Republic of Iraq
Ministry of Higher Education
and Scientific Research
University of Babylon
Faculty of Engineering

High Performance of All Optical Orthogonal Frequency Division Multiplexing Based Light Fidelity System for Outdoor Communication

A Thesis

Submitted to the Faculty of Engineering, University of Babylon in Partial Fulfillment of the Requirements for the Degree of Doctorate of Philosophy in Electronics and Communications Engineering.

by

Marwa Jaleel Mohsin

Supervised by

Prof. Dr. Ibrahim Abdullah Murdas

2023 A.D. **1444 A.H.**

بِسْمِ اللَّهِ الرَّحْمَٰنِ الرَّحِيمِ

﴿ هُوَ الَّذِي جَعَلَ الشَّمْسَ ضِيَاءً وَالْقَمَرَ نُورًا وَقَدَّرَهُ مَنَازِلَ لِتَعْلَمُوا عَدَدَ السِّنِينَ وَالْحِسَابَ ۚ مَا خَلَقَ اللَّهُ ذَٰلِكَ إِلَّا بِالْحَقِّ ۚ يُفَصِّلُ الْآيَاتِ لِقَوْمٍ يَعْلَمُونَ ﴾

صَدَقَ اللَّهُ الْعَلِيّ الْعَظِيم

سورة يونس (٥)

Abstract

Light Fidelity (Li-Fi) was presented as a promising technology for the fifth generation and beyond to overcome the Radio Frequency (RF) spectrum crunch in wireless communication networks and perform high-speed transmission, it is considered an excellent alternative to the RF in the wireless network for the past few years due to its many benefits.

This work proposed a simulated ultra-high-speed Li-Fi system suitable for outdoor applications where the light signal is sent over an unguided and unlimited path called a free-space optical (FSO) channel link. Laser diode LD is utilized as an optical source to eliminate the limitation of conventional Li-Fi systems in terms of Light Emitting Diode (LED) bandwidth, transmission bitrate, and transmission distance.

The proposed Li-Fi system offered high performance and immunity to free space channel attenuation due to utilizing All-Optical Orthogonal Frequency Division Multiplexing (AO-OFDM) architecture by implementing Inverse Fast Fourier Transform/Fast Fourier Transform (IFFT/FFT) completely in the optical domain without reacquiring the electrical component, which limits the system speed and performance. The proposed system succeeds to create the orthogonality optically between subcarriers through proposed a new scheme of Optical Frequency Comb Generator (OFCG) for visible band applications to generate multi carriers from single continues laser diode with tunable property. The proposed OFCG is simple with more efficient power and excellent flatting of comb lines, the number of generating frequency lines was 52 with a power stronger than 2 dBm and fluctuation less than 0.5 dB over a 470 GHz bandwidth.

AO-OFDM signal generated between eight and sixteen channels over 180 or 340 GHz of bandwidth respectively, through implementing optical IFFT at the transmitter side based on OFGC, Dense wavelength Division multiplexing DWDM,

and optical combiner at the transmitter side, each channel with 20 G symbol/s and utilizing Dual-polarization- In phase/Quadrature phase DP-IQ modulation with Quadrature phase shift keying QPSK and 16- Quadrature amplitude modulation QAM schemes making the system with transmitted signal has approximately ~5dB of a peak-to-average power ratio (PAPR) and spectral efficiency SE of 4 and 8 bit/s/Hz for QPSK and 16-QAM respectively. At the receiver side to recover the signal of each channel, Optical FFT is implemented based on a special structure of multi-Mode interference (MMI) and time delays.

This work has been done using VPI design suite software version 9.8 which is suitable for this work and the system achieved a well-received power with a high data rate reaching 1.28 Tbps and a low Bit Error Rate (BER) of about 1×10^{-10}.

Various optical signal-to-noise ratio (OSNR) values (0-35dB) and FSO path links (1 to 10 km) under different turbulence and weather conditions were utilized to test the behavior of the proposed system.

This study extensively examined and simulated the atmosphere attenuation using MATLAB with various conditions and evaluated the influence of these conditions on the proposed Li-Fi system design. The system demonstrated a decent performance with BER at approximately 1×10^{-3} and received a signal of -45 dBm for 10 km and under significant turbulence.

Dedications

To…

My Parents, husband,

and

Lovely children

"Raneem & Ayham"

Researcher

Supervisor Certification

I certify that this Thesis entitled "***High Performance of All Optical Orthogonal Frequency Division Multiplexing Based Light Fidelity System for Outdoor Communication***" was prepared by ***Marwa Jaleel Mohsin*** under my supervision at the Department of Electrical Engineering, College of Engineering, University of Babylon, as a partial fulfillment of the requirements for the degree of Doctorate of Philosophy in Electronics and Communications Engineering.

Signature:

Name: ***Prof. Dr. Ibrahim Abdullah Murdas***

(Supervisor)

Date: / / 2023

In view of the above recommendation, I am forward this Thesis for discussion by the Examination Committee.

Signature:

Name: ***Prof. Dr. Qais Kareem Omran***

(Head of Electrical Engineering Dept.)

Date: / / 2023

Examining Committee Certificate

We certify that we have read this Thesis entitled "***High Performance of All Optical Orthogonal Frequency Division Multiplexing Based Light Fidelity System for Outdoor Communication"*** and as an examining committee, examined the student, "***Marwa Jaleel Mohsin***", in its contents and that in our opinion it meets the standard of a thesis for the degree of Doctorate of Philosophy in Electronics and Communications Engineering.

Signature:
Name: ***Asst. Prof. Dr. Wasan Kadhim Saad***
(Member)
Date: / / 2023

Signature:
Name: ***Prof. Dr. Haider J. Abd Nasar***
(Member)
Date: / / 2023

Signature:
Name: ***Prof. Dr. Yousif Al Mashhadany***
(Member)
Date: / / 2023

Signature
Name: ***Prof. Dr. Kasim Karam Abdallah***
(Member)
Date: / / 2023

Signature:
Name: ***Laith A. Abdul-Rahaim***
(Chairman)
Date: / / 2023

Signature:
Name: ***Prof. Dr. Ibrahim Abdullah Murdas***
(Supervisor)
Date: / / 2023

Signature:
Name: ***Prof. Dr. Qais Kareem Omran***
(Head of Electrical Engineering Dept.)
Date: / / 2023

Signature:
Name: ***Prof. Dr. Hatem Hadi Obeid***
(Dean of College of Engineering)
Date: / / 2023

Acknowledgements

*Praise is to the **Almighty Allah** the most gracious and most merciful for enabling me to present this work.*

*I would like to express my sincere thanks and gratitude to my supervisor Dr. **Ibrahim A. Murdas** for his guidance, supervision and efforts during this work.*

I would like to thank the University of Babylon/ Electrical Engineering Department, faculty members and all the Electrical Engineering Department staff for their support and assistance.

I would like to thank my colleagues and all friends who helped and encouraged me throughout this work.

Finally, I am indebted to my family for their care, patience and support during my years of study.

Marwa

List of Contents

List of symbols

Symbol	Meaning
x_m	Time domain FFT input signal
X_k	Frequency domain input to IFFT block
E_k	The frequency domain samples
ε_m	The time domain samples
$\Delta\varphi$	Phase difference between two consecutive time instances
Δf	line width of the laser diode
f_k	The frequency of the k^{th} line
f_{CF}	The frequency central line
N_{sc}	Total number of subcarriers or channels
$x(t)$	The transmitted electrical signal
ω	Angular frequency
$\emptyset$	The phase of the transmitter LD
c_{ki}	Complex data of i^{th} signal symbol on the k^{th} subcarrier
T_s	The symbol period
f_{CF}	The center frequency of the OFDM system
A_K	The initial amplitude of the k^{th} subcarriers
$h_{(t)}$	The channel impulse response
$w(t)$	The channel noise
$i(t)$	The instantaneous photodetector current
η_{eq}	The quantum efficiency
α	The absorption coefficient
d	The distance
ξ	Electron-hole pair contribution to photocurrent
R	The reflection coefficient at the air-semiconductor interface
$n(x)$	X noise component
$n_{xl}(t)$,	The in-phase noise components of the x polarization
$n_{xQ}(t)$	The quadrature-phase noise components of the x polarization
$n_{yl}(t)$	The in-phase noise components of the y polarization
$n_{yQ}(t)$	The quadrature-phase noise components of the y polarization

$I_x(t)$,	The in-phase component of the incoming signal in the x polarization
$Q_x(t)$	The quadrature-phase component of the incoming signal in the x polarization
$I_y(t)$	The in-phase component of the incoming signal in the y polarization
$Q_y(t)$	The quadrature-phase component of the incoming signal in the y polarization
$A_{lo,x}$	The LO amplitude in the x-polarization
$A_{lo,y}$	The LO amplitude in the y-polarization
$\theta_{lo}(t)$	The phase/diversity receivers
P_e	Total power emitted from the transmitter (dBm)
S_r	The receiver sensitivity (dBm)
A_{geo}	The geometric attenuation loss (dB)
A_{atmo}	losses resulting from absorption and scattering in the atmosphere (dB)
$A_{scintillation}$	The attenuation due to scintillation
P_R	The received power
P_T	The transmitter power
G_T	The effective gain of the transmitter
G_R	The effective gain of receiver
L_P	The free space path loss
A	The effective optical telescope area
λ	The wavelength of the signal
θ_{div}	Beam divergence angle
S_L	The spot surface of emission beam at distance *L*
θ	The beam divergence angle
$S_{capture}$	The capture area of the receiver or detector (m^{-1})
$\gamma_t(\lambda)$	The total attenuation or extinction coefficient (km^{-1})
α_m	The absorption coefficients of the molecular
α_a	The absorption coefficients of the aerosols
β_m	The scattering coefficients of the molecular

β_a	The scattering coefficients of the aerosols
σ	The extinction cross-section
N	The concentration of molecules
α_{abs}	The effective absorption particle cross-section
N_{abs}	The absorption particle concentration
α_{scat}	The cross-section parameter
β_{scat}	The Rayleigh scattering
N_{scat}	The particle concentration
α_m	The Rayleigh scattering cross-section
N_m	The air molecules' number density
α_a	Mie scattering cross-section
β_λ	The atmosphere attenuation coefficient
T_{th}	The transmittance threshold level
α_{rain}	Rain attenuation
$n(r)$	refractive index at any point (r) in space
P	The atmosphere pressure in mbar
T	The temperature in Kelvin K.
l_0	The inner scale of the turbulence
L_0	The outer scale of the turbulence
C_T^2	The temperature fluctuation structure constant
σ_r	The radial variance
C_n^2	The turbulence strength
w_0	The beam waist at the transmitter aperture
I	The intensity or signal irradiance.
k	The wave number
σ_{turb}	The atmosphere attenuation due to turbulence or scintillation
$E_{n,k}$	The amplitudes of components
$\theta_{n,k}$	The phases of components

List of Abbreviations

Abbreviation	Full name
ADC/DAC	Analogue to digital convertor/Digital to analogue convertor
AO-OFDM	All optical- Orthogonal frequency division multiplexing
AP	Access point
BER	Bit error rate
CCI	co-channel interference
CO-OFDM	Coherent- Orthogonal frequency division multiplexing
DD-OFDM	Direct detection- Orthogonal frequency division multiplexing
DP-IQ	Dual polarization- in-phase Quadrature polarization
DWDM	Dense Wavelength division multiplexing
EOC/OEC	Electrical-to-optical converter/optical-to-electrical convertor
e-OFDM	Electrical- Orthogonal frequency division multiplexing
FOV	field of view
FSO	Free space optic
IEEE	Institute of Electrical and Electronics Engineers
IF	intermediate frequency
IFFT/FFT	Inverse Fast Fourier transform/Fast Fourier transform
IM	Intensity modulation
IM/DD	Intensity modulation/ Direct detection
IoT	Internet of things
BPSK	Binary phase shift keying
QPSK	Quadrature phase shift keying
QAM	Quadrature amplitude modulator
IR	Infrared
IrDA	Infrared association
IROWC	Infrared optical wireless communication
ISI	inter-symbol interference
LD	Laser diode
LECS	local edge computing system
LEDs	Light emitting diodes

Li-Fi	Light Fidelity
LO	local oscillator
LOS	Line of sight
LPWAN	low-power wide-area network
MCM	multicarrier modulation
MIMO	Multiple input-Multiple output
MLL	mode-locked laser
mm waves	millimeter waves
MMI	Multi-mode interferometer
MZM	Mach-Zehnder Modulator
OFCG	optical frequency comb generator
OFDM	Orthogonal frequency division multiplexing
OLT	optical line terminal
O-OFDM	Optical- Orthogonal frequency division multiplexing
OOK	ON-OFF keying modulation
OPLL	optical phase lock loop
OSNR	Optical signal to noise ratio
OWC	optical wireless communication
P/S	Parallel to serial
PAM	Pulse amplitude modulation
PBS	Polarization beam splitter
PPM	Pulse position modulation
QOS	Quality of Service
RF	Radio frequency
RGB	Red, Green, Blue
RIN	relative intensity noise
S/P	Serial to parallel
SLED	super luminescent-LED
SMD	service-mounted device
SOPs	state of polarization
UI	users’ interface
UTROV	Un-Tethered Remotely Operated Vehicle
UV	Ultraviolet

UVC	Ultra violet communication
UWB	ultra-wideband wireless system
V2I	Vehicle-to-Infrastructure
V2V	Vehicle-to-Vehicle
VCSEL	Vertical-cavity surface-emitting laser
VLC	Visible Light communication
VLLC	visible laser light communication
WDM	Wavelength division multiplexing
Wi-Fi	Wireless fidelity
µFSO	Micro-free space optic (Underwater communication)
µLED	Micro-LED
5G	Fifth generation

List of Figures

List of Tables

Chapter one

Introduction

Chapter one

Introduction

1.1 Background

Light for communication is one of the oldest methods used to communicate between people since ancient times. Greeks and Roman used it as a communication tool between people. Roman used a plate with polished material to reflect the sunlight and carry the signals for a long distance. Optical wireless (OW) existed in ancient times, such as semaphores, ship flags, and fire or smoke signals. Semaphore lines based on optical communication were evened in 1790 and developed by the French Claude Chappe in 1792, the first virtual telegraphy system used to transfer information between the cities. Modern communication was expanded and exponential growth in its experience and application due to extraordinary developments that the world witnessed at various levels of life in general and in the communication field in particular [1-3].

Due to the importance of communication systems in human life, modern techniques and tools were invented, whether wired or wireless, to overcome the communication revolution [2]. Nowadays, the fastest growing technology in wireless networks where everything in the world is connected wirelessly, various wireless communication technologies are available, and the most efficient are operated in Radio Frequency (RF) spectrum [4, 5].

The electromagnetic spectrum is made up of all sorts of things, including radio waves, visible light, infrared, X-ray, Gamma rays etc.; some of these rays are pretty dangerous [4]. The radio frequency spectrum is a small part of the electromagnetic spectrum. Fig. 1.1 displays the RF spectrum classification.

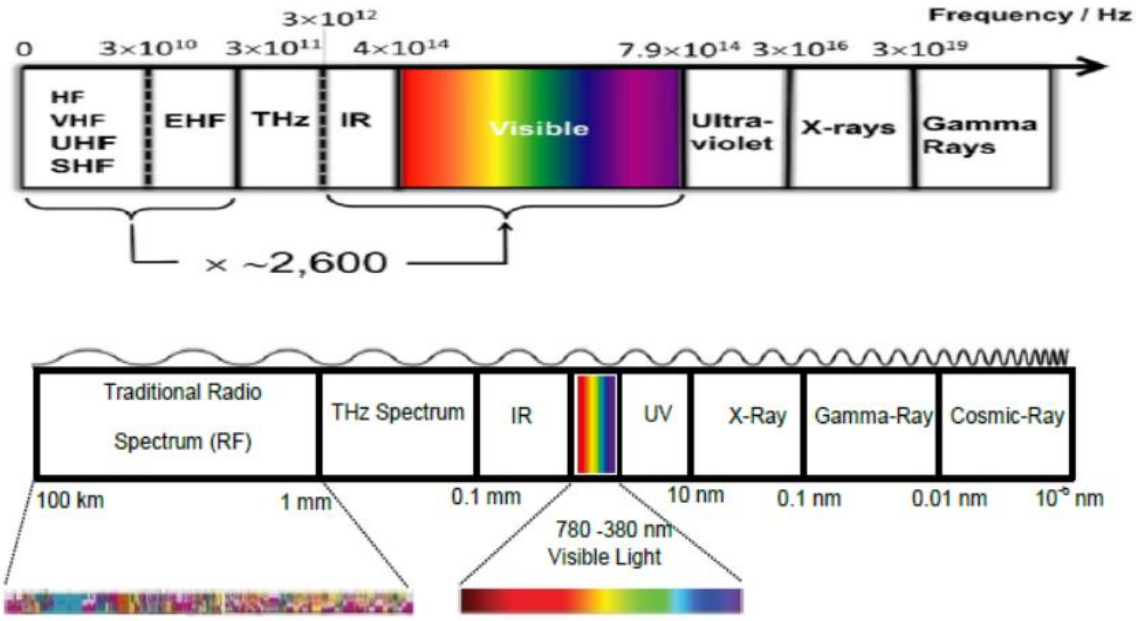

Figure 1.1 Radio Frequency spectrum[1, 6]

On the cusp of Fifth Generation 5G and beyond, where the Internet of Things (IoT) has become an essential issue. There is a considerable increase in network traffic where life becomes data. This data is not only generated by humans as it is primarily knowing this data generated by machines and things such as things at home, office, oven, car, watch etc., all these generated data at the high data rate. IoT devices are connected to the internet by a wireless network, and the resource to do that is the Radio Frequency spectrum. Unfortunately, spectrum crunch occurs due to an oversupply of available Radio Frequencies. Eventually, RF technology like Wi-Fi will no longer keep up with demand [7].

Many studies improve that reduce the available RF spectrum and couldn't meet the demand of network connectivity, such as high bit rate, lower cost, and better Quality Of Service (QOS), so it is necessary to find alternatives. Therefore, various technology enters the race to provide ultra-fast wireless communication

system like optical wireless communication (OWC) (indoor or outdoor), ultra-wideband wireless system (UWB) etc.[1, 6, 7].

1.2 OWC classification

OWC system was introduced for short-range communication more than two decades ago, and it has many merits rather than FR, such as high bandwidth, cost-effectiveness and robustness against multipath fading [2].

OWC used IR, visible light and UV wavelengths as unguided light to carry a signal. Combined infrared and visible Light spectrum are 2600 timed of radio frequency spectrum (300GHz)., as shown in Fig. 1.1 [7]. The Modern optical wireless communication (OWC) is classified as illustrate in Fig. 1.2 [2].

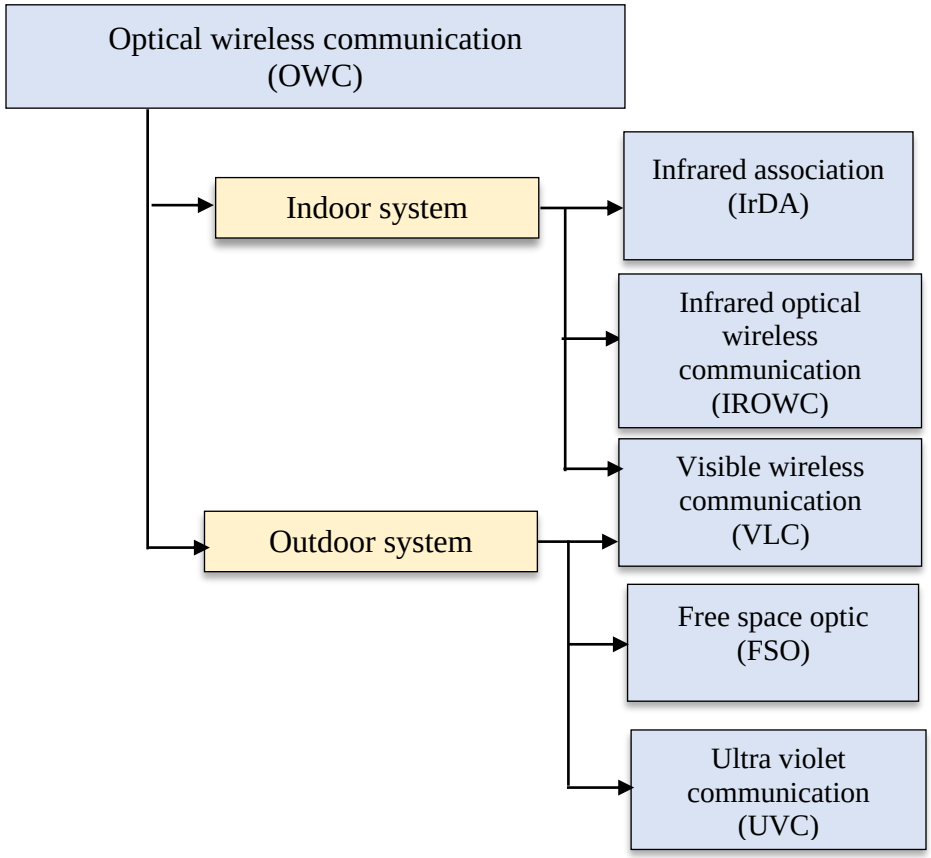

Figure 1.2 Classification of OWC

1.2.1 Indoor Optical Wireless Communication

OWC included Indoor communication systems that utilized IR and VLC ranges; VLC is getting much attention nowadays. VLC is one type of optical communication that utilized visible signals from the electromagnetic spectrum in the frequency range between 430THz-790THz or 380nm-780nm of wavelengths [2]. VLC stands for utilizing the visible band's light wave-free space propagation as a transmission channel for communication. However, illumination and communication can be provided through VLC. VLC is characterized by a very high bandwidth, secured, low power consumption, no health hazard and licenses free channel [2, 7, 8].

Light emitting diodes (LEDs) with white illumination are preferred for VLC due to their merits, such as long lifetime and energy efficiency (10 times greater than incandescent bulbs)[9]. VLC enables Light Emitting Diode (LED) to transmit the information by modulating the illumination level coded by Intensity Modulation (IM), and the receiver can detect the data using Photodetector (PD); the process happens so fast that the eye couldn’t perceive it. VLC provide a point-to-point communication channel between the transmitter (LED) and receiver (PD) [10, 11]. This technology is known as green technology and can replace RF in many important places such as hospitals and Airports. In 2011, the IEEE certified the 802.15.7 standard for VLC with a data rate ranging from 11 Kbps to 96 Mbps [10].

1.2.2 Outdoor Optical Wireless Communication

For outdoor OWC can be classification in to:

I. Outdoor Visible Light communication

Outdoor short-range optical wireless communication Known as outdoor VLC with communication links few meters, there are many VLC outdoor promising systems

such as VLC-IoT and Vehicle-to-Vehicle (V2V) or Vehicle-to-Infrastructure (V2I) [11, 12].

II. Free space optical (FSO) communication

FSO refers to long-range communication that reaches a few kilometers and is preferred for communicating between buildings[9, 13], as shown in Fig. 1.3

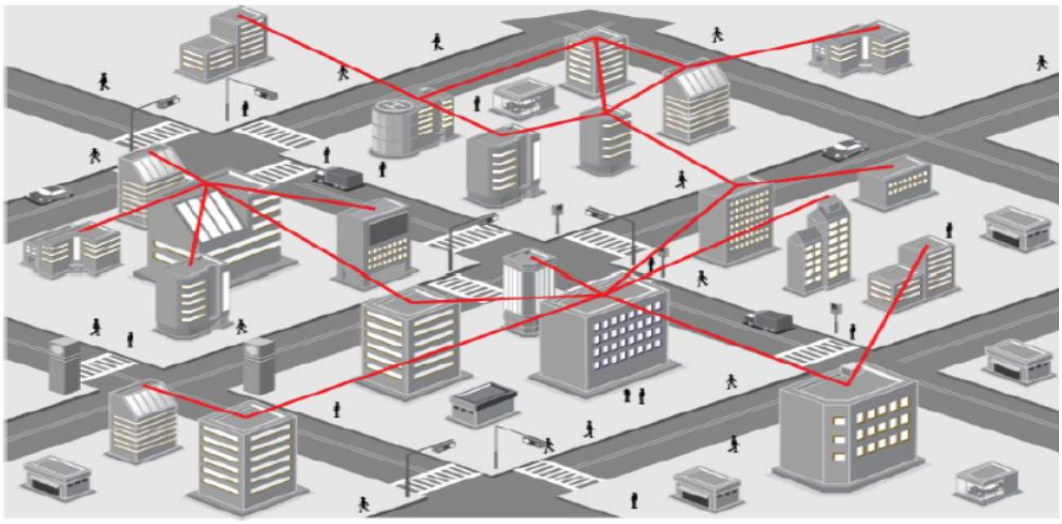

Figure 1.3 FSO network [10]

FSO is a high data rate (Mbps to 10 Gbps) and unlicensed spectrum channel and immunity against any RF signal of link and devices, utilized IR and VLC as a carrier to achieve high data rate transmission with enormous bandwidth (hundreds of terahertz). Therefore, FSO is more cost-effective and attractive in civil and military applications than the traditional optical fiber network. Furthermore, there is a repaid evaluation of FSO technology and taking the leading role in the indoor and outdoor application for the next-generation networks [7, 14]. Figure 1.4 illuminates the capacity of wireless technology with maximum transmission distance.

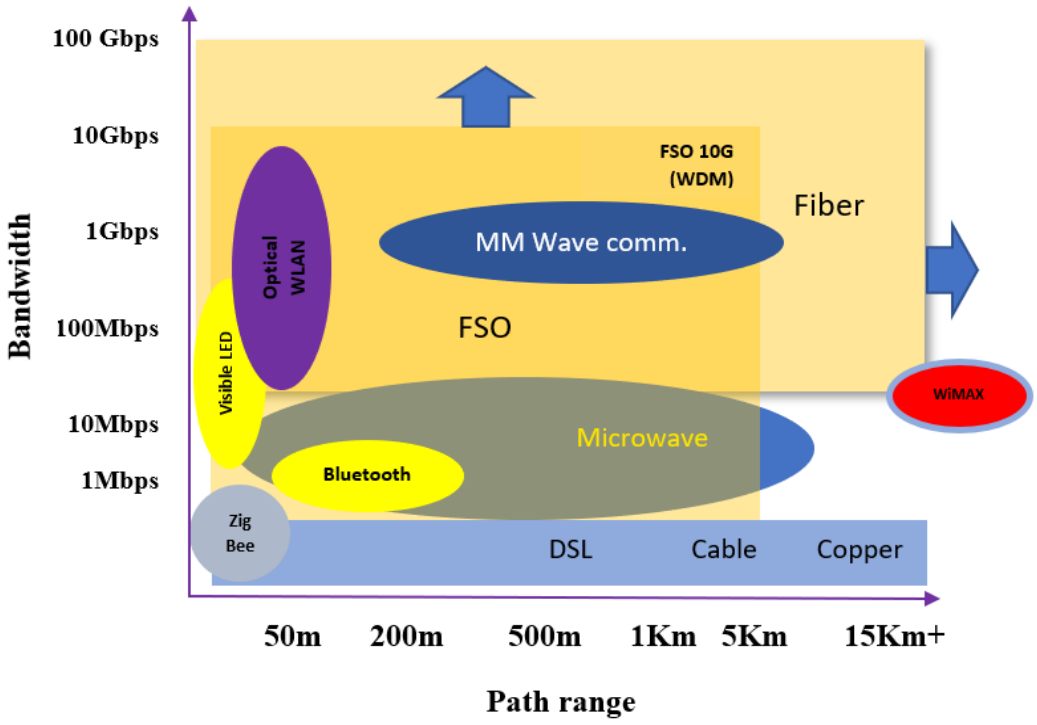

Figure 1.4 Wireless communication technologies [8]

LEDs and low-power laser diodes LDs are used as optical carriers for data transmission in the atmosphere. However, LED is preferred for indoor FSO applications. For example, in Japan in 2003, successful data transmission with a VLC system was carried out using LED at the Nakagawa Laboratory at Keio University [6].

With a 5G, high data rates are required up to 10 Gbps. Therefore, FSO is a good candidate for using LDs rather than LEDs due to the extremely high data rate reaches to Terabits [8,10].

There are two crucial challenges with FSO, Atmospheric losses and Weather attenuation. Each type causes a different effect on the transmitted signal. Atmospheric attenuation causes scintillation, and weather attenuation causes power loss [10]. Each one will explain in detail in chapter two.

1.3 Visible light communication applications

There are many vital applications of VLC, such as:

i. **Vehicle-to-vehicle communication (V2V)**: can be advantageous, from the vehicle lights to communication between vehicles for safety or with existing traffic infrastructure [2, 6].

ii. **Hospitals and industries**: VLC human safety and didn't interfere with other electromagnetic waves radiated from some hospital devices [2, 6].

iii. **Underwater communication (UWC):** Due to the conductivity of the water, RF waves don't travel well in the sea. Therefore, VLC is a good candidate for underwater communication. One application of UWC is Un-Tethered Remotely Operated Vehicle (UTROV). Different jobs can be implemented underwater through UTROV, such as deployment opportunities and observatory maintenance of the oceans [2, 6]. Studies achieve 20-30 m light propagation using LEDs with an average power consumption of 500mW and data rates between (9600-38400) bps [10, 6].

iv. **Li-Fi:** One of the most promising communication technologies for modern life coined by German researcher Harald Haas in 2011 was Light-Fidelity (Li-Fi) [2,9]. Li-Fi can be defined as a bidirectional wireless communication technology, that is fast, secure, and fully networked. Moreover, it enables us to move to the higher frequencies in the RF spectrum (such as IR and VLC) to utilize as a medium for transmit and receive the data [9].

Li-Fi supports mobility and multiuser access, such as point-to-multipoint or multipoint-to-point, establish a very small optical wireless network (called attocells) with seamless handover [10,7]. Figure 1.5 explains the principle of Li-Fi and its applications [11, 7].

Li-Fi support different applications for 5G and beyond, such as Internet of Things (IoT) and mobile systems, with speed up to 10 Gbps, which is 250 times greater than super-fast broadband speed [6, 10]. Li-Fi will explain in detail in chapter two.

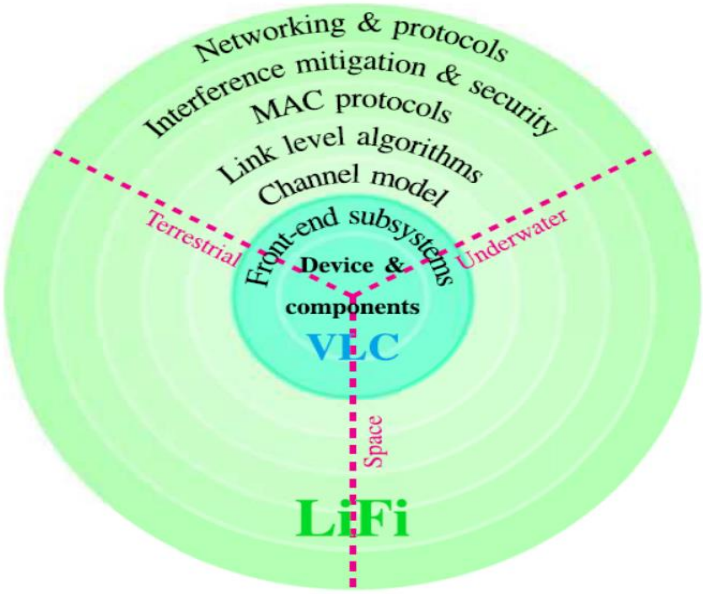

Figure 1.5 The principle of Li-Fi and its applications [11]

1.4 Literature survey

C. Ying et al. (2015) [15] achieved 20 Gbps with good BER (10^{-6}) and clear constellation performance over a 6m free-space link due Li-Fi optical system by utilizing Vertical-cavity surface-emitting laser (VCSEL). It is a developed technology of visible laser light communication (VLLC) (375-685nm) using an external light injection technique. The modulation scheme was 16QAM-OFDM. The OFDM signal was generated offline using MATLAB with 256 subcarrier and electrical 256-FFT.

D. Tsonev et al. (2015) [16] Appling three experimental scenarios of using LD for fully indoor illumination and transmitting/receiving the information with a high data rate. First: utilizing an array of three RGB LDs and estimated the data

rate at a distance of 30 cm achieving overall data rate from the three LDs is 14 Gb/s with BER 6.07×10^{-4}. Second: occupy the entire visible light spectrum for transmitted by using 12 RGB triples operating at a different wavelength with an allocated 10nm for each stream of information to fit 36 parallel information streams, the data rate achievable with this scenario 105 Gb/s with 2.04×10^{-3}. Third: using single RGB triple for front-end indoor communication only without illumination by mounted on the ceiling, providing a 1 m^2 coverage area and 2.88m distance; with this scenario, the overall data rate can achieve about 3.34 Gb/s and BER 2.33×10^{-3}.

M. Ayyash et al. (2016) [17] proposed a hybrid of Wi-Fi-Li-Fi system with three scenarios for connection to the internet and compared them using a single access point AP for both Wi-Fi and Li-Fi systems. The first scenario for connection to the internet using Wi-Fi (30 Mbps at 15m), the second same the first system only the downlink of a user connected to the Li-Fi, which is hybrid (73Mbps at 2m), and the third is an aggregation of both superior scenario (95 Mbps at 2m), Wi-Fi and Li-Fi in parallel. The comparison includes the average throughput for the three scenarios at a different distance (between 2 to 10m); the throughput decreases with distance, and the throughput of the Hybrid systems is double of the Wi-Fi, and the aggregation system is triple the throughput achievable of Wi-Fi.

H. Chun et al. (2016) [18] implemented WDM between different color LEDs (red RC-LED, green and blue µLEDs) for multiplexing to generate white light and transmitted different data streams. The combination was based on VLC and studied the data rate variation based on the effect of light color. They achieve 10.4 Gb/s and BER between 2.8×10^{-3}- 3.4×10^{-3} using LED-based WDM with a 1.5m distance between the transmitter and receiver. Furthermore, they used DC-biased

optical orthogonal frequency division multiplexing for communication due to high spectral efficiency over the all schemes of optical OFDM.

A. A. Mohamed et al. (2017) [19] Enhanced the FSO transmitted system by stimulating a transmitted system based on DWDM-OFDM under different weather conditions. It utilized some techniques such as CO-OFDM and spatial diversity to minimize the effect of atmospheric attenuation. As a result, 20-channel DWDM with CO-OFDM and DD-OFDM over the FSO channel was successfully demonstrated. The data rate was 10Gbps over 100 to 500 Km of range. A transmitter modulated the light of CW laser diode (1550nm and 20dBm power) with QAM scheme. It mapped the symbols serial to parallel implementing OFDM with 104 subcarriers and 128-electrical FFT and adding a cyclic prefix. Under these different weather conditions, the system shows a low bit rate and good Q-factor.

R. J. L. Ferreira et al. (2017) [13] presented a practical and simulated confirmation of an all-optical fast Fourier transform (FFT), which is based on optical interferometry. This FFT is employed for the dropping of an OFDM carrier. QPSK scheme was employed to modulates the OFDM signal at 75 Gb/s. With channel spacing about 12.5 GHz, it was proved that the optical frequency created optical comb-based laser gain-switched. In addition, it produced a comb line that used only three of these subcarriers to modulate three channels, each with 25Gbps. Compared between SNR and BER.

R. Bian et al. (2018) [20] Experimentally demonstrated a transmission system with 10.2Gbps using three LEDs characterized by high brightness and utilizing WDM-VLC link without an equalizer. The system applying WDM for three different color LEDs, red, green, and blue, for enhancing the spectral efficiency OFDM was implemented with Hermitian symmetry for real and positive signal

due to IM/DD. BER about 3.8×10^{-3}. The proposed system can be integrated as transmitter and receiver units to be suitable for real applications like the internet of thinks IoT.

C. Verma et al. (2018) [21] simulated a communication system-based VLC using Opti-system to transmit 10 Gbps by modulating data on a CW laser diode with 450nm wavelength as an optical source transmitted it through a free space optic link with a length of 250 m. This system's benefit is improving the overall VLC system for Free-space communication in terms of high data rate, high speed, and high transmission distance. The modulation scheme was OFDM-4QAM. In addition, the proposed stimulated system achieves a clear constellation diagram.

R. A. Othman et al. (2018) [8] designed a simple Li-Fi system integrated with IoT to transmit audio signals. The system consists of the transmitter transmitting an audio signal represented by a cell phone, which acts as an audio source with LED as a light source to modulate the signal. The receiver was a solar cell used to detect the received signal, demodulate it and send it to the speaker.

A. R. Ndjiongue and H. C. Ferreira (2018) [22] described the probability of using VLC for outdoor applications and discussed promising outdoor VLC applications such as V2V and R2V. They explained the challenges that obstacle the outdoor VLC application with a different type of noise. They make a simple communication system that allows up to 10 MHz for the transmitter: two LEDs, white and RGB-LED, to achieve the communication using OOK and CSK techniques. For the receiver, they used a single photodiode PD and a matrix of color photodiode PDs. The transmitter and receiver were aligned and studied the variation of outdoor intensity at along daylight.

A. Israr et al. (2019) [23] presented a solution to the Li-Fi system to compensate for the problem of FSO attenuations by proposing a 4×4 MIMO-FSO system with a different modulation scheme. The performance of the proposed system was analyzed with different length distances, transmitting power, and attenuation factors and observed the effect on Q-factor and eye diagram. The system transmitted high bandwidth data from a pseudo-random generator and modulated it using a Mach-Zehnder modulator with a CW laser beam diagram. Different modulation scheme was utilized, such as NRZ, RZ, and CSRZ. MIMO was implemented with four transmitters and receiver. The operating frequency was 1550nm, achieving a data rate 2.5 Gbps over 1-10Km. Q-factor 900-100 with attenuation (1-10 dBKm) respectively.

R. George et al. (2019) [24] used an Arduino Uno microcontroller to design a communication system based on VLC to control the speed of two motor vehicles by modulating the light intensity generated from LED as an optical carrier with the data. The data was exchanged between the transmitter and receiver (the two vehicles) to control the speed of the motor, reducing road accidents.

M. Adel et al. (2020) [25] simulated and studied the FSO transmitting system under diverse weather and pointing errors. The system was implemented under clear weather, Haze, and Fog, tested in the constellation, eye diagram and received SNR. Achieving maximum bit rate reaches 128 Gbps, applying QPSK modulation to modulate the light of laser diode source, estimated the eye diagram among different distances 15, 25, and 35Km.

C. Lee et al. (2020) [26] implemented a Li-Fi system with laser light as an optical source. They employed white light SMD (service-mounted device containing blue LD with phosphor to generate the white light) to increase the data rate. For the purpose to maximize the capacity of the channel, QAM-OFDM was utilized and

achieved 11 Gb/s for 5m distance with single SMD and 1.7 Gb/s with 50m, although 22.45 Gb/s at 3m distance with dual SMD and two-channel WDM. the two LD are simultaneously transmitted the data within wight light of MSD.

H. Haas et al. (2020) [27] motivated the importance of Li-Fi to be a very timely technology due to 6G for cellular communication. Therefore, they designed a hybrid Wi-Fi/Li-Fi system developed in the classroom, including eight AP (Li-Fi attcell) with existing two Wi-Fi AP. The Li-Fi AP have a coverage area of 2.5 to 3.5 m diameter of circular coverage. The designed system supports 8 users with 43 Mbps, which is 344 Mbps for each classroom.

J. Hoxha et al. (2020) [29] presented a simulated system to implement AO-OFDM through six 10 G Boud rate channels using a wavelength selective switch WSS over 800 Km fiber channel link with 19-39dB. They also presented a new way to improve traditional AO-OFDM by confining the extending spectral of the particular subcarrier. This method improved the Q-factor (3dB) and increased the spectral efficiency (14%).

R. Bian et al. (2021) [30] presented experimental results based on LED VLC to achieve 15.73Gb/s with FEC through 1.6m. Furthermore, to increase data rate and feasibility, WDM-OFDM between four channels (four different LEDs colors), achieve BER (28×10^{-4}). Table 1.1 shows a brief comparison between previous works.

Table 1.1 Comparison between previous studies

Ref.	Work type	Optical source	Modulation	Distance	Data rate (bps)	channel link	BER
[15] 2015	Experiential	LD	e-OFDM 16QAM-	6m	20 G	Free-space	10^{-6}

[16] 2015	Experiential	LDs	-	6cm 93 cm 2.88m	14G 105G 3.34G	indoor	~ 6×10^{-4} ~ 2×10^{-3} ~ 2×10^{-3}
[17] 2016	Experiential	LEDs	IM-DD	2-10m	95 M	indoor	-
[18] 2016	Simulated	LEDs	WDM-DCO-OFDM	1.5m	10.4G	indoor	~ 3×10^{-3}
[19] 2017	Simulated	LDs	CO-OFDM	100-500Km	10 G	FSO	20-5 (Q-factor)
[13] 2017	Simulated	LDs	AO-OFDM (QPSK)	Back-to-back	75G (3-channel of 25G)	direct	10e-3to 10e-16
[20] 2018	Experiential	Three LEDs	DCO-OFDM IM/DD WDM	-	10.2 G	Direct	3.8×10^{-3}
[21] 2018	Simulated	LDs	e OFDM-4-QAM	250m	10 G	FSO	Clear constellation diagram
[23] 2019	Simulated	LDs	4×4 QAM-MIMO	1-10Km	2.5 G	FSO	900-100 Q-factor
[25] 2020	Simulated	LD	QPSK	15,25,35 Km	128 G	FSO weather condition	Open eye diagram
[26] 2020	Experiential	Laser SMD	QAM-e OFDM	5m 50m	11G 1.7G	Indoor	2.98×10^{-3}
		Dual SMD	QAM-e OFDM WDM	3m	22.45G	Indoor	-

[29] 2020	Simulated	laser	AO-OFDM	800 Km	6channel of 10G Boud rate	Fiber	Q-factor ~20
[30] 2021	Experiential	LEDs	e-OFDM WDM	1.6m	15.73G	Indoor	28×10^{-4}
Our 2022	Simulated	LD	AO-OFDM	1-10 Km	1.28T	FSO	~10e-10

As shown in Table 1.1, many studies implemented the Li-Fi system in various ways under various conditions. This study designed a Li-Fi system-based AO-OFDM suitable for long-range outdoor Li-Fi applications. This work is typically similar to the reference [13], which simulated a back-to-back AO-OFDM system between three channels only and achieve BER between 10e-3 and 10e-16. The reference [25] is also similar to this study in the Li-Fi principal system, but the reference didn't implement OFDM architecture. Furthermore, the reference [29] is more similar to the current study but implemented AO-OFDM in different way, based on wavelength selective switch WSS, and the channel link was optical fiber.

1.5 Problem statement

Li-Fi system is a promising technology for the fifth generation and beyond due to its features, it can be utilized for many important applications in our life. Unfortunately, From the literature review, Li-Fi system-based traditional LEDs have several limitations such as:

1. The short range of transmission distance.
2. Low transmission data rate about of 1Gbps.
3. LEDs' lifetime is reduced with a temperature rise.
4. The modulation bandwidth is limited to several of MHs.

5. Attenuation due to path loss (such as ambient light). interference between symbols, known as inter-symbol interference (ISI), which is caused by multipath propagation, and interference between channels, known as co-channel interference (CCI), which is caused by numerous transmitters [2, 10].

1.6 Thesis objectives

1. To eliminate the limitation of the Li-Fi system in terms of LEDs bandwidth, transmission bitrate, and transmission distance, design and simulate an ultra-high-speed Li-Fi system that utilized a laser diode as an optical source rather than traditional LEDs.
2. To maximize the exploitation of channel capacity offered by the VLC band, design and simulate a Li-Fi system-based all-optical OFDM architecture as a multicarrier transmission system.
3. To overcome the requirement of the electrical components which limit the system performance or speed, create the AO-OFDM signal successfully by implementing IFFT/FFT completely in the optical domain.
4. To generate several subcarriers from a single CW laser source that offers flexibility and tunability for creating the orthogonality between these subcarriers.
5. To improve the system performance in term of BER , received power, data rate and link range , and compare current findings results with recent work at the same conditions.

1.7 Thesis contributions

The main contribution of this study is:

1. Designed and simulate ultra-high speed and long-range Li-Fi system suitable for outdoor applications due to utilizing the laser diode as optical carrier rather than traditional LEDs.
2. Design and simulated a new scheme of Li-Fi system based all-optical OFDM architecture.
3. Design and simulate a new optical frequency comb generator OFCG system, which is a vital element to implement the orthogonality optically between subcarriers.
4. Tested the behavior of the proposed Li-Fi system-based AO-OFDM under different free space turbulence and weather condition in terms of data rate, BER, received power.

1.8 Thesis organization

This Thesis contains five chapters organized as follows:

Chapter one: Presented an introduction to the Li-Fi system and its limitations, related work, goal, contributions for this study.

Chapter two: The principles of Li-Fi systems and AO-OFDM architecture were discussed in chapter two.

Chapter three: Presented a simulation for the proposed designed system of outdoor Li-Fi system based on AO-OFDM architecture.

Chapter four: The simulated results of the proposed system were illustrated in chapter four.

Chapter five: conclusions for this study and some prospects for future work were given in chapter five.

Chapter two

Theory aspects of Li-Fi communication systems

Chapter two

Theory aspects of Li-Fi communication systems

2.1 Introduction

An overview of OWC in a general way and the Li-Fi system in a specific way is discussed in this chapter. The central concept of the Li-Fi system and all-optical OFDM architecture is deeply demonstrated in next sections.

2.2 OWC principles

OWC is a wireless connecting system-based optical spectrum that provides ultra-high data rate service across a communication distance of up to 10,000 km and it can be utilized for indoor and outdoor applications. A wide range of unlicensed spectral wavelength (700-10000nm) can be conveying by Indoor and outdoor optical wireless communication systems and provide protocol linkages with cost-effective and high data rates [31, 32].

OWC systems are problematic because of their susceptibility to the obstacles and their restricted capacity for power transmission. So, the cohabitation of OWC and RF systems can provide a practical solution to the enormous needs of impending 5G and beyond communication systems. Fig. 2.1 shows the principle of OWC [33, 34].

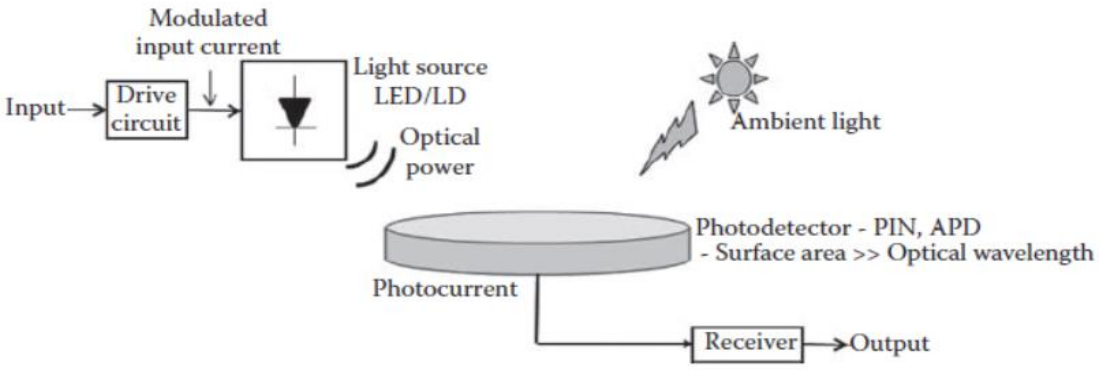

Figure 2.1 OWC system in a block diagram [40]

OWC system can be physically configured into four categories as shown in Fig. 2.2.

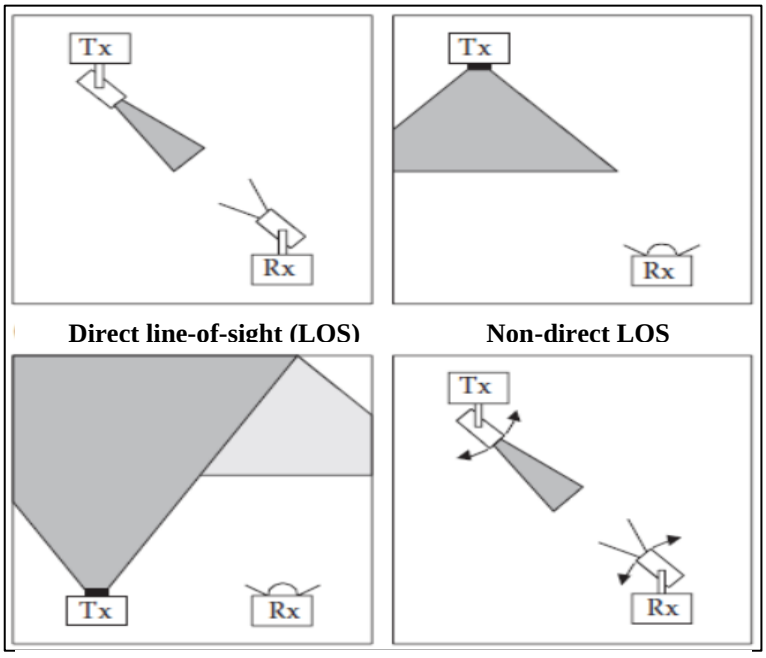

Figure 2.2 OWC physical configuration [40]

i. **Direct line-of-sight (LOS)** It is a point-to-point communication technique that offers more security and high data rate about hundreds of MHz and above (more than 100 Gbps with WDM). It is designed to maximize power efficiency and minimize multipath distortion-induced ISI. It can be applied for indoor

environments but is more suitable for outdoor applications with link lengths ranging from a few meters to 5km. The optical transmitters are characterized by low power consumption, a very narrow beam with a small terminal, minimal aperture size, and high-power flux density at the receiver (photodetector) with a large field of view (FOV) aperture. The data rate is limited in LOS links with free-space path loss than multipath dispersion and does not undergo multipath-induced signal distortion. The noise results from ambient light such as the sun and can be rejected by utilizing a receiver with a narrow field of view (FOV). LOS link has several demerits, such as small coverage area and roaming problems with indoor applications. LOS can't support mobile users due to alignment between the transmitter and receiver [35-37].

ii. **Non-direct LOS** It is point-to-multipoint communication that offers robustness and is suitable for indoor applications. It has the most flexible configuration and can achieve a broader coverage area to scatter from the surfaces within the room. The beam of the transmitters and the receiver field of view (FOV) are wide. For indoor IR systems, the multipath fading does not result due to the multipath propagation; the receiver detector size is larger than the wavelength, it increases the inter-symbol-interference (ISI) and limits the system data rate to a few Mbps. The receiver detected a high portion of light from different directions accruing high path loss and contending multipath-induced dispersion; furthermore, it requires higher transmitted power. The OWC connection cannot work in a high-light environment because it degrades link performance [41,42].

iii. **Diffused:** It is referred to as non-directional or non-LOS configuration and it is often used for LAN ad hoc networks where precise alignment or LOS

between the transmitter and receiver is not necessary. Although diffused OWC indoor configurations are adaptable and may be utilized for infrastructure and ad-hoc networks. They suffer from significant path loss, which ranges from 50 to 70 dB with a 5 m horizontal spacing and can be exacerbated by obstructions. However, a receiver with a wide field of view (FOV) to gather signals reflected from walls, ceilings, and other objects would increase system mobility but lowering data rates owing to multipath interface (ISI) problems [40, 41].

iv. **Tracked:** The tracked base station (transceiver) located at the ceiling and focused to the tracked receiver (mobile station), which is placed at the table top height, for this scenario less power is required for tracked than the diffused link. With a tracked link, the multipath interface ISI and ambient light interference are reduced due to the narrow-transmitted beam and tiny receiver FOV. It results in a higher data rate (about 1 Gbps) and greater power efficiency [35, 38].

2.3 Li-Fi Technology Principle

It is a bidirectional and high-speed OWC technology that utilized visible light waves instead of radio waves as a carrier to bear the data. Hence, it is also known as optical Wi-Fi [39, 40].

Li-Fi is a form of VLC (380-780nm) and a subset of OWC. Li-Fi utilized the light waves generated from LEDs or LDs on the visible light band to propagate through free space as a transmission medium to communicate. Li-Fi was invented to overcome the crisis of the RF spectrum with the revolution of IoT on the cusp of entering the fifth generation of wireless communication and beyond. As previously mentioned, if the Li-Fi system is applied for a short distance and in

closed places, it is called indoor Li-Fi; typically, LEDs are used. However, Free space optical communication (FSO), often known as an outdoor optical Li-Fi system, is a kind of free space optical communication. It is used when a Li-Fi signal spreads across a significant distance of unguided channel links such as atmosphere, air, and water [6, 44, 45].

The outdoor Li-Fi system has utilized LDs and provides a higher transmission speed. FSO is considered a viable technology due to its wide application for the next generations' communication. Therefore, this study focused on FSO communication in detail and showed this system's cons and pros. Furthermore, it presents a Li-Fi system suitable for outdoor applications [41-43].

2.3.1 Free-space optics (FSO)

It is a branch of OWC and forms a high-speed outdoor wireless communication system. FSO links for outdoor applications provide performance comparable to optical fiber along a route link ranging from a few hundred meters to a few kilometers. It allows high-speed transmission over various applications and is an excellent alternative to RF links [44].

FSO is a high-speed Line-of-Sight technology utilized light as a carrier to transmit information offering performance similar to optical fiber communication over a path link (hundred meters-kilometers). However, unlike today's internet backbone in which data travel through optical cables, the light propagates directly into free space, such as air, vacuum and outer space. As a result, it has several advantages, such as theoretically transmitting information at almost unlimited throughput and almost anywhere with a satellite, ship or airplane [35, 45].

Point-to-point FSO link utilizing the light produced by LEDs or LDs as optical carriers to bear the signal and propagate through free space. LEDs and LDs emit light in the range of visible and IR spectrum (380-1000nm).

The optical transmitter power of FSO systems is up to 100mW, and the receiver requires a sufficient power margin to deal with the attenuation induced due to atmospheric and meteorological conditions. Fig. 2.3 shows the basic principle of the FSO system. [7, 35, 45]

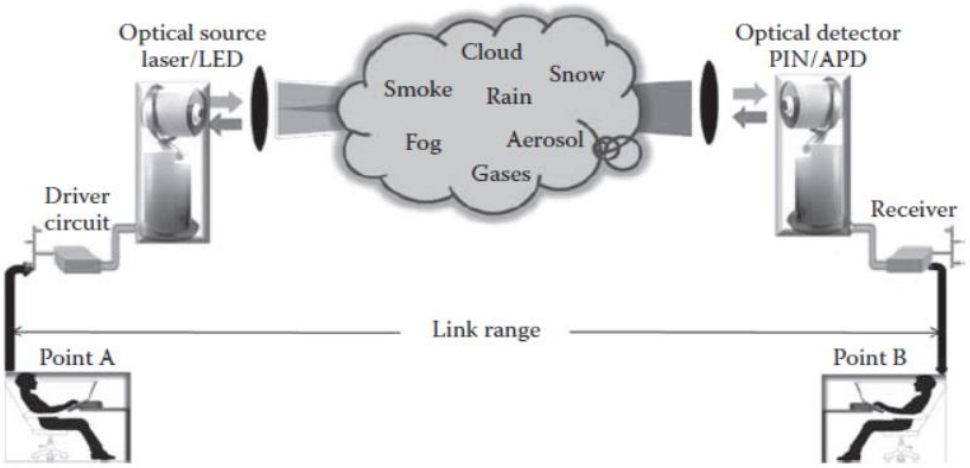

Figure 2.3 FSO communication link [40]

FSO communication system transmitted data modulated in optical carriers' phase, frequency, or intensity (LDs and LEDs). As illustrated in Fig. 2.4, it needs obstacle-free point-to-point communication between two identical transceivers at either end of the connection [7, 44].

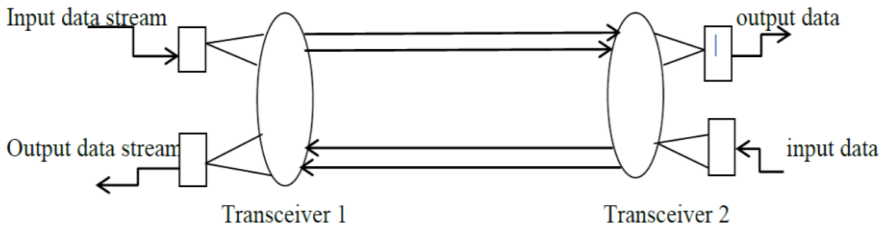

Figure 2.4 Typical point-to-point FSO setup [42]

FSO system can be used for: chip-to-chip communication, IR or VLC, inter-building communication, Free space laser communication like airborne, spaceborne and deep space missions, Ground satellite laser link (Bidirectional), Satellite to satellite cross-link, Up and down link between aircraft and platforms [6, 10, 49].

2.3.2 FSO merits

FSO communication link presented lower path attenuation and more immunity against interference compared to the millimeter waves (mm waves) and RF links due to the narrow beam between the transmitter and receiver, and it offers: Long transmission distance, High bit rate (several Gigabytes) for any transmission system, Immunity from interference with other electromagnetic devices, no health hazards, high secure technology with a low probability of interaction and detection (LPI/LPD), low BER, No Fresnel zone is necessary, Low maintenance, Absence of side lops, License free, and low cost [45-47].

2.3.3 FSO limitations

Despite all the benefits mentioned above, FSO is line-of-sight, so the link between the transmitter and receiver must be free of physical obstacles. There are several parameters affected by a transmitted signal through its propagation in free space and degrade the reliability and quality of the transmission, such as: pollution, shadowing, beam divergence, atmospheric turbulence, weather or meteorological conditions, interference with ambient light, pointing stability in wind [39,41,52]

2.4 Li-Fi communication system fundamentals

Outdoor Li-Fi communication systems can be classified into three stages, as shown in Fig. 2.5.

i. **Optical transmitters:** LDs are considered optical sources to radiate the light through the atmosphere and follow the Beer-Lamberts Law.

ii. **Free-space transmission channel**: Attenuation from weather conditions such as gases, aerosols, temperature and pressure variation (scintillation), cloud, rain, smoke, and fog.

iii. **Optical receiver:** It is used to process the received signal. Each stage will be explained in detail in the next sections.

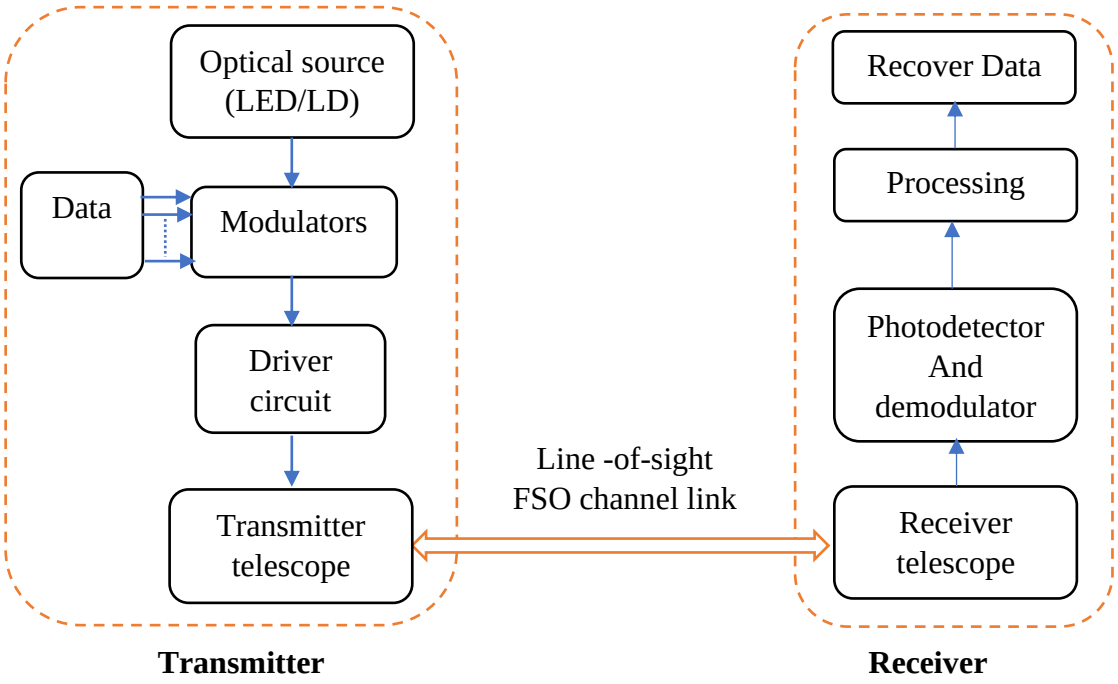

Figure 2.5 Outdoor Li-Fi communication system scheme

2.5 Optical transmitters

2.5.1. Light source operating windows

The light source utilized for Li-Fi systems emits light over various electromagnetic spectrum frequencies from VLC to IR. These wavelengths take a great interest in OWC. Fig. 1.1 shows the electromagnetic spectrum and the classification of windows for OWC [39,43]. The electromagnetic spectrum of OWC is categorized as:

i. **Visible light communication (VLC)** 400-700 nm is the visual range of the human eye. 495-570 nm (green part) used for underwater OWC due to low attenuation with this window.

ii. **IR Region:** used for OWC and outdoor point-to-point FSO channel link, it can be categorized into:

   a) **Near IR(IR-A)** (780 to 1400 nm): It is used in optical fiber and wireless communication. The band between 800-900 nm is commonly utilized for early optical fiber communication, while the band between 1260-1360 is utilized for long-haul optical fiber communication. Most commercial FSO systems operate at 750-850 nm

   b) **Short wavelength IR (IR-B)** (1400 - 3000 nm) 1530-1560 nm is used for long-distance optical fiber and FSO. The emitted optical power with wavelength band 1550 nm could reach up to 10mW for OWC link. The transmission in this band cannot hurt the delicate retina because it cannot get past the corneal filter.

   c) **Mid wavelength IR (IR-C)** from 3000 to 5000 nm.

   d) **Long wavelength IR (IR-D*)*** from 8000-15000 nm [40].

Some requirements are considered when designing a system, such as component availability, transmitted power, and the price. The most commercial outdoor Li-Fi

system or FSO communication systems operate near IR between 750-850 nm and 1520-1600 nm. 1520-1600 nm is more convenient for FSO systems due to many resources, such as much power that can be transmitted to overcome the atmospheric attenuation (aerosols), eye safety, and component availability despite being more expansive than the range 750-850nm [39-40].

The commercial FSO system operates in a window between 850-1550 (it's also used in optical fiber) with lower cost, while other available windows 300-500 nm and 800-1400 nm, but the availability of the component in this window are limited and more cost [41, 54].

The light sources for Li-Fi systems must have appropriate characteristics such as wavelength, linewidth, numerical aperture, high radiance with a small surface emitting area, high modulation bandwidth, great consistency, and long life. Several optical light sources can be used with Li-Fi systems, but the most common are incoherent optical sources-light emitting diode (LED) and coherent optical source-Laser diode (LD). The operation of both depends on the electronic excitation of semiconductor materials. Both offer small size, high brightness in the visible wavelength, emission property at the range of frequencies or single frequency, and low forward drive current and voltage [48-50].

2.5.2 Light sources

The most recent published studies employed LEDs for both functions as an optical source to transmit data and illumination at the transmitter for the communication systems due to the benefits of LEDs such as small size, small power consumption, long life, and low cost. However, it has some limitations, such as nonlinearity, low efficiency in electro-optic power conversion (usually 10–40%), limited carrier lifetime, and a high RC parasitic effect that limits modulation bandwidth to tens

of MHz's So, it is used for short link transmission up to kilometers, characterized by moderate data rate, so it is limited for indoor applications [50-52].

LEDs are required to emit the white light with a wavelength from 400 to 700nm. There are two prominent ways of producing white light from LEDs. First is the blue light emitted from LED with a yellow phosphor coating. This type is characterized by low modulation bandwidth due to low response and does not support complex modulation. The second is red, green, and blue LEDs chip are encapsulated to mix the lights and results in white light. This second kind can support sophisticated modulation and large data rates because of its rapid reaction speed, although it comes at a greater price [50, 52].

Micro-LED (μLED)/super luminescent-LED (SLED) is used to guarantee an increased bandwidth of about 1.5GHz but is limited by intrinsic carrier life. It is classified as high bandwidth optical source between LED and LD.[7, 26, 53].

Due to the highly directional beam profile of the laser diode LDs, it is preferred for long transmission distances and is suitable for outdoor applications. A special type of laser diode with phosphor coating (to emit white light) is also used in Li-Fi systems with a data rate of about a few Gbps called white laser or laser light. White LD has shown a good alternative to traditional LED owing to qualities such as a high data rate of Gbps, high modulation bandwidth of more than 10GHz, high electro-optic power conversion efficiency (30-70 %) and linear electrical to optical conversion characteristics [53-55].

LEDs/LDs have similar supplied power (10-50 mW) and produce light over a wide frequency range in electromagnetic spectrum from VLC to IR. Table 2.1 shows a brief compression between available light sources. This study focused on laser diode as an optical source with a coherent detection scheme [53, 54].

Table 2.1 Types of Li-Fi transmitters with their characteristics [31]

	LED	µLED	Laser diode	Laser Light
	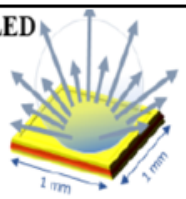	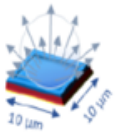	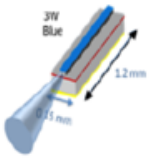	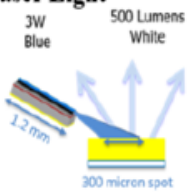
Area	0.1~1mm²	<0.01mm²	<0.2mm²	~0.01mm²
Limiting factor	$\tau_{RC}(\sim 1ns)$	$\tau_{carrier}(\sim 0.1ns)$	$\tau_{photon}(\sim 1ps)$	$\tau_{photon}(\sim 1ps)$
Bandwidth	~10MHz	<1.5GHz	10~20 GHz	10~20 GHz
Power$_{out}$	>1W	~µW	>1W	>1W
Eye safe	Yes	Yes	No	Yes

2.5.3 Laser diode LD

Light Amplification by Stimulated Emission of Radiation (LASER) is a technique where the incident photon makes the stimulated electron go down and emits a photon with the phase and frequency identical to the incident photon. Its light amplification is rarely used for this purpose. It emitted monochromatic light with a narrow band of 0.1-5nm. In laser, the conversion method is relatively efficient than LEDs. LED requires 150 mA of forwarding current to give out 1 mW power, whereas laser diode needs only 10 mA current is needed to radiate the same power. Table 2.2 shows a brief comparison between LED and LD performance [49, 50, 56].

Table 2.2 LED and LD comparison [40]

Characteristics	LED	LD
Optical output power	Low power	High power
Optical spectral width	25-100nm	0.01-5 nm
Modulation bandwidth	Tens of KHz to handers of MHz	Tens of KHz to tens of GHz
E/O conversion efficiency	10-20%	30-70%
Eye safety	Considered eye safe	Must be rendered eye safe
Directionality	Beam is border and spreading	Beam is directional and high collimated
Reliability	High	Moderate
Coherent	Noncoherent	Coherent
Temperature dependent	Little	Very
Drive and control circuitry	Simple to use and control	Threshold and temperature compensation circuitry
Cost	Low	Moderate to high
Harmonic distortion	High	Less
Receiving filter	Wide-increase noise floor	Narrow-low noise floor

Laser for communication is similar in concept to the optical fiber cable, but the difference is transmission channel media. Since the speed of light in air is quicker than glass and free license, FSO is classified as optical communication at the speed of light [54, 57]. Fig. 2.6 illustrate the laser beam propagation through free space.

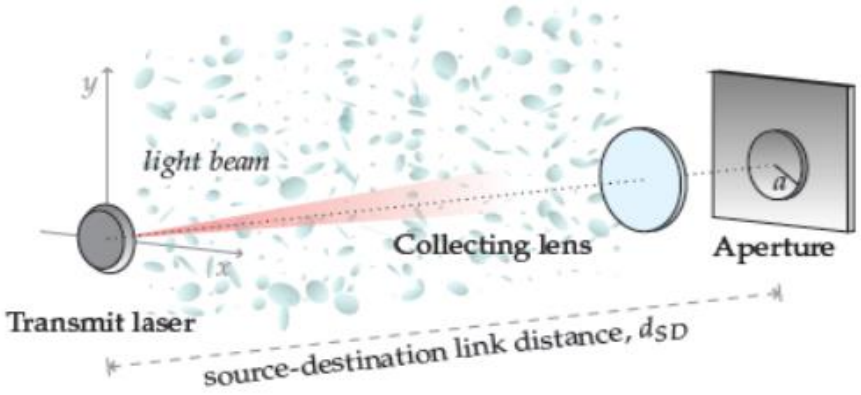

Figure 2.6 Laser beam propagation through the FSO link [54]

2.6 Optical modulation

There are two methods to convert the electrical signal to optical one, direct or external modulation.

i. Direct Modulation

Its known also non-coherent detection, only the intensity of the emitted light from LEDs or LDs is utilized to convey the data or information. There is no local oscillator LO at the receiver and the photodetector directly detects the variation of transmitted light intensity to convey the information. This method is called intensity modulation/direct detection IM/DD. That means the transmitter modulated the instantaneous power of the optical carrier to the electrical signal rather than amplitude, frequency or phase. However, the receiver utilized a photodetector for the down-converted technique in which the instantaneous power produced the electrical signal. This kind of detection is also recognized as envelope detection [40]. IM/DD scheme is the most commercial FSO system due to its simplicity for implementation and lower cost. It offers hundreds of Mb/s. The instantaneous photodetector current for a given incident power and can be written as:

$$i(t) = \frac{\eta_{eq}\, q\lambda}{hc}\, MP(t) \tag{2.1}$$

where *M* is the photodetector gain factor with a unity value for the PIN detector. η_{qe} is quantum efficiency and defines the ratio of electrons–hole pairs produced by a photodetector in a given time is termed the quantum efficiency η:

$$\eta_{eq} = \frac{Electrons\ out}{photons\ input} \tag{2.2}$$

$$\eta_{eq} = (1 - R)\xi(1 - e^{-\alpha d}) \tag{2.3}$$

where d is the distance at which optical power is absorbed, α is the absorption coefficient, electron-hole pair contribution to photocurrent is expressed as a ξ, and R is the reflection coefficient at the air-semiconductor interface. A photodetector's quantum efficiency is often used as a measure to describe it [35, 39]. This kind is unsuitable for data transfer speeds higher than 2.5 Gbps [58, 59]. Fig. 2.7 illustrates the principal scheme of IM/DD system.

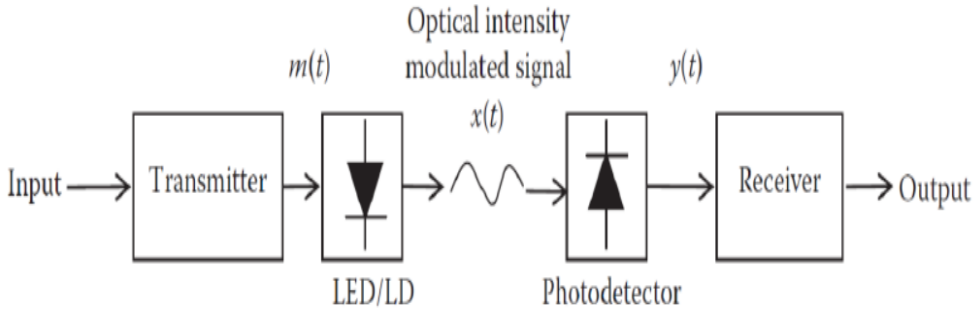

Figure 2.7 IM/DD communication [44]

ii. External modulation

External modulator uses electrical and optical signals at the same time. The optical power level of laser light, rather than the amplitude, fluctuates in response to the electrical signal. Hence, a stable signal amplitude emitted from the laser source improves the system performance in data rate due to the stability of the source

signal amplitude. As a result, external modulation can achieve 10 Gbps or greater [60]. Fig. 2.8 shows external modulation scheme.

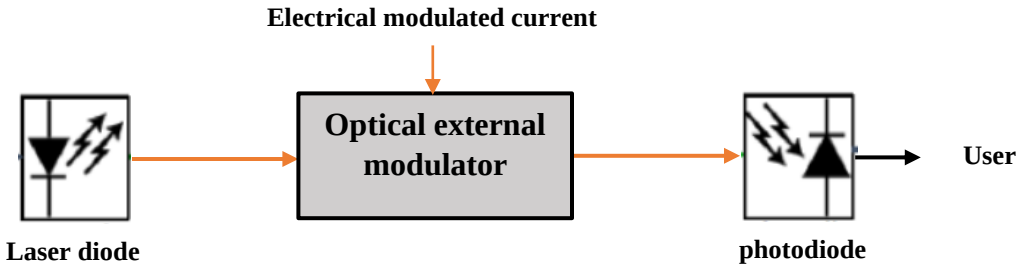

Figure 2.8 External modulation scheme [60]

Li-Fi has been employed to increase or maximize the transmission data rate. However, the suitable modulation scheme for Li-Fi system falls into:

i. **ON-OFF keying modulation (OOK)** This is a simple modulation technique which is represented ON (1) and OFF (0); where each symbol interval is represented through a light pulse. This type of modulation is characterized by low energy and spectral efficiency. Estimating the instantaneous coefficient of the channel fading is required to perform dynamic thresholding for optimal signal detection [3]. 5Gbps can be achieved with this modulation schemes and higher transmission with higher order modulation schemes.
ii. **Pulse position modulation (PPM)** This energy-efficient modulation approach does not need dynamic thresholding for the best signal detection. However, PPM suffers from ISI due to multipath propagation.
iii. **Pulse amplitude modulation (PAM**) Dispersive optical wireless channels' frequency selectivity causes ISI and nonlinear signal distortion at the front-end LED. Therefore, these three types of modulation are used for single-carrier modulation only [3, 9].

Due to meeting the needs for high-capacity transmission systems, two issues arise to raise the data rate beyond 100 Gbps per wavelength [10].

a) **Bandwidth expansion:** One way to increase the transmission system capacity is by increasing the bandwidth per wavelength optically or electrically. There are two techniques to increase the capacity in optical communication; the first technique is wavelength division multiplexing (WDM), in which several optical carriers are added to expand the bandwidth. The Other method is overcoming the bandwidth limitation of electrical components such as ADC/DAC by utilizing CMOS technology. For example, 6 GHz is only supported with ADC/DAC, and it is cost-effective to cross the barrier of 100Gbps.

b) **Enhancing spectral efficiency:** Spectral efficiency is the most important advantage of optical communication. The spectral efficiency of intensity modulation IM/DD systems and binary modulation do not go beyond 1 bits/s/Hz. Various innovative modulation schemes were invented to increase the capacity of the transmission system, such as signal amplitude, phase, and polarization. The advanced modulation schemes with coherent detection can be easily achieve several bits/s/Hz. Multi-carrier is more efficient in bandwidth but less energy efficient than single carrier modulation [3, 61].

One of the most common and effective multicarrier and advanced modulations is orthogonal frequency division multiplexing OFDM. OFDM greatly attracts direct detection and coherent modulation for long-haul transmission. Moreover, the coherent system with OFDM can achieve high spectral efficiency, high bandwidth, and simple channel and phase estimation [62, 63].

2.7 OFDM in Optical Communications

Typically, intensity modulation/direct detection IM/DD was employed to encode the intensity of the LEDs and LDs with a Li-Fi systems. To encode large data values, OFDM was implemented. OFDM is an efficient and popular technique for multiplexing/demultiplexing technology applied in wired and wireless systems permitting multiuser to transmit the information simultaneously and provide simplicity with flexibility. Although OFDM has been extensively studied in RF, it is recently applied in optical communications world. OFDM is a multicarrier modulation (MCM) in which the information is distributed among multiple carriers with lower data rates instead of a single carrier, so the spectrum is divided into many subcarriers. The modulation is performed in each carrier independently with a lower data rate beam [63, 64]. OFDM has several important advantages: 1) high speed and long-haul data transmission,2) Good solution for ISI, by moving the channel to multiple flat channels that effectively reduce the effect of channel dispersion, 3) great performance in a multipath fading channel, 4) high spectral efficiency, 5) facilities the estimation of the channel phase in the time domain. In contrast, OFDM has the following two disadvantages:1) great peak to average power ratio (PAPR) and 2) more sensitive to the phase noise and frequency offset [65-67].

The linearity of the transformation for the optical transmitter and optical receiver is the primary factor in the optical implantation of OFDM. The complex value of the electrical signal may be linearly up converted to the optical signal in one of two ways: first, by utilizing electrical OFDM, and second, by using an IQ mixer. The fundamental step in constructing OFDM is the multiple channels or subcarriers must be allowed to overlap with orthogonality constraints in OFDM

and this procedure can be accomplished by utilizing invers fast Fourier transform/fast Fourier transform (IFFT/FFT) [67, 68].

OFDM is divided into three groups depending on the IFFT/FFT implementation procedure. Electrical OFDM uses IFFT/FFT in the electrical domain, whereas All-optical-OFDM (AO-OFDM) uses FFT/IFFT in the optical domain and Optical-OFDM (O-OFDM) combine electrical processing with optical processing [64, 69]. Even though O-OFDM has many features, it restricted by the electrical components' symbol rate and bandwidth to implemented IFFT/FFT, such as analogue-to digital convertor/ digital-to analogue convertor (ADC/DAC), serial-to-parallel (S/P), and parallel-to-serial (P/S). While with AO-OFDM maximize the data flow and spectral efficiency through creating the orthogonality between the subcarriers in optical domain without required to these electrical component [70-72]. This study focused on AO-OFDM architecture; it will be explained in details in the following sections.

2.8 All-optical OFDM

IFFT/FFT is utilized completely in the optical domain to avoid large modulators bandwidth and high-speed DAC, significantly increasing the system data rate and spectral efficiency; the system is called AO-OFDM. AO-OFDM is employed where the OFDM transmitter has multiple optical subcarriers are produced. The optical IFFT/FFT (OIFFT/OFFT) circuits realized without electrical-to-optical converter/optical-to-electrical convertor (EOC/OEC) on the transmitter and receiver side. As a result, the integrated passive optical component in the OFFT/OIFFT circuit has the necessary temporal delays and phase shifts, it can be offered high speed and low power consumption [29, 70].

AO-OFDM employs optical delay lines and phase shifts to accomplish IFFT/FFT entirely in the optical domain [89] The forward and reverse FFT are considered as:

$$\varepsilon_m = \sum_{k=0}^{N-1} E_k \, e^{-i\frac{2\pi}{N}mk} \tag{2.4}$$

$$E_k = {}^{1}/_{N} \sum_{m=0}^{N-1} \varepsilon_k \, e^{i\frac{2\pi}{N}km} \tag{2.5}$$

Where E_k is the frequency domain samples and ε_m is the time domain samples, m and K is the position,$0 < m, k < N$, where N is total number of samples. While $tm{=}m\tau$ and $\omega k{=}k\delta$ represented the frequency and time position, respectively.

AO-OFDM system architecture can be implemented by different methods to form OIFFT/OFFT, such as fewer optical time lens, optical couplers, phase shift and coupler, Fiber Brag Grating, series of cascaded Mach-Zehnder interferometer, Wavelength selective switch WSS and Array wavelength grating AWG [13, 73].

This study implemented AO-OFDM signal-based OFCG and DWDM. The General block diagram of all-optical OFDM transverse for outdoor applications is shown in Fig. 2.9.

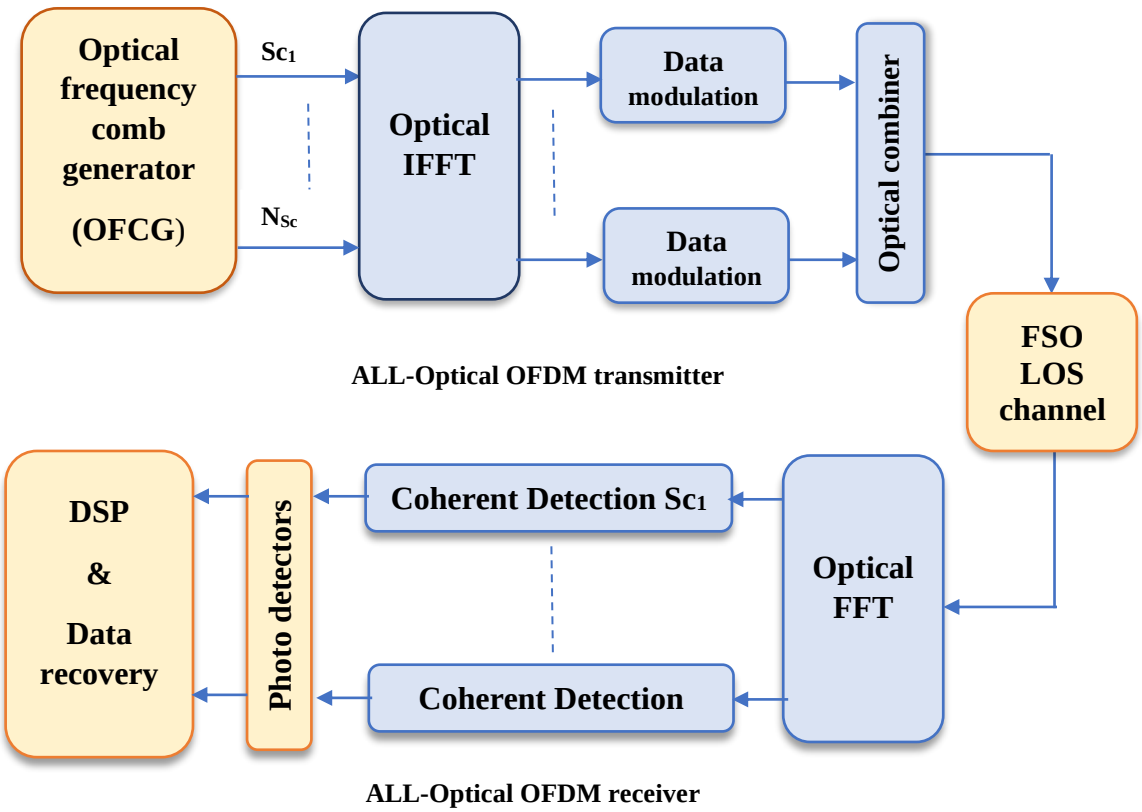

Figure 2.9 AO-OFDM system architecture

2.8.1 All-optical OFDM transmitter

AO-OFDM signal produces at the transmitter side through two stages:

i. Optical frequency comb generator OFCG

The optical subcarriers are already in the optical domain in AO-OFDM system rather than O-OFDM, the subcarrier frequencies are generated in the RF domain then upconverted in the optical domain. AO-OFDM signal is created directly in the optical domain by modulating many of optical subcarriers without needing electronic IFFT processing. The optical subcarriers can be generated through the OFCG[74].

OFCG is a vital component source for many applications based on multi-wavelength sources such as optical frequency measurement, OFDM , microwave photonic signal processing, optical arbitrary waveform generation and dense wavelength division multiplexing [74, 75]. OFCG is used in optical communication techniques such as dense wavelength division multiplexing (DWDM), optical orthogonal frequency division multiplexing (O-OFDM), and time division multiplexing (TDM). The basic principle of OFCG is to generate a set of optical signals or harmonics from a single optical source with maximum exploitation of the optical bandwidth, the spacing between these harmonics is tunable. Can benefit of OFCG by reducing the optical sources in the optical line terminal (OLT) side with providing broad bandwidth and high transmission data rate [76, 77].

The key characteristics of OFCG are equal frequency spacing between lines, optical spectrum flatness, the narrow linewidth of each comb line, low implementation cost and wide spectrum wavelength range [75, 78]. Many different techniques were presented by many studies over the last years each one has its merits and demerits, these techniques were categorized into two methods, electrical and optical, the electrical one was limited by the bandwidth of the electrical components while the optical method allowed broader bandwidth, therefore the optical method is the most prevalent in the researches nowadays [79, 80]. For the optical method, one technique to implementation OFCG by using mode-locked laser (MLL) such as in [81, 82], the mean disadvantages of this method are the stability and it’s hard to tunable the spacing between lines, because of the carrier frequency depending on the cavity of the laser diode due to the environments, for stable operation, it required a complicated feedback loop for stable operation [83, 84].

An optical frequency comb generated some narrowband optical lines from a single CW laser, as shown in Fig. 2.10, starting from CW emission frequency (f_0) and equidistantly spaced over frequency generated Δf [85, 86]. A laser light with frequency f_0 has amplitude A_0 and phase φ_0. The laser phase noise is moduled as a function of the probability density function.

$$f(\Delta\varphi) = \frac{1}{2\pi\sqrt{\Delta f dt}} \cdot e^{-\Delta\varphi^2 / 4\pi\Delta f dt} \tag{2.6}$$

Where $\Delta\varphi$ is the phase difference between two consecutive time instances and Δf is the line width of the laser diode, between two subsequent time is a Gaussian stochastic variable with zero mean and variance of $2\pi\Delta f$. The output of OFCG consists of a series of harmonic tones with the following components: $f_0 + n\Delta f$, where Δf is adjustable, and $n = [0,1,2,\dots.]$ is the number of the harmonics [103].

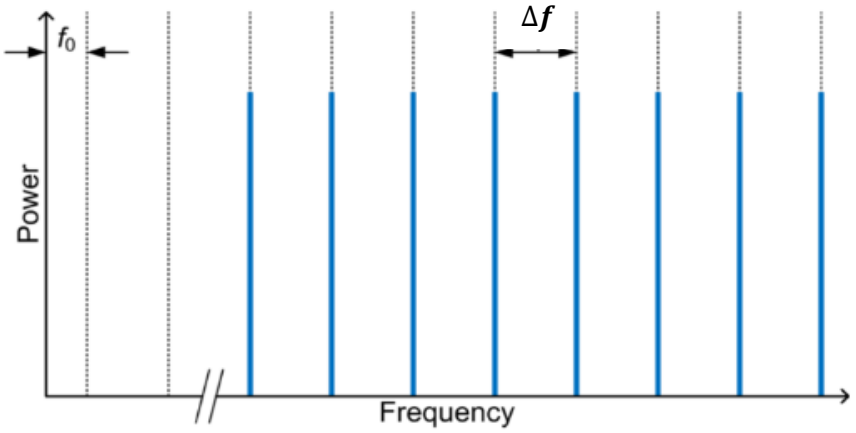

Figure 2.10 OFCG lines [86]

In the time domain, the OFCG lines correspond to a train of optical pulses. OFCG is necessary for AO-OFDM systems because different subcarriers must be produced from the same laser source to keep the orthogonality between the OFDM subcarriers [103, 104].

The frequency of the central line of the OFCG is equal to the frequency of the derived laser while line spacing frequency Δf is controlled by the used RF source. The frequencies of the OFCG lines (i.e., optical subcarriers) are governed by the following equation:

$$f_k = f_{CF} - (N_{sc}/2 - k)R_s \qquad \text{K=1,2,…}N_{sc} \qquad (2.7)$$

where f_k and f_{CF} are the frequency of the kth line and central line, respectively. Note that central line carriers the index $k = N_{sc}/2$; in this case $fN_{sc}/2 = f_{CF}$. The polarization state of the electrical field emitted from the laser is controlled to achieve a linearly polarized field with a 45° polarization angle. The state of polarization of each comb line is identical to that of the input laser. The 45° polarization angle ensures that each comb line can be resolved into two equal-power orthogonal polarization components, TE (or X) and TM (or Y). This is useful for the operation of DP-IQ optical modulators that will be used later to embed the data on the comb lines [103, 104].

ii. Optical IFFT

It is possible to get AO-OFDM by using inverse fast Fourier transform (IFFT) only in the optical domain and not with electrical parts. It transforms frequency domain info such as the amplitude and phase of the subcarriers for each AO-OFDM symbol into time domain. Fig. 2.11 illustrate the general schematic of OIFFT.

The basic principle of optical IFFT demultiplexing or splitting the OFCG subcarriers or lines to modulate each one individually as a single carrier (to decrease the modulation bandwidth) and then couple to create an AO-OFDM signal [87]. The key principle of performing the orthogonality between these subcarriers is that Boud rate of modulation subcarriers must be equal to the OFCG

spacing [88]. For the modulation process, the QAM scheme is taking place, in order to produce a kind of modulation capable of offering high levels of spectrum efficiency. The QAM modulation uses both the amplitude and phase components of optical signals. The QAM signal is formed by modulating and combining two carriers that are 90° out of phase (i.e., sine and cosine). They are in quadrature as a consequence of the 90° phase difference. One signal is often called the "I" or "in-phase" signal, while the other is called the "Q" or "quadrature" signal. The overall signal is made up of both the I carrier and the Q carrier, which both have changes in amplitude and phase. The I/Q modulator comprises two Mach-Zehnder modulators (MZM) and an upconverter for converting the complex OFDM signal (I/Q component) to the optical domain. As a result, we can be written the modulated signal as:

$$E(t) = x(t)\exp(j\omega_{LD1} + \emptyset_{LD1}) \tag{2.8}$$

Where $x(t)$ is the transmitted signal, ω is angular frequency, and $\emptyset$ the phase of the transmitter LD. After that, each modulated subcarrier is combined using an optical beam combiner device and all subcarriers ready to transmit through an optical channel [29, 89, 90]. The optical input field to the DP-IQ QAM modulator is given as:

$$E_{in}(t) = \sqrt{P_t}\, exp[j(2\pi f t)] \tag{2.9}$$

where P_t is the optical signal power and f is the optical frequency? If this field is linearly polarized with a 45-polarization angle, then each polarization modulator is pumped with $\sqrt{P_t/2}$ amplitude field.

The equations below show how these fields fed into the I-MZM and Q-MZM modulators:

$$E_{in-I(t)} = \sqrt{P_t/_4}\cos(2\pi f t) \tag{2.10}$$

$$E_{in-Q(t)} = \sqrt{P_t/_4}\sin(2\pi f t) \tag{2.11}$$

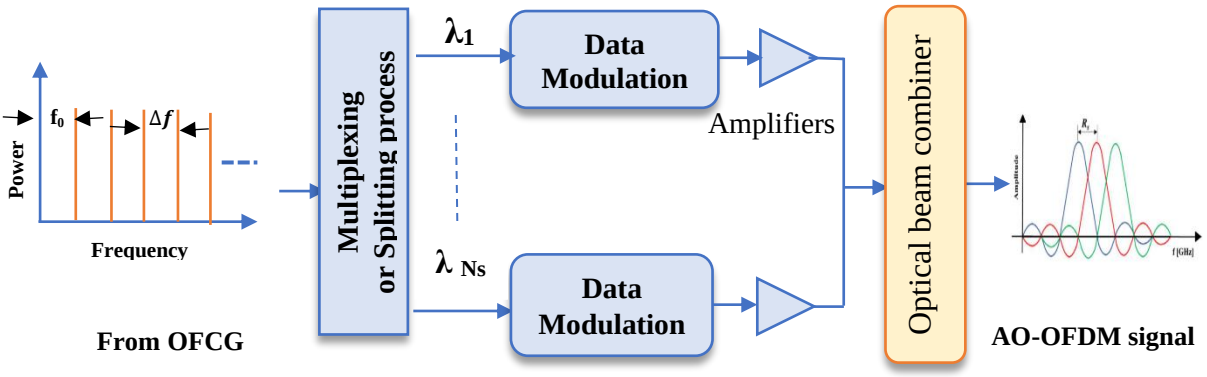

Figure 2.11 Optical IFFT

The spectrum of each AO-OFDM subcarrier S_B is a Sinc function with nulls overlapping with the centers of the other subcarriers. It gives the orthogonal feature of OFDM, assuming that each symbol interval is a square waveform S_B.

$$s_B(t) = \sum_{i=-\infty}^{\infty}\sum_{k=1}^{N_{sc}} c_{ki}.\exp\left(j2\pi f_{CF}.(t-iT_s)\right).rect\left(\frac{t}{T_s}-i-\frac{1}{2}\right) \tag{2.12}$$

$$s_B(t) = \sum_{k=1}^{Nsc} A_K.sinc(T_s.(f-f_{CF})) \tag{2.13}$$

$$A_k = \sum_{i=-\infty}^{\infty} c_{ki}\,T_s.\exp\left(-j2\pi i\,T_s.f\right) \tag{2.14}$$

where c_{ki} is complex data of ith signal symbol on the kth subcarrier, T_s is the symbol period, f_{CF} is the center frequency of the OFDM system, A_k is the initial amplitude of the kth subcarriers [29, 90].

AO-OFDM symbol of duration $T = 1/f_s$ can be expressed for a single polarization as:

$$s(t) = \sum_{k=0}^{N_s-1} X_K \, .rect(\frac{t}{T}). e^{-j2\pi f_k t} \quad (2.15)$$

where X_K is the kth complex symbol of a pseudo-random symbol sequence (PRSS), and$f_k = k/T$ (k=0, 1…, Ns-1) are subcarriers center frequencies [29].

2.8.2 All-optical OFDM receiver

After passing the signal through the FSO channel with different path lengths and attenuation, the signal at the receiver is denoted by:

$$E_{r(t)} = E(t) \otimes h_{(t)} + w(t) \quad (2.16)$$

Where $h_{(t)}$ and $w(t)$ are the channel impulse response and channel noise respectively. The received signal was subjected to a set of optical couplers and delayer to implement All-optical FFT before utilized to the coherent receiver.AO-OFDM receiver classified into four sub-stages:

i. Demultiplexing all optical OFDM

OFFT can be implemented in the optical domain by different techniques as explained in [29, 87, 88, 91-93], this study successes to implemented OFFT through utilizing a set of optical multi-mode interference (MMI) and optical delays, as shown in Fig 2.12. It's called OFFT and differs from the electronic implementation because the OFFT requires passive components with low power consumption compared with devices for electronic FFT [34].

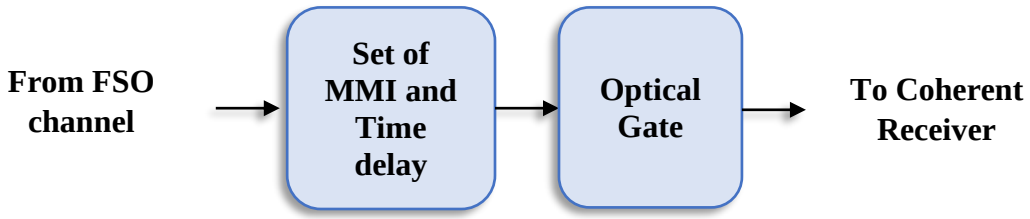

Figure 2.12 Optical FFT

MMI is a device that distributes optical power from one or several input ports among several output ports and is based on destructive/constructive interferences occurring in the MMI area with many guided modes. MMI have many potential applications such as couplers, splitters, combiners, mode converters, filters, etc. After an OFFT module which recover or separates the OFDM signal subcarriers, a bank of optical gates for the sampling process was performed, where the electrical signal controls the gate that switches the optical data signal. The sampling process can create the phase and amplitude information for AO-OFDM symbol. This process can be implemented after optical FFT or photodetectors without changing the overall operation. The optical sampling model is a more effective process than electrical or optical noise filtering. The photodetector must have a wide enough bandwidth to capture the tiny autocorrelation patterns [73, 93].

ii. Coherent detection

The received optical signal is mixed with a continuous laser CW wave of the local oscillator before being utilized in the photodetector. It offers better performance than IM/DD in terms of higher receiver sensitivity, background noise rejection, and mitigation of turbulence induced fading at the expense of implementation complexity. The information is modulated in the optical carrier's intensity, phase and polarization. This study focuses on coherent detection due to its benefit and offers high-speed communication networks with the simplicity of installing,

monitoring and maintenance [7, 69]. Fig. 2.13 shows the coherent detection scheme.

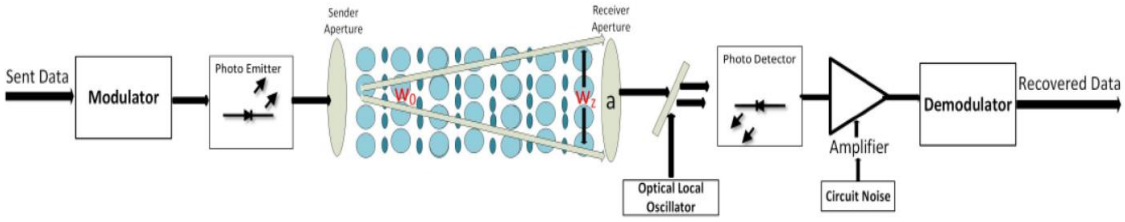

Figure 2.13 Coherent detection scheme [8]

Heterodyne and homodyne are two kinds of coherent detection based on whether or not the local oscillator's frequency is set near the optical signal frequency. The difference is only the phase or frequency of the local oscillator. The incident radiation is the same as the local oscillator frequency in the homodyne detection scheme, making the system expensive. The frequency of the local oscillator and incoming radiation does not match for heterodyne detection scheme. A new frequency is produced when the two signals are mixed, called intermediate frequency IF. The thermal and shot noise can be reduced with this scheme. Due to the drifting of an optical source over time, IF can be regularly observed and the local oscillator frequency is adopted according to the changes to maintain IF constant [9, 60].

The SNR sensitivity is the same for both types. Both require polarization diversity detector or polarization controller to align the state of polarization (SOPs) of local oscillator with received signal. To recover the in phase *I* and quadrature *Q* of the received signal in case of homodyne, it needs optical hybrid, which required twice as much optical component, on the other image rejection filter and twice as much photodetector bandwidth is required for heterodyne receiver. The sensitivity of the coherent detection receiver depends on the SOP of the incoming signal (the incoming signal polarization's commonly misaligned with SOP of LO) if there is

no polarization controller. To solve this problem, polarization diverse architecture can be employed [67].

For coherent detection; balanced detection is usually introduced into the coherent receiver as a means to suppress the dc component and maximize the beat between the signal and the LO. A balanced laser is used to restrain the direct current component and decrease the laser relative intensity noise RIN (power instability of the laser diode). A single balanced coherent receiver illustrated in Fig. 2.14, a 3dB optical coupler combines the received optical signal ($E_R(t)$) with the LO signal ($E_{LO}(t)$) and adds 180 phase shifts to either the optical signal or the LO field before dividing it into two equal portions and using it to drive two different photodetectors [67]. For the sake of simplicity, the received signal is assumed to be corrupted only by noise and not by channel dispersion.

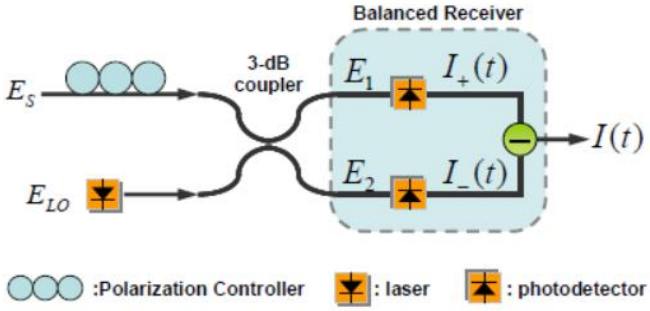

Figure 2.14 Balanced receiver [19]

The photocurrents of Balanced Coherent Detection Receiver are [31]:

$$I_1(t) = \frac{1}{2}\,\Re|E_1(t)|^2 \qquad (2.17)$$

$$I_2(t) = \frac{1}{2}\,\Re|E_2(t)|^2 \qquad (2.18)$$

where $\Re$ is the photodiode responsivity, $E_1(t)$ and $E_2(t)$ are the sum and the difference of the electric fields, respectively, given by as follows:

$$E_1(t) = \frac{1}{\sqrt{2}} [E_s(t) - jE_{LO}(t)] \quad (2.19)$$

$$E_2(t) = \frac{1}{\sqrt{2}} [-E_s(t) + jE_{LO}(t)] \quad (2.20)$$

For balanced quadrature coherent receiver, The Polarization beam splitter (PBS) receive the incoming signal after optical FFT to divide the incoming signal with arbitrary SOP into two orthogonal linear polarization components. It is fed into dual polarization coherent receiver (two homodyne I/Q receivers) for detecting both I and Q components for each polarization. DSP for Dual polarization coherent receiver is similar to the single carrier coherent receiver, which includes automatic frequency control, subcarrier separation, adaptive equalizer, carrier recovery, and data demodulation [10, 19].

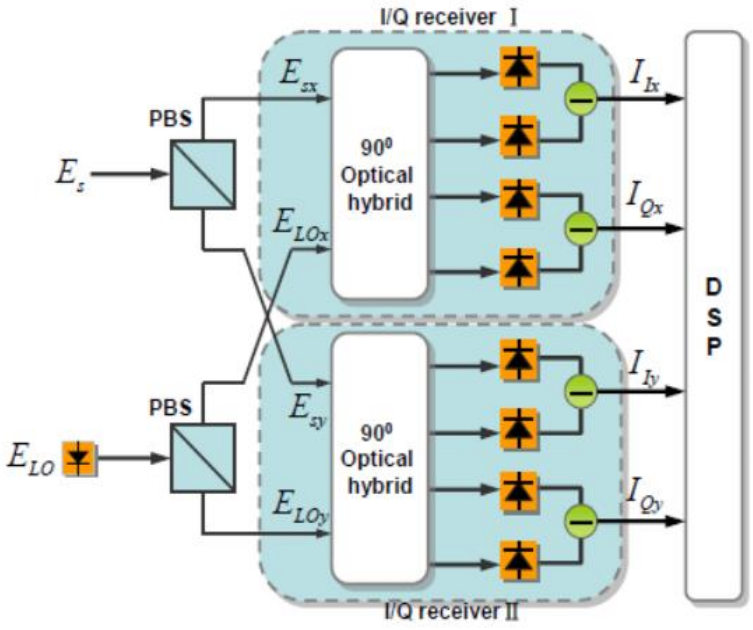

Figure 2.15 Configuration of a phase and polarization diversity receiver [19]

Fig 2.15 illustrates the schematic of phase and polarization diverse receiver. It can detect multiple signal polarization for the incoming optical signal. Two PBS, two 90^o optical hybrid components, and four balanced receivers are employed in

phase/polarization diversity coherent receivers to convert the optical signal into electrical and after that analogue to digital convertors. Internally, the 90° optical hybrid device produces an optical signal with a 90° phase shift using the optical signal from the local oscillator. In addition, optical pre-amplification technique may improve sensitivity in coherent detection. According to [31, 94], an analogous electrical field is generated by the two noise components (x,y):

$$n(x) = \left(n_{xl}(t)\cos(2\pi f_{LO}t) - n_{xQ}(t)\sin(2\pi f_{LO}t)\right) + \left(n_{yl}(t)\cos(2\pi f_{LO}t) - n_{yQ}(t)\sin(2\pi f_{LO}t)\right) \quad (2.21)$$

where $n_{xl}(t)$, $n_{xQ}(t)$ and $n_{yl}(t)$, $n_{yQ}(t)$ denote the in-phase and quadrature-phase noise components of the x polarization and y polarization, respectively. The outputs of the PBSs are:

$$E_{R,x}(t) = (I_x(t) + n_{xI}(t))\cos(2\pi f_{LO}t) - (Q_x(t) + n_{xQ}(t))\sin(2\pi f_{LO}t) \quad (2.22)$$

$$E_{R,y}(t) = (I_y(t) + n_{yI}(t))\cos(2\pi f_{LO}t) - (Q_y(t) + n_{yQ}(t))\sin(2\pi f_{LO}t) \quad (2.23)$$

where $I_x(t)$, $Q_x(t)$ and $I_y(t)$, $Q_y(t)$ represents the in-phase and quadrature-phase component of the incoming signal in the x polarization and y polarization, respectively.

$$E_{1,2} = \frac{1}{2}\left[E_{R,x}(t) \pm A_{lo,x}\cos\left(2\pi f_{LO}t - \theta_{lo}(t)\right]\right, \quad (2.24)$$

$$E_{3,4} = \frac{1}{2}\left[E_{R,x}(t) \pm A_{lo,x}\sin\left(2\pi f_{LO}t - \theta_{lo}(t)\right]\right, \quad (2.25)$$

$$E_{5,6} = \frac{1}{2}\left[E_{R,y}(t) \pm A_{lo,y}\cos\left(2\pi f_{LO}t - \theta_{lo}(t)\right]\right, \quad (2.26)$$

$$E_{7,8} = \frac{1}{2}\left[E_{R,y}(t) \pm A_{lo,y}\sin\left(2\pi f_{LO}t - \theta_{lo}(t)\right]\right \quad (2.27)$$

where $A_{lo,x}$ and $A_{lo,y}$ are the LO amplitude in the x-polarization and y polarization, respectively. $\theta_{lo}(t) = 2\pi\Delta f t + \theta$, and θ is a random phase shift. The balanced receivers' output current may be expressed as:

$$I_1 = \Re[\langle E_1^2\rangle - \langle E_2^2\rangle] \quad (2.28)$$

$$I_2 = \Re[\langle E_3^2\rangle - \langle E_4^2\rangle] \quad (2.29)$$

$$I_3 = \Re[\langle E_5^2\rangle - \langle E_6^2\rangle] \quad (2.30)$$

$$I_4 = \Re[\langle E_7^2\rangle - \langle E_8^2\rangle] \quad (2.31)$$

The following describes I_1:

$$I_1 = \Re|(E_1^2 - E_2^2)|$$

$$= \frac{\Re}{4}\Big[\langle\big[E_{R,x}(t) + A_{lo,x}\cos(2\pi f_{Lo}t - \theta_{lo}(t))\big]^2\rangle - \langle\big[E_{R,x}(t) - A_{lo,x}\cos(2\pi f_{Lo}t - \theta_{lo}(t))\big]^2\rangle\Big]$$

$$= \frac{\Re}{4}\Big[\langle\big[(I_x(t) + n_{xI} + A_{lo,x}\,cos\,(\theta_{lo}(t)))\cos(2\pi f_{LO}t) - (Q_x(t) + n_{xQ})\sin(2\pi f_{LO}t)\big]^2\rangle - \langle\Big[\big[(I_x(t) + n_{xI} - A_{lo,x}\cos(\theta_{lo}(t))\cos\,(2\pi f_{LO}t) - (Q_x(t) + n_{xQ}(t))\sin(2\pi f_{LO}t)\big]^2\Big]\rangle\Big] \quad (2.32)$$

I_1 can be expressed using the trigonometric equation:

$$I_1 = \big|\Re A_{lo,x}[I_x(t) + n_{xl}(t)]\cos\big(\theta_{lo}(t)\big) - \Re A_{lo,x}\big[Q_x(t) + n_{xQ}(t)\big]\sin\big(\theta_{lo}(t)\big)\big| \quad (2.33)$$

Similarly, I_2, I_3, and I_4 can be defined as:

$$I_2 = \Re A_{lo,x}[I_x(t) + n_{xl}(t)]\sin\big(\theta_{lo}(t)\big) - \Re A_{lo,x}\big[Q_x(t) + n_{xQ}(t)\big]\cos\big(\theta_{lo}(t)\big) \quad (2.34)$$

$$I_3 = \Re A_{lo,y}\left[I_y(t) + n_{yl}(t)\right]\cos\left(\theta_{lo}(t)\right) - \Re A_{lo,y}\left[Q_x(t) + n_{yQ}(t)\right]\sin\left(\theta_{lo}(t)\right) \quad (2.35)$$

$$I_4 = \Re A_{lo,y}\left[I_y(t) + n_{yl}(t)\right]\sin\left(\theta_{lo}(t)\right) - \Re A_{lo,y}\left[Q_x(t) + n_{yQ}(t)\right]\cos\left(\theta_{lo}(t)\right) \quad (2.36)$$

$\theta_{lo}(t) = 0$ represents the optimal case for homodyne phase/diversity receivers. After that, the currents of the balanced receiver are:

$$I_1 = \Re A_{lo,x}[I_x(t) + n_{xl}(t)], \quad (2.37)$$

$$I_2 = \Re A_{lo,x}\left[Q_x(t) + n_{xQ}(t)\right], \quad (2.38)$$

$$I_3 = \Re A_{lo,y}\left[I_y(t) + n_{yl}(t)\right], \quad (2.39)$$

$$I_4 = \Re A_{lo,y}\left[Q_y(t) + n_{yQ}(t)\right], \quad (2.40)$$

It depicts the optical preamplifier signal's divided I and Q components in the x and y polarizations.

As showed in [95], When the signal and LO are same polarization, the electrical fields $E_{1,2,3,4}$ incident on both upper and lower photodiodes are given by:

$$E_1 = \frac{1}{2}\left(E_R + E_{LO}\right) \quad (2.41)$$

$$E_2 = \frac{1}{2}\left(E_R - E_{LO}\right) \quad (2.42)$$

$$E_3 = \frac{1}{2}\left(E_R + jE_{LO}\right) \quad (2.43)$$

$$E_3 = \frac{1}{2}\left(E_R - jE_{LO}\right) \quad (2.44)$$

Output photocurrents from balanced photodiodes are given by [87]:

$$I_I(t) = I_{I1}(t) - I_{I2}(t) = \Re\sqrt{P_R P_{LO}}\, cos\{\theta_R(t) - \theta_{LO}(t)\} \quad (2.45)$$

$$I_Q(t) = I_{Q1}(t) - I_{Q2}(t) = \Re\sqrt{P_R P_{LO}}\, sin\,\{\theta_R(t) - \theta_{LO}(t)\} \quad (2.46)$$

2.9 FSO Channel Fundamental

For an outdoor Li-Fi system, the channel link is the atmosphere. The atmosphere is a dynamic and complex environment that affects optical beam propagation characteristics due to the atmospheric turbulence and metrological condition-induced phase and amplitude fluctuation. Atmospheric turbulence causes amplitude/phase fluctuations of optical signal due to random variation of the air refractive index along the path link. It causes a significant decline in the performance of the optical wave system. Furthermore, power loss of optical signals results from metrological conditions such as rain, haze, cloud, fog, smoke, and snow [3, 96, 97]. Fig. 2.16 shows FSO communication channel attenuation.

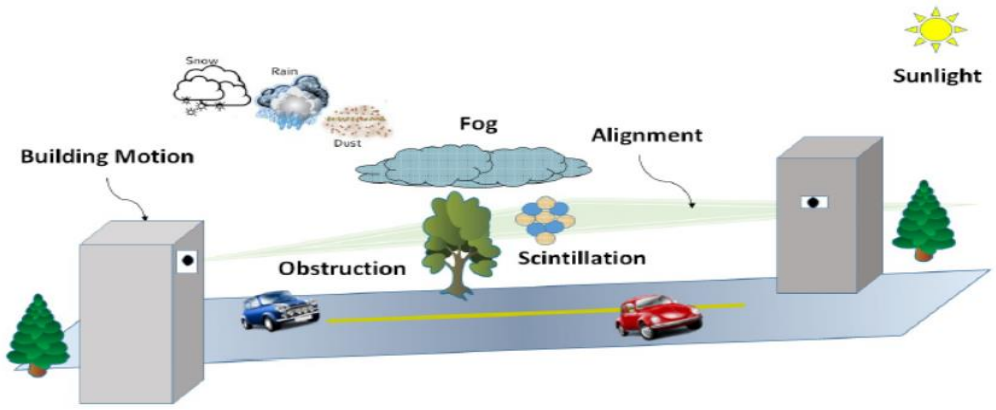

Figure 1.16 FSO communication channel attenuation [1].

During the transmission data of the FSO communication system, the transmitted power reduced gradually along the path due to the channel turbulence. To quantify the performance of FSO communication system, link margin or fade margin are vital factors which describe FSO link's performance. It describes the ability of a system to deliver sufficient optical power in the worst atmospheric condition. It must be positive and maximum for a reliable connection. Link margin can be calculated as:

$$M_{link} = P_e - S_r - A_{geo} - A_{atmo} - A_{scintillation} - A_{system} \quad (2.47)$$

P_e Total power emitted from the transmitter (dBm), S_r receiver sensitivity (dBm) (depend on system bandwidth or data rate), A_{geo} the geometric attenuation loss (dB), A_{atmo} losses resulting from absorption and scattering in the atmosphere (dB), $A_{scintillation}$ attenuation due to scintillation, A_{system} all other system losses [98, 99].

The primary atmospheric process causes influence of optical signal during the propagation, these influences include: Beam divergence or Geometric loss, Atmospheric attenuation (absorption and scattering), Weather conditions (rain, fog, haze…etc.), Atmospheric turbulence (index of refractive turbulence IRT, known scintillation).

2.9.1 Beam divergence or geometric loss

Optical radiation travelling through the atmosphere spreads out or diverges from its propagation path length because of diffraction. This phenomenon is known as beam divergence or geometric losses resulting in a portion of the transmitted beam not reaching the telescope receiver aperture[99, 100]. Fig. 2.17 explain the beam divergence phenomena.

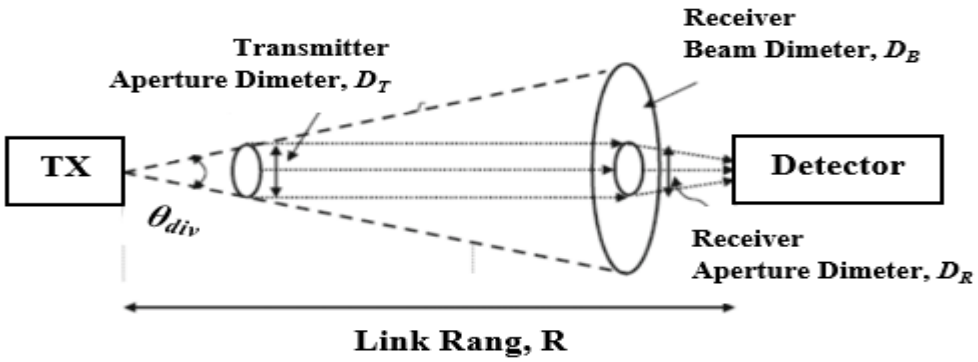

Figure 2.17 FSO geometric loses [101]

Geometric losses for FSO channel link are a fixed value that does not change with time depending on the following FSO components: Transmitter beam width, Divergence angle (θ), Path length (L), Transmitter and receiver aperture diameters.

In FSO, typically at 1km of propagation, the beam spreads about 1-5 m in dimeters. The received power formula:[101]

$$P_R = P_T \cdot G_T \cdot G_R \cdot L_P \tag{2.48}$$

Where P_R received power, P_T transmitter power, G_T effective gain of the transmitter, G_R effective gain of receiver, L_P free space path loss. The free space path loss can be defined as:

$$L_P = \left(\frac{\lambda}{4\pi \cdot R}\right)^2 \tag{2.49}$$

R is the path length. The gain of the transmitter and receiver telescope is:

$$G_t = \frac{4D_T}{\lambda^2} \quad , \quad G_r = \frac{\pi D_R}{\lambda^2} \tag{2.50}$$

Where: A effective optical telescope area, λ wavelength of the transmitter signal. The received power is:

$$P_R \approx P_T \left(\frac{D_T D_R}{\lambda\, R}\right)^2 \approx P_T \left(\frac{4}{\pi}\right)^2 \left(\frac{A_T A_R}{\lambda^2 R^2}\right) \tag{2.51}$$

The diffraction-limited beam divergence loss or geometric loss in dB is:

$$A_{geo} = -10\left[2log\left(\frac{4}{\pi}\right) + log\left(\frac{A_T A_R}{\lambda^2 R^2}\right)\right] \tag{2.52}$$

Adjusting the aperture of the receiver lens to match the divergence angle of the laser beam may help overcome or minimize beam divergence [102] . The divergence angle is inversely proportional to the beam divergence angle for the diffraction-limited case as:

$$\theta_{div} = \frac{\lambda}{D_T} \tag{2.53}$$

And beam sold angle Ω expressed as:

$$\Omega = \frac{\pi\,\theta^2}{4} \tag{2.54}$$

θ beam divergence angle (mrad), λ laser beam wavelength, $\mathcal{D}$ the aperture size. For a perfectly aligned transmitter and receiver, a narrow beam is preferred to reduce the pointing losses when the center of the beam doesn't directly face the receiver. For non-diffraction limited case: [100, 103]

$$\frac{P_R}{P_T} = \frac{D_R^2}{(D_T + \theta_{Div}\,R)^2} \tag{2.55}$$

And the beam divergence angle in dB:

$$A_{Geo} = -20\log\left[\frac{D_R}{(D_T + \theta_{Div}\,R)}\right] \tag{2.56}$$

The geometric attenuation can be expressed as:

$$A_{geo} = \frac{S_L}{S_{capture}} = \frac{\pi/_4 (L.\theta)^2}{S_{capture}} \tag{2.57}$$

S_L spot surface of emission beam at distance L, L Path length or distance between transmitter and receiver in km, θ beam divergence angle, $S_{capture}$ capture area of the receiver or detector (m^{-1})[100, 104]. Table 2.3 shows the relation between divergence, path length, and spot diameter.

Table 2.3 The relation between divergence, path length, and spot diameter [100]

Divergence	Range	Spot dimeter
0.5 mrad	1.0 Km	~0.5 m (~20 in)
2.0 mrad	1.0 Km	~2.0 m (~6.5 ft)
4.0 mrad	1.0 Km	~4.0 (~13.0 ft)

2.9.2 Atmosphere attenuation

The atmospheric channel is different from the conventional Gaussian-noise channel, which consists of tiny practical suspended in the atmosphere such as gases, molecules and aerosols. The optical beam through the FSO propagation suffers from absorption and scattering due to the atmosphere containing aerosols and gas molecules. In addition, the effect atmosphere channel is statistical due to its random nature[98, 105].

The attenuation due to these molecular and aerosols causing absorption and scattering of the received optical signal causing transmission power reduction due to the affection on mean value of the optical signal. On the other hand, distortion of the optical signal is caused by fluctuation of the atmospheric reflective index of the optical signal around the mean [46, 100, 106].

Beer-Lambert law (BLL) show behavior of optical field propagation as a function of path length (L) or distance. Beer Lamber's law covers the:

$$T(\lambda, L) = \frac{P_t}{P_r} = exp(-\gamma_t(\lambda)L) \tag{2.58}$$

$$A(dB/Km) = 10\ log_e\ [\gamma(\lambda)] \tag{2.59}$$

Where P_r, P_t are the received and transmitter optical power, respectively. L transmitter and the receiver gap (km), $\gamma_t(\lambda)$ is total attenuation or extinction coefficient (km^{-1}). It's also known as an optical depth which describes the amount of extinction due to absorption and scattering that occurs through the medium. γ is the wavelength of the optical source such as laser diode, depends on path integrated distortion along the LOS of the atmospheric constituents and is defined as $\gamma = -10\ log_{10}T = 4.43\tau_{od}$, τ_{od} of 0.7, the corresponding loss is 3dB.

The atmosphere contains molecular parts (gases) and causes attenuation. The absorption and scattering of the optical light caused by these particles, and it is a

complex casing power transmission loss process. Aerosols consist of tiny particles suspended in the sphere with various shapes, such as a sphere or irregular. Therefore, the atmosphere attenuation is stated as:

$$\gamma_t(\lambda) = \alpha_m(\lambda) + \alpha_a(\lambda) + \beta_m(\lambda) + \beta_a(\lambda) \quad (2.60)$$

Where α_m , α_a and β_m , $\beta_a$are the absorption and scattering coefficients of the molecular and aerosols, respectively [35, 100, 101].

2.9.2.1 Absorption

As mentioned earlier, the atmosphere contains various particles causing the signal beam's absorption along the transmitted signal's propagation path. The absorption particles are divided into molecules (due to gases) and aerosols (suspended particles) absorption. Due to these molecules' components and when these molecules' quantum states are exposed at greater energies, the tight photon is absorbed, causing the reduction in optical energy. Some extinguished photons turn their energy into kinetic energy or heat, resulting in a loss of power.

Atmospheric molecular characterized by its index reflection, the extinction coefficient (α) is an important quantity for absorption and scattering. The equation (2.48) connects the extinction coefficient (α) to the index of refraction's imaginary part (k):

$$\alpha = \frac{4\pi K}{\lambda} = \sigma\, N \quad (2.61)$$

Where σ is the extinction cross-section and *N* is the concentration of molecules. Atmosphere attenuation $\tau = exp(-\beta L)$, were

$$\beta = \beta_{abs}\, \beta_{scat} \quad (2.62)$$

$$\beta_{abs} = \alpha_{abs} N_{abs} \left[{}^{1}/_{Km}\right] \quad (2.63)$$

α_{abs}, effective absorption particle cross-section [km^2] and N_{abs}, absorption particle concentration [1/km^3][100].

The concentration and kind of gas molecules affect the absorption coefficients. The absorption strongly depends on the transmitter beam wavelength (λ), such as a wavelength below 200 nm absorbed or blocked by O_2 and O_3. The absorption appears due to water vapor near IR wavelength, and CO_n and NO_n absorb the light beam for higher wavelength. For FSO communication system, the laser source is selected in a window of transmittance between 600-1000 nm to avoid most absorption [40, 114, 120]. Fig. 2.18 explain the transmittance windows.

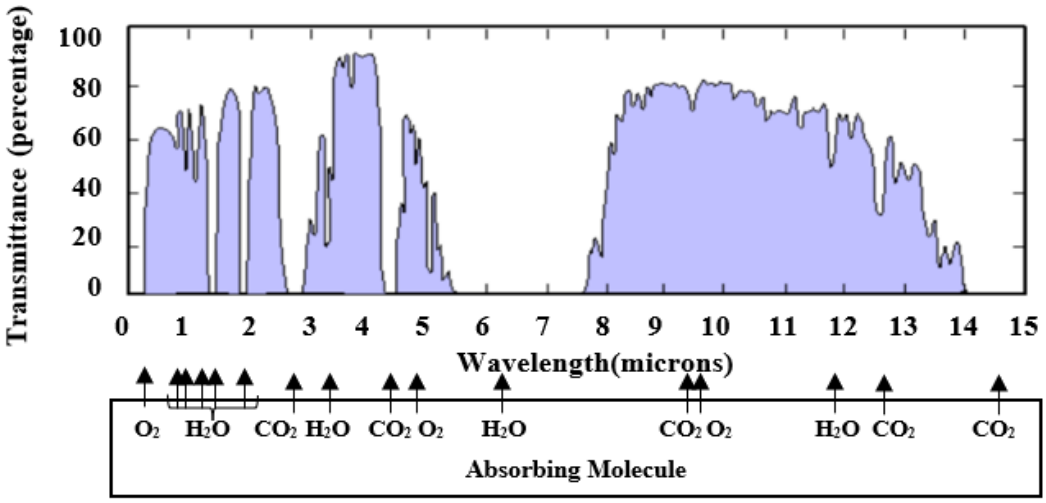

Figure 1.18 Transmittance of light through the atmosphere [107]

IR and visible transmission window represented a narrow absorption line. Therefore, the losses due to the atmospheric absorption for FSO communication can be reduced by adopting or choosing the range of transmitted wavelength within minimal absorption or low losses window, which is in the Visible and IR reign and the coefficients of the attenuation dominated by the scattering only as:[35, 100, 101]

$$\gamma_t(\lambda) \cong \beta_{al}(\lambda) \tag{2.64}$$

2.9.2.2 Scattering

The scattering causes redirection of the light energy along the straight-line path due to colliding the light with particles in the atmosphere. The atmospheric molecular interacts with photons and causes some of them to be extinguished. At the same time, particular constituents scatter the photons, the size of atmospheric distributions ranging from a few μm to 15 cm. Three types of light scattering can be classified based on the size of the existing particles in the atmosphere involving:[100, 105]

i. **Rayleigh scattering** for the small size of particles compared with the incident light wavelength (atmosphere molecules)

ii. **Mie scattering** by colliding particles comparable with the incident light wavelength.

iii. **On-selective scattering** by the large size of colliding particles compared with the incident light wavelength. Figure 2.19 shows the scattering types.

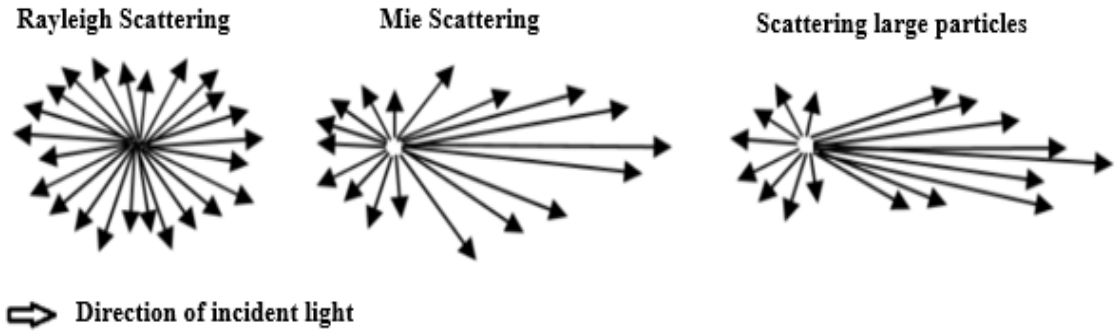

Figure 2.19 Atmosphere scattering types [100]

During the propagation, the scattering is affected by the radius of the encountered particles r_p to describe the characteristics of the size parameter x_0 as: $x_0 = 2\pi r_p/\lambda$, If $x_0 \ll 1$ Rayleigh scattering is processed, $x_0 \approx 1$ Mie scattering is processed, $x_0 \gg 1$ non-selective is processed.

The scattering coefficients may be computed from the particle concentration and effective cross-section.

$$\beta_{scat} = \alpha_{scat} N_{scat} [{}^{1}/_{Km}] \quad (2.65)$$

β_{scat} is either Rayleigh (molecular) β_m or Mie (aerosols) β_a scattering.

α_{scat} is a cross-section parameter [km^2], N_{scat} is a particle concentration [1/km^3].

The total scattering can be written as: [114]

$$\beta_{scat} = \beta_m + \beta_a [{}^{1}/_{Km}] \quad (2.66)$$

Table 2.4 explains how light is scattered by various scattering particles exist in the atmosphere.

Table 2.4 scattering process for various scattering particles [42]

Types of particles	Radius (μm)	Size parameters (X_O)	Scattering regime
Air molecules	0.0001	0.00074	Rayleigh
Haze particles	0.01-1	0.074-7.4	Rayleigh – Mie
Fog droplets	1-20	7.4-147.8	Mie- Geometric
Rain droplets	100-1000	740-7400	Geometric
Snow flakes	1000-5000	7400-37000	Geometric

i. Rayleigh scattering

Rayleigh scattering is the term used to describe scattering by molecules and atmospheric gases that are significantly smaller than the wavelength of the incoming light. The following expression gives the Rayleigh scattering coefficient:

$$\beta_m = \alpha_m N_m [{}^{1}/_{Km}] \quad (2.67)$$

α_m the Rayleigh scattering cross-section [km^2], N_m air molecules' number density [1/km^3]. Reflection cross-section of Rayleigh scattering depends on the incoming wavelength in an inverse manner:

$$\alpha_m = \frac{8\pi^3(n^2-1)^2}{3N^2\lambda^4}[Km^2] \quad (2.68)$$

Where: n the index of refraction, λ the incident light wavelength [m], *N* the volumetric density of the molecules [1 /km^3]. The simplified Rayleigh scattering equation is:

$$\beta_{Rayleigh}(\lambda) = 0.827 N_P A_P^3 \lambda^{-4} \quad (2.69)$$

N_P density (number) of particles per unit volume along the propagation distance, A_p represents the cross-sectional area of scattering, λ wavelength of incident light which is inversely proportional with scattering. It means more scattering with a shorter wavelength is responsible for sky blue color during the day. Since Rayleigh scattering predominates in the ultraviolet to visible range, it is negligible in the infrared waveband [101, 106].

ii. Mie scattering

Mie scattering is used for the size of particles diameter identical or 1/10th of incident wavelength. Mie scattering is the major reason for atmosphere attenuation in FSO and terrestrial altitude. Moreover, Mie scattering represents a complete analytic solution to Maxwell's equation for radiation scattering only adequate for spherical particles [45].

The transmitted optical beam in FSO is attenuated due to fog and haze, which makes the fog and haze the mean attenuator of optical power and irradiance. The attenuation reaches hundreds of dB/km. Mie scattering attenuation coefficients is:

$$\beta_a = \alpha_a N_a \left[{}^{1}/_{Km}\right] \quad (2.70)$$

α_a Mie scattering cross-section [km2], N_a the number (density) of air particles [1 /km^3]. It is challenging to foresee attenuation because the aerosol's composition, concentration, and distribution are spatially and temporally varying. In addition, the concentration of these particles is closely related to visibility.

The absorption by aerosol or fog particles is insignificant since their imaginary component of refractive indices is extremely low in this spectral range, and the diffusion by atmospheric molecules (Rayleigh scattering) is negligible.

$$\beta_{scat} = \beta_a \tag{2.71}$$

The atmospheric attenuation τ is expressed as:

$$\tau = exp(-\beta_a L) \tag{2.72}$$

The atmospheric attenuation (τ) in dB is given as:

$$\tau = 4.3429\, \beta_a L \ \ [dB] \tag{2.73}$$

The atmosphere factors which cause absorption and scattering of optical signal beam are predictable (weather conditions) such as fog, rain, snow, and sand, explained in next section [115, 114].

2.9.3 Weather condition

The weather condition is another FSO channel attenuation which affects the transmitted light beam, such as fog, rain, haze and other forms of participation [104, 108]

i. Fog Attenuation

The most harmful atmospheric factor is foggy and can sometimes make the link useless. The fog attenuation is classified based on light, moderate, and thick fog density. The system performance can be improved for light fog by increasing the transmitted power while can be used multi-hop link for thick fog conditions. For example, with light fog, BER reaches 10e-3 for a path length of 1km.

Visibility is an easily obtainable parameter and is used to measure attenuation. A basic rule known as the Koschmieder low is used to gauge fog density depending on visibility. Koschmieder low[108, 109].

$$\beta_\lambda = \frac{10\ log_{10} T_{th}}{V(Km)} \left(\frac{\lambda}{\lambda_0}\right)^{-q} (dB/Km) \tag{2.74}$$

The optical attenuation due to fog can be written with T_{th} 5% as:

$$\beta_\lambda = \frac{13}{V} \left(\frac{\lambda}{550}\right)^{-q} (dB/Km) \tag{2.75}$$

β_λ atmosphere attenuation coefficient, T_{th} transmittance threshold level, T_{th} level mostly used values of 2 and 5%, λ transmitted signal wavelength λ_0 the reference visibility 550 nm, q size distributed of scattered particles (distribution coefficient)[105, 110]. The attenuation due to fog and haze conditions can by calculated by:

$$A_{fog} = \exp(-\alpha_{fog} L) \tag{2.76}$$

$$\alpha_{fog} = \frac{3.91}{V} \left(\frac{\lambda}{550}\right)^{-q} \tag{2.77}$$

$$A_{fog}(dB/Km) = 10\ log_e\ [\alpha_{fog}] \tag{2.78}$$

For calculating the attenuation of optical signal due to fog scattering, there are two most common models Kim model and Kruse Model to describe the factor (q). For Kim model:

$$q = \begin{cases} 1.6 & if\ v > 50Km \\ 1.3 & if\ 6Km < v < 50Km \\ 0.1v + 0.34 & if\ 1Km < v < 6Km \\ v - 0.5 & if\ 0.5Km < v < 1Km \\ 0 & if\ v < 0.5Km \end{cases} \tag{2.79}$$

For Kruse model :

$$q = \begin{cases} 1.6 & if\ v > 50Km \\ 1.3 & if 6Km < v < 50Km \\ 0.585v^{1/3} & if\ v < 6Km \end{cases} \quad (2.80)$$

This equation suggests that there is less attenuation at higher wavelengths. However, Kim model shows no wavelength dependent on attenuation with visibility of less than 500m. Therefore, the impact of Mie scattering cannot be removed by selecting or modifying the transmitted wavelength since the transmitted wavelength is insensitive to the wavelength at poor visibility. Fog and haze attenuation strongly depends on the propagation wavelength, with lower attenuation and a larger wavelength [98, 100, 109].

ii. Rain attenuation

The attenuation due to the rain and snow is relatively low than fog attenuation and its wavelength independent. This attenuation increases with rainfall or snowfall rate. The rain scattering coefficient of the rainfall depends on the size of the raindrop. This size (100-1000 μm) is significantly greater than the optical signal. Therefore, the laser beam can pass through the raindrop particle with less scattering [98, 108].

The rain attenuation depends on the precipitation intensity (R) in (mm/hr). Therefore, as the raindrop rate increases, the raindrop size also increases.

The attenuation of rain can find by:[98, 101]

$$\alpha_{rain} = 1.076 * R^{2/3} \quad (2.81)$$

The losses due to rain and snow are:

$$\delta_{rain} = \frac{2.9}{V} \quad (2.82)$$

$$\delta_{Snow} = 20\ \delta_{rain} \quad (2.83)$$

$$A_{rain} = \exp(\beta_{rain\,scat} L) \quad (2.84)$$

2.9.4 Atmospheric turbulence

Atmospheric turbulence is another factor that must be considered in the FSO communication systems, even with clear weather. There is a temporal and spatial random variation of the atmosphere's refractive index along the course of an optical beam travelling through the atmosphere due to the inhomogeneity of the atmosphere in terms of temperature and pressure. Inhomogeneity of the atmosphere results from the formation of eddies or discrete cell (cells having size 0.1-10cm) that acts as refractive prisms with various size and indices of refraction [3, 101, 106]. Fig. 2.20 illustrates the atmospheric turbulence due to eddies and their affection for the transmitted signal.

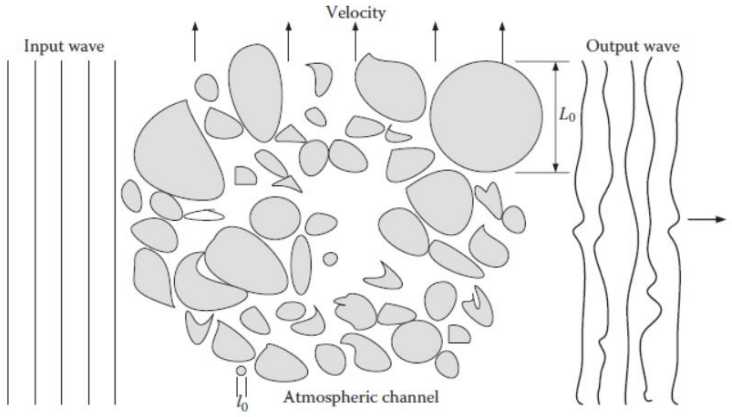

Figure 2.20 Atmospheric channel with turbulent eddies [41]

The interaction between the turbulence medium and the transmitted laser beam causes random variation in laser beam phase and amplitude. The refractive index at any point (r) in space can be written as:

$$n(r) \cong 1 + 79 \times 10^{-6} \left(\frac{P}{T}\right) \quad (2.85)$$

P atmosphere pressure in mbar, T temperature in Kelvin K.

Here, the molecules or aerosols' ability to absorb or scatter light is not taken into account. The temperature structure function for refractive index, $D_T(r)$ is typically measured by utilized a pair of sensors with a small distance separation between them. The temperature structure function can be expressed as:

$$D_T(r) = \langle [T(x) - T(x+r)]^2 \rangle \tag{2.86}$$

T is absolute temperature, $\langle . \rangle$ temporal average, r gap between two sensors.

For homogeneous and isotropic conditions, where inertial convective turbulence is present. Kolmogorov represent the function of the temperature structure as follows:

$$D_T(r) = C_T^2 r^{2/3} \qquad l_0 \ll r \ll L_0 \tag{2.87}$$

l_0, L_0 are represent the inner and outer scale of the turbulence, C_T^2 temperature fluctuation structure constant. On the propagation route, it is measured by calculating the mean square temperature between two places separated by a specific distance ($Deg^2/m^{2/3}$) [101, 109, 111]. The effect of atmospheric turbulence caused:

a) ***Beam wander:*** The beam is deflected due to large-scale turbulence causing random changes in the reflection index. If the received aperture diameter is greater than the Fresnel zone $(L/K)^{0.5}$, where k is optical wave number $k = 2\pi/\lambda$. The deflection effect due to beam wanders is assumed to be insignificant. The radial variation caused by the beam wander is:

$$\sigma_r = 1.83\, C_n^2 \lambda^{-1/6} L^{17/6} \tag{2.88}$$

σ_r is the radial variance, L is traveling beam distance.

C_n^2 is a turbulence strength ($m^{-2/3}$), an important parameter to measure fluctuation strength in the refractive index called refractive index structure constant. It is

considered the most critical factor along the propagation path characterizing atmospheric turbulence's effect. C_n^2 depicts the atmosphere turbulence, it depends on various vectors such as altitude, wind, geometrical location and the time of day. Higher altitude, lower turbulence and smaller value of C_n^2 due to colder and less dense air gas. C_n^2 ranging between 10^{-12} $m^{-2/3}$ and 10^{-17} $m^{-2/3}$. Typically, strong turbulence is 10^{-12} $m^{-2/3}$ or larger, and weak turbulence is $10^{-17} m^{-2/3}$, as shown as follows:

$$C_n^2 = \begin{Bmatrix} 10^{-17} & weak\ turbulance \\ 10^{-15} & moderate\ turublence \\ 10^{-12} & stronge\ trubulance \end{Bmatrix} \quad (2.89)$$

C_n^2 can be written using Gladstone's law:

$$C_n^2 \cong \left[79 \times 10^{-6} \frac{P}{T^2}\right]^2 C_T^2 \quad (2.90)$$

Less beam wander for longer wavelengths compared with shorter ones[101, 111].

b) ***Beam divergence:*** adding divergence into the transmitted optical beam. Due to diffraction theory alone, the turbulence-induced beam spreads. The laser in practical has Gaussian's form intensity profile, and over long path length L the beam waist w_b was expanded and can give by:

$$w_b^2 = \left(\frac{4L^2}{k^2 w_0^2}\right) + 3.58\, C_n^2\, L^3\, w_0^{-1/3} \quad (2.91)$$

w_0 is the beam waist at the transmitter aperture [106].

c) **Scintillation:** It is the most noticeable effect in FSO communication. It causes intensity fluctuation to the traveling beam even with small propagation path length (fading the received optical signal), degrading the overall system performance. In addition, scintillation is caused due to small variations in the temperature creating fluctuation in the refractive index. As

the propagation beam passes through the fluctuation, it focuses and defocuses, creating destructive and constructive interference with different parts of the light wave, causing spatial coherence losses [112, 113]. Fig. 2.21 shows the Scintillation affection.

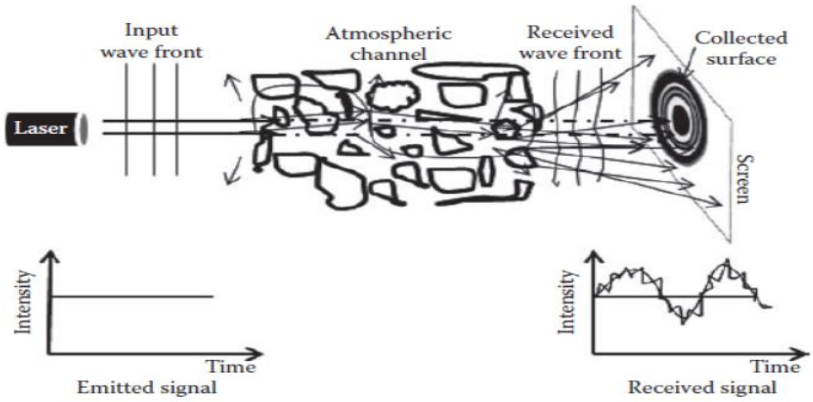

Figure 2.21 The affection of scintillation [35]

σ_i^2 represents the scintillation index and defines the intensity fluctuation as its normalized variance. It can be written as:

$$\sigma_i^2 = \frac{\langle (I - \langle I \rangle)^2 \rangle}{\langle I \rangle^2} = \frac{\langle I^2 \rangle}{\langle I \rangle^2} - 1 \tag{2.92}$$

I =|E|^2 is the intensity or signal irradiance.

The Scintillation effect for small fluctuation follows log-normal distribution characterized by the variance σ_i^2 given by:

$$\sigma_i^2 = 1.23\, C_n^2\, k^{\frac{7}{6}}\, L^{\frac{11}{6}} \tag{2.93}$$

$k = 2\pi/\lambda$ is the wave number, longer wavelength experience smaller variance, the Scintillation effect for large fluctuation:

$$\sigma_{high}^2 = 1 + 0.86\left(\sigma_i^2\right)^{-2/5} \tag{2.94}$$

Shorter wavelengths experience smaller variance. Therefore, the Scintillation effect can be mitigated or neglected by utilizing aperture averaging (large receiver area). The averaging aperture factor is the ratio of intensity variation of fluctuation of a receiver with diameter (D) to appoint receiver. This factor tails off beyond a certain receiver size for a given degree or range of turbulence [100, 106], as Fig. 2.23 shows.

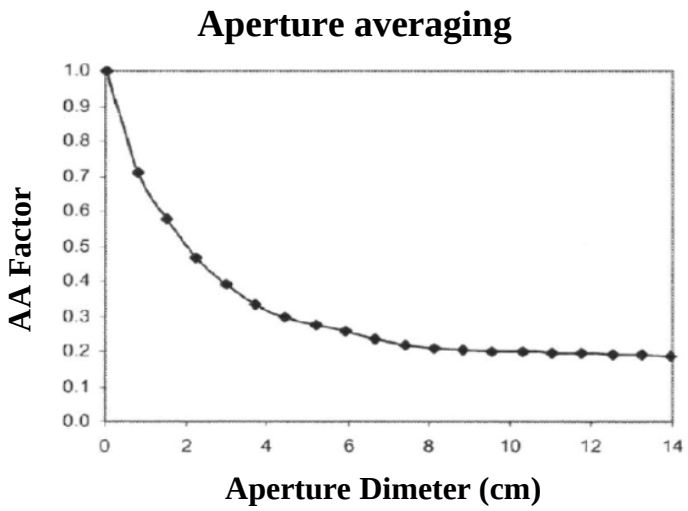

Figure 2.22 Aperture averaging factor vs receiver diameter [106]

The atmosphere attenuation due to turbulence or scintillation (dB/km) can be expressed by Rytov formula:

$$\sigma_{turb} = 2 \times \sqrt{23.17 \times k^{7/6} \times C_n^2 \times L^{11/6}} \qquad (2.95)$$

The fundamental determinant of C_n^2 is temperature; greater optical wavelengths result in increased scintillation. It may be possible to reduce or minimize the effect of turbulence through diversifying propagation routes, such as employing wider aperture receivers, and MIMO approaches. Finally, turbulence is a random phenomenon, and there is no way to know the FSO scintillation signal amount at any moment [98, 113].

2.10 The mitigation techniques of Atmosphere conditions

Different techniques for mitigation of the effect of weather conditions and atmospheric turbulence have been presented by researchers for several years to improve FSO communication systems in terms of BER [114-116], such as: Diversity techniques, aperture averaging, forward error correction, different modulation and coding techniques, etc. Table 2.5 provides an overview of various methods.

Table 2.5 summary of FSO attenuation and mitigation process

Sr. No.	Weather condition	Effects	Mitigation techniques
1	Aerosols, smoke and gases etc.	Scattering of the light (Mie/Rayleigh scattering)	• increase transmitter power • Different diversity techniques
2	Rain, snowfall, haze, etc.	Photon absorption	• Increase transmitted power
3	Fog (Thin fog, Tick fog)	Scattering of light	• Use longer wavelength laser • Hybrid FSO/RF • Increase transmitted power
4	Atmosphere turbulence	Irradiance fluctuation, phase fluctuation, beam spreading, beam broadening	• Diversity techniques • Different modulation and coding techniques. • Forward error correction

Chapter Three

Suggested Li-Fi system design and simulation

Chapter Three

Suggested Li-Fi system design and simulation

3.1 Introduction

The information presented in the previous two chapters has been used as a foundation to design an outdoor high-speed Li-Fi system based on AO-OFDM under different weather conditions and atmospheric turbulence. This chapter presents the proposed Li-Fi system-based AO-OFDM in detail. The system was simulated through VPI photonic design suite 9.8 and analyzed in terms of BER, constellation diagram, and received power with different FSO path links from 1 to 10 km and under different free space turbulence and weather conditions.

3.2 Proposed system design

Figure (3.1) depicts the proposed Li-Fi system, which is divided into three stages:

First: **All-Optical OFDM Transmitter**, this part receives digital data (zeros and ones) from eight or sixteen channels and transmits it through orthogonal subcarriers to the induced AO-OFDM signal. This scenario is implemented as follows:

- **i.** OFCG-based single CW laser diode.
- **ii.** Optical IFFT accomplished IFFT entirely in the optical domain using DWDM, dual polarization IQ modulation, and optical beam combiner.

Second: **FSO channel link** with different atmosphere attenuation.

Third: **All-Optical Receiver** recovers and processes the received signal through Optical FFT, sampling process, coherent receiver with dual polarization IQ

demodulators and DSP for signal recovery. Fig. 3.1 shows the proposed system for Li-Fi-based AO-OFDM. The following sections go into more detail about each stage. Fig. 3.2 and Fig. 3.3 are described in an abbreviated way the proposed system as a flowchart for transmitter and receiver respectively.

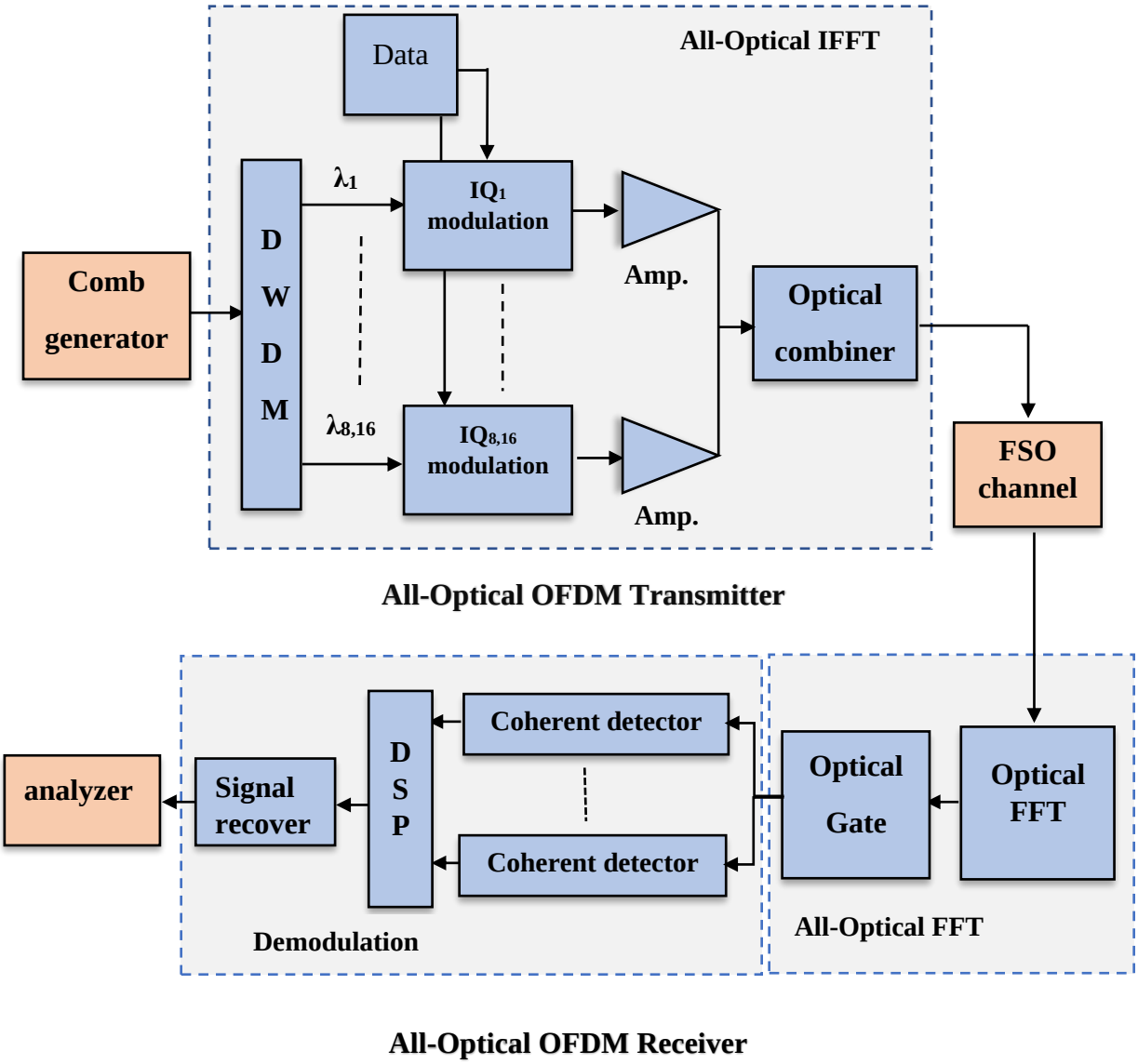

Figure 3.1 The proposed Li-Fi system-based AO-OFDM

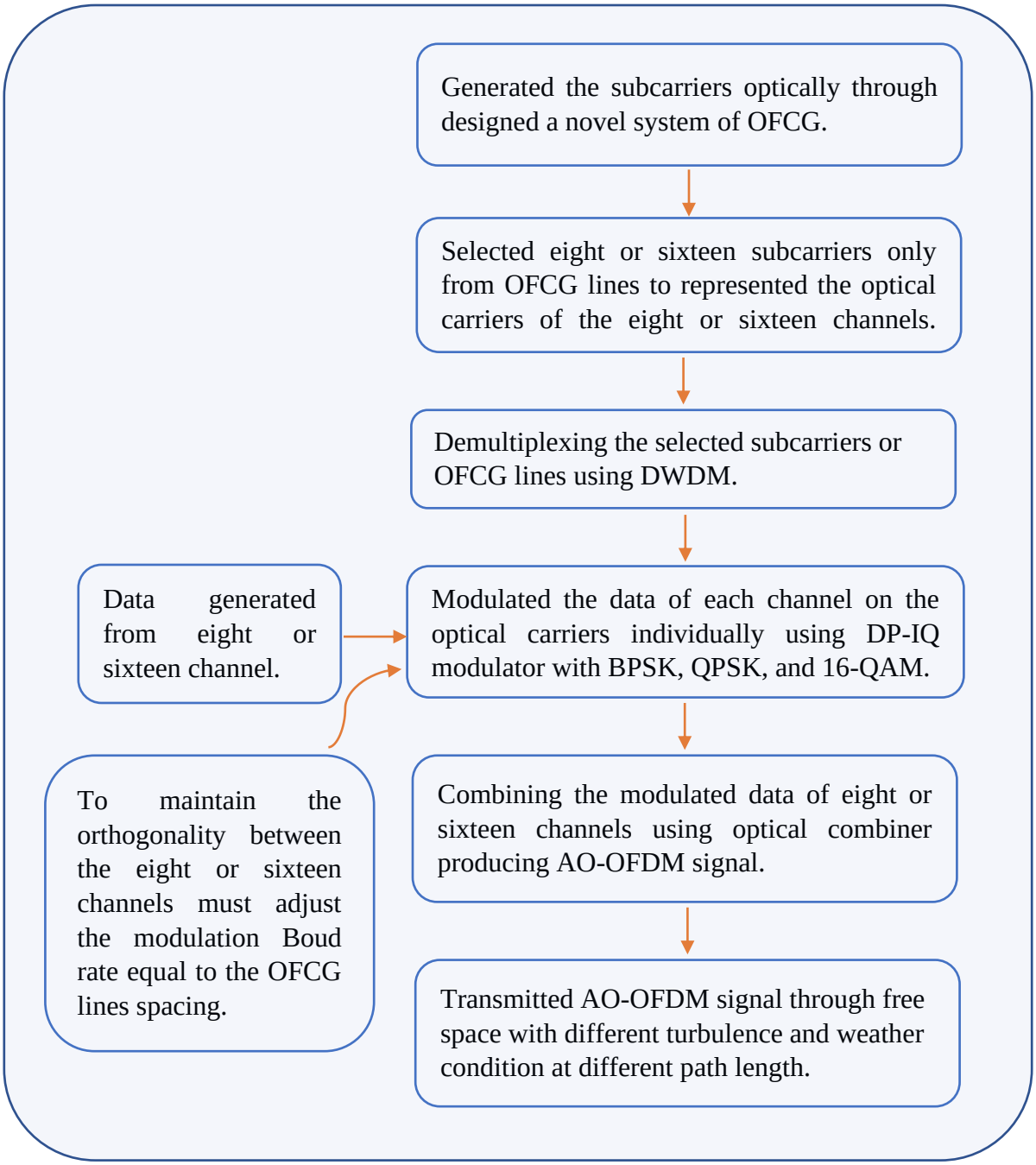

Figure 3.2 AO-OFDM signal generator steps of Li-Fi system at transmitter side

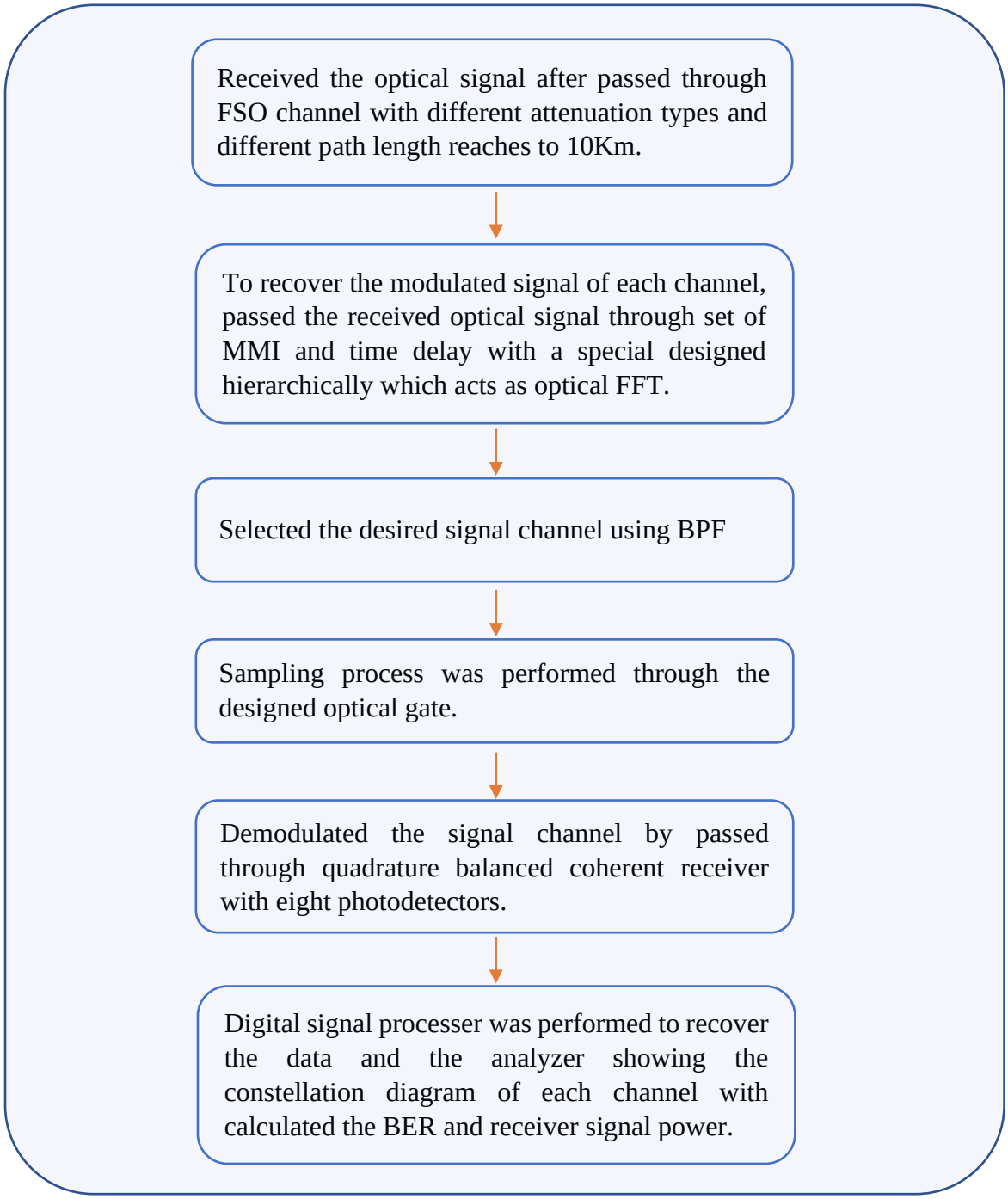

Figure 3.3 AO-OFDM signal generator steps of Li-Fi system at receiver side

3.2.1 All-optical OFDM transmitter

The transmitter side modulates the data it receives from the channels on the optical multi-carrier to broadcast the AO-OFDM signal. This scenario can be implemented through:

i. Optical frequency comb generator (OFCG)

As the previous chapter explains, OFCG is an optical source with multi-wavelengths. It can be advantageous in reducing the number of optical laser sources at the optical line terminal (OLT), increasing the transmission data rate of the system (due to multi carriers or multi-user systems) and bandwidth of data transmission. OFCG is essential to perform the orthogonality between the subcarriers and maintain the optical Inverse Fast Fourier transform (IFFT) at the transmitter side. Several requirements must be available for OFCG, such as stable frequencies (comb lines) with an equal phase shift and the spectral frequency of optical lines must be characterized by flatness [80].

The current study presents a new OFCG design system to generate optical comb frequency lines for visible light communication applications and DWDM applications over a wide bandwidth.

The design of OFCG is based on a single CW laser source, an amplitude modulator, two Mach-Zehnder modulators (MZM), an RF signal generator, and phase shift as shown in Fig. 3.4.

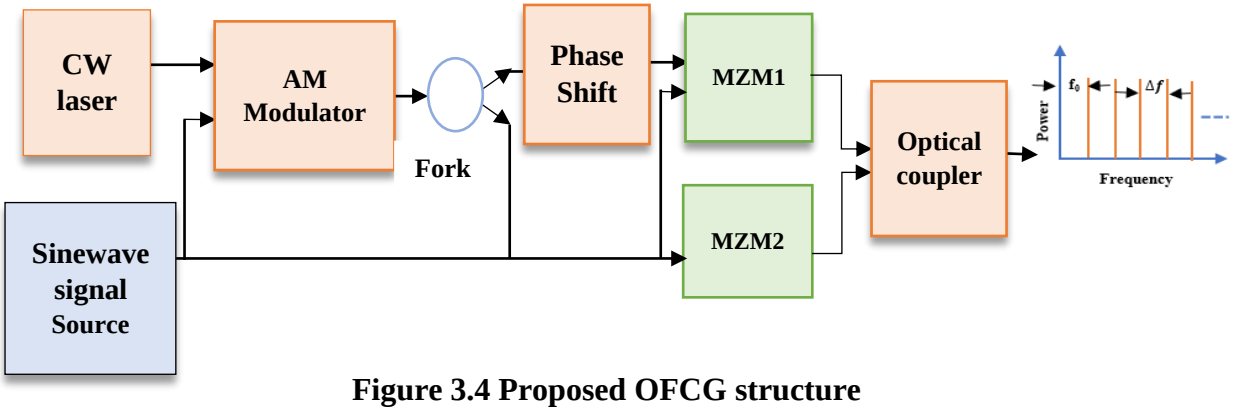

Figure 3.4 Proposed OFCG structure

The CW laser source was emitted at a frequency 500THz (λ= 600nm). The light of the laser source has a frequency f_0, amplitude A_0 and phase φ_0. The probability density function was used to module the laser phase noise as written eq. 2.5.

The amplitude modulator gave a sequence of harmonic tones with $f_0 + n\Delta f$ components, where Δf is the RF signal frequency, and $n = [0,1,2,\dots.]$ is the number of the harmonics. References [17,22] give the output field of AM as follows:

$$E_k = |E_0| \sum_{n=\infty}^{-\infty} E_{n,k} \cos\left[2\pi(f_0 + nf)t + \theta_{n,k}\right] \quad (3.1)$$

$E_{n,k}$ and $\theta_{n,k}$ are the amplitudes and phases of components, respectively. the amplitudes and phases formula as follows:

$$E_{n,k} = \frac{1}{2}\left[\cos(b_k + n)\frac{\pi}{2}\right] J_n\left(\frac{c_k \pi}{4}\right) \quad (3.2)$$

$$\theta_{n,k} = [1 + n + (-1)^n]\frac{\pi}{2} + n\phi_1 + n\phi_k \quad (3.3)$$

b_k represents the DC offset, c_k represents the amplitude from peak-to-peak (PP) and ϕ_k denotes the phase of the k[th] modulator. The amplitude modulator's output was provided directly to the MZM_2, and the phase-shifted modulator's output

f_0+$n_{max}f$ was applied to MZM_1. The same RF signal drives all the modulators, and the spacing of the generator comb lines could be tunable by RF signal frequency. The input RF signals to MZM_1 and MZM_2 can be given as $E_1\cos(2\pi f_s t + \Delta\varphi)$ and $E_2\cos(2\pi f_s t)$, respectively. where $\Delta\varphi$ is the phase shift, E_1 And E_2 the amplitude of the RF signal [85, 117].

When applied (3.2) to the input of MZM_1 and MZM_2, the output can be given as:

$$E_{MZM1}(t) = \frac{\sqrt{2}}{2}\,|E_0|\,\sum_{n=-\infty}^{\infty} E_{n,k}.\left[J_n\left(-\frac{\pi E_1}{V_{\pi 1}}\right).\exp\left(j\frac{\pi V_{bais1}}{V_{\pi 1}}+\right.\right.$$
$$\left.\left.J_n\left(\frac{\pi E_1}{V_{\pi 1}}\right)\right].\cos\left[2\pi(f_0+nf)t+(\theta_{n,k}+\Delta\varphi)\right] \quad (3.4)$$

$$E_{MZM2}(t) = \frac{\sqrt{2}}{2}\,|E_0|\,\sum_{n=-\infty}^{\infty} E_{n,k}.\left[J_n\left(-\frac{\pi E_2}{V_{\pi 2}}\right).\exp\left(j\frac{\pi V_{bais2}}{V_{\pi 2}}+\right.\right.$$
$$\left.\left.J_n\left(\frac{\pi E_2}{V_{\pi 2}}\right)\right].\cos\left[2\pi(f_0+nf)t+\theta_{n,k}\right] \quad (3.5)$$

The proposed OFCG system was characterized by simplicity and produced many strong, flat comb lines from a single laser diode (with 35mW average power and light of 600 nm) over a wide range of wavelengths bandwidth reaches to 470 GHz, these comb lines started from $f_0 = 500THz$ (emission frequency). Furthermore, the spacing between comb lines ($\Delta f = 5,10,20\,GHz$) was easily adjustable by varying the frequency of RF signal generator, this is an important feature to confirm the orthogonality between the sub-carriers for implemented optical IFFT at transmitter side.

To maintain the best performance of OFCG in terms of combs flatness, the proposed system was tested with different MZM chirping factors (α=3,5, and 7). All the parameters used for designing the OFCG system are explained in Table 3.1.

Table 3.1 The parameters of proposed OFCG

The Device	Parameter	Value
CW Laser	Emission Frequency	500 THz λ=600nm
	Average Power	35 mW
	Linewidth	100 kHz
	Azimuth	45 deg
Phase Shift	Frequency Offset	160 GHz
RF Signal	Frequency	5,10,20,40 GHz
	Amplitude	2 a.u.
	Bias	1 a.u.
MZMs	Extinction Ratio	35 dB
	Alpha Factor	3, 5, 7
Over all OFCG system	Band width	470 GHz
	No. of comb lines	52, 48, 24
	Fluctuation power [dBm]	4.44

ii. Optical IFFT

This work succeeded in inducing the AO-OFDM signal by utilizing IFFT in the optical domain. Fig. 3.5 explains the OIFFT stage. OIFFT process was generated based on:

a) Dense wavelength division multiplexing (DWDM)

The OFCG lines started from 500 THz, represented by f_0 were separated by $\Delta f = 20\text{GHz}$ are demultiplexed using DWDM, which contains eight or sixteen bandpass filters, Gaussian transfer function, and center frequencies (f_c) started at 500THz and increased gradually by 20 GHz. The central frequencies of these

filters matched the OFCG lines. Gaussian transfer function with bandwidth << Δf ensured line separation with low-noise bandwidth. Demultiplexing the comb lines provided sub-carrier frequencies into eight of sixteen for the eight or sixteen channels (N8,16); each frequency represented the optical carrier for single channel and was fed into the modulators.

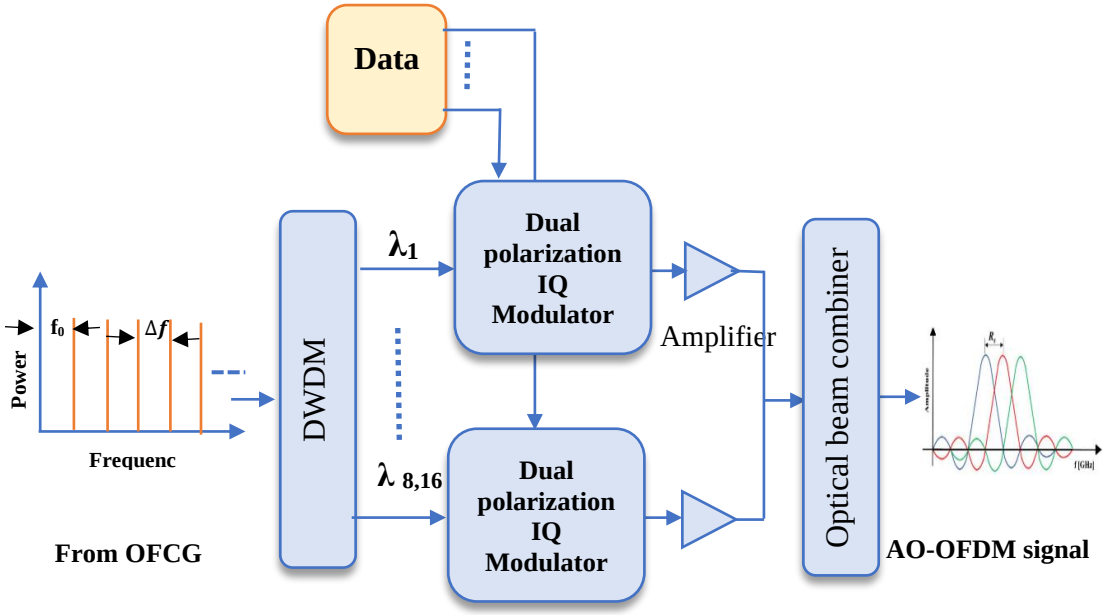

Figure 3.5 AO-OFDM transmitter

b) Dual polarization IQ modulation

After demultiplexed process using DWDM, the comb lines passed through the Dual polarization IQ modulator which separated the polarization of the signal (x, y) using PBS and then modulated each one individually with two types of modulation scheme: QPSK and 16-QAM symbols. Fig. 3.6 explains dual polarization IQ modulator.

The key principle of achieving the orthogonality between these sub-carriers was making the modulation baud rate equal to the spacing between the sub-carrier's frequencies generated by the OFCG which is 20 GHz.

Data was divided into 8 or 16 channels ($N_{8,16}$) and encoded using dual-polarization IQ modulator with OFCG subcarriers. The modulation rate was 20 G Symbol/s (for each polarization), equal to the comb lines and DWDM spacing.

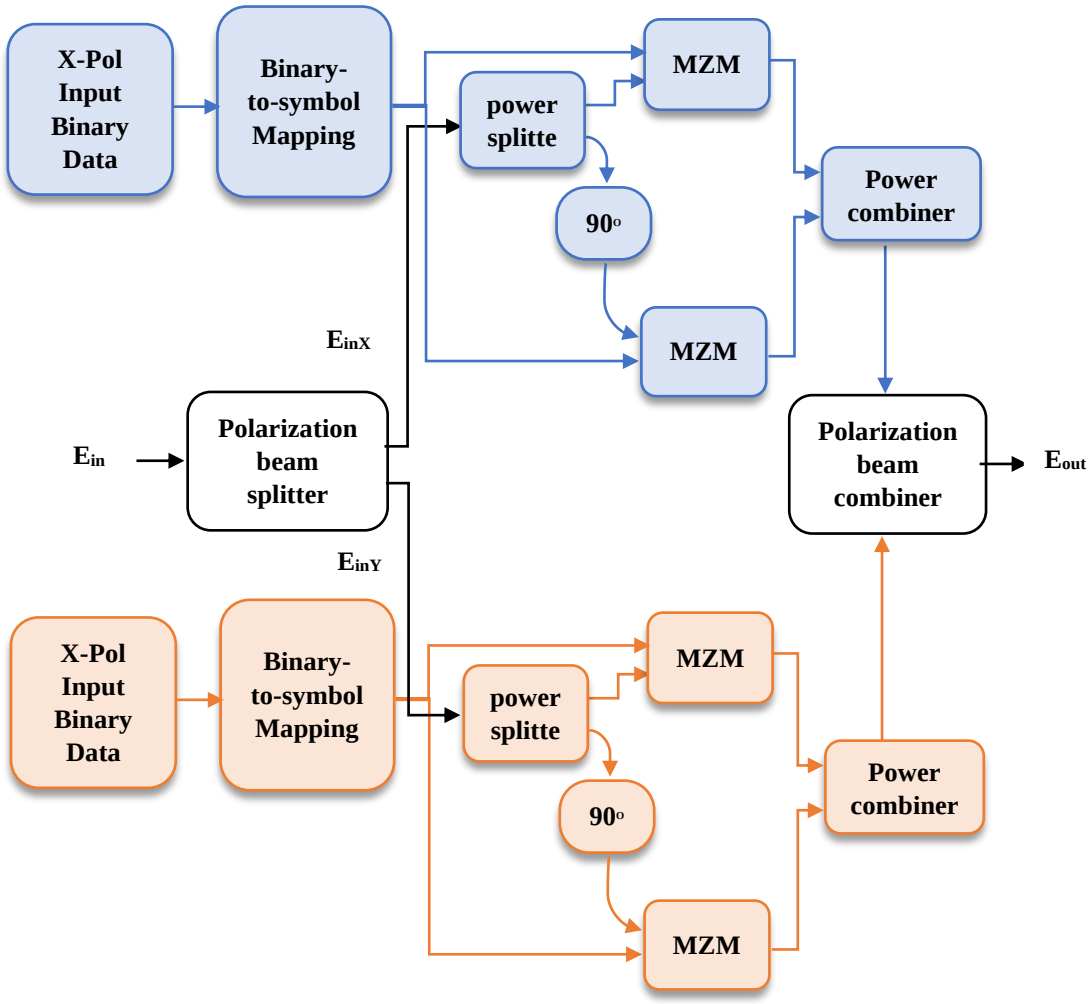

Figure 3.6 Dual polarization IQ modulator

The optical modulator was implemented using DP-IQ QAM modulator. The modulator contains two identical sections driven by the input optical carrier's *X* and orthogonal polarization components *Y*. Two sequences of input data were used to modulate the input optical carrier; one sequence for each carrier polarization component. Depending on the M-QAM modulator format employed, the serial data bits were transformed into a collection of symbols, and the final group was mapped to points in IQ space. The resultant RF drive signals are created. As shown in Fig. 3.4. First, an optical input field E_{in} was splitted by polarization splitter into orthogonally polarized components, E_{inx} and E_{iny}. Then, each one of these two components were splitted by an optical power splitter into two carrier components. One carrier component E_{in-I} directed to an MZM, acted as an amplitude modulator driven by the RF-drive signal I. The second carrier component E_{in-Q} was subjected to a 90° phase shift and then used to feed an MZM driven by an RF-drive Q component.

c) Optical Amplifier and combiner

The outputs of the eight or sixteen channels ($N_{8,16}$) after the modulation the resulting optical signal were individually amplified using a booster optical amplifier (OA) with a power control scheme (1W output). OFDM symbols were generated by combining the channels' output using an optical combiner. The resulting optical spectrum signal was an orthogonal eight- or sixteen-Sinc signal, suitable for transmission through an optical oscilloscope via a free-space optical channel.

The total bitrate R_b carried by the AO-OFDM subcarriers was computed from ($R_b = 2R_s\, N_{sc} log_2 M$), where R_s is rate of single channel, M is the modulation order and the number 2 is used to ensure the DP modulation. Note that each of the

M symbols contains m = $\log_2$M bits. The spectral efficiency (total transmitted bit rate / optical bandwidth of the system) was given by:

$$SE = \frac{R_b}{\Delta f N_{sc}} = \frac{2R_s N_{sc} log_2 M}{\Delta f N_{sc}} = 2log_2 M \quad (3.6)$$

Equation 3.6 reveals that the SE was determined only by the modulation format and was independent of several optical subcarriers and subcarrier frequency spacing. For QPSK- and 16-QAM signals, the SE is 4 and 8 bits per second per Hz, respectively.

As a result, the transmitted signal has an acceptable peak to average power ratio PAPR value 5~6 dB over 180 GHz and 340 GHz of bandwidth for eight and sixteen channels respectively. Table 3.2 explains the transmitter parameters of Li-Fi system-based AO-OFDM architecture.

Table 3.2 The transmitter parameters of Li-Fi system-based AO-OFDM architecture.

The device	Parameter	Value
DWDM	Filter type	Bandpass
	Filter function	Gaussian
	Bandwidth	1GHz
	Center frequency spacing	20 GHz
	No. of channel (N)	8,16
IQ Modulation	Sample frequency	4.6e11 Hz
	Baud rate	20 GHz
	Bit per symbol	2, 4 Bits
Amplifier	Amplifier type	Power control
	Output power	1W
	Maximum gain	30 dB
	Output power	≅ 0dBm
	Bandwidth	180, 340 GHz

Transmitted signal	Sample frequency	640 GHz
	PAPR	5~6 dB
	SE	4,8 bit/sec/Hs

3.2.2 FSO channel modeling

i. Clear weather condition

Scintillation, a crucial free space channel connection parameter, deteriorates the whole system's performance even in clear weather by producing intensity fluctuations to the travelling beam even with short propagation paths (fading the received optical signal). Additionally, a slight change in temperature's effect on scintillation causes a change in the refractive index. As a result, the propagation beam focuses and defocuses as it passes through the fluctuation, producing both negative and positive interference with a separate portion of the light wave.

The light signal generated from the proposed system with 180 and 340 Gbps bandwidth for 8 and 16 channels, respectively, propagated through an FSO channel with Different levels of path length and scintillation based C_n^2. Equation (2.86) was used to represent weak, moderate, and strong turbulence.

The system was tested and examined under these circumstances using the FSO channel link of VPI design suite to replicate the Scintillation model. Table 3.3 shows the FSO scintillation channel parameters.

Table 3.3 FSO channel parameters

Parameters	Values
Length (Km)	1:10 Km
C_n^2	$10^{-17}, 10^{-15}, 10^{-12}$
Launch Waist	2e-2
Receiver Aperture Diameter	10e-2

ii. Weather condition

The atmospheric channel was modelled using MATLAB, and the behavior of signals under the modelled channel with various wavelengths was evaluated. The atmosphere attenuation was computed for different path lengths of 1-10 km based on visibility using two models, Kim's and Kruse's. Due to lower absorption attenuation and falls with visible band , 600 nm was chosen for the Li-Fi system optical source. This wavelength was used to determine fog attenuation under various degrees of fog and haze attenuation. Rain attenuation is a separate wavelength that is affected by the precipitation rate. This study modelled and calculated rain attenuation for different presentation intensity levels. All the calculated attenuation values are utilized in addition to the scintillation effect of FSO channel link of the proposed Li-Fi system.

3.2.3 All-optical receiver

The schematic of all-optical Li-Fi coherent receiver was illustrated in Fig. 3.1. The optical signal received from the FSO link output is split into N_{sc} components by the receiver, and each subcarrier was handled separately. The next section goes into further depth about the received signal.

i. Demultiplexing all optical OFDM (OFFT)

The received optical signal was derived into a set of optical interference and time delay to perform optical FFT. An optical multi-mode interference (MMI) or Mach-Zehnder interferometer (MZI) with optical delays divided the received signal into $N_{8,16}$ components.

MMI distributes optical power from one or several input ports among several output ports. It is based on destructive/constructive interferences occurring in the MMI area with many guided modes. Therefore, MMI have many potential applications, such as couplers, splitters, combiners, mode converters, filters, etc. The Fig. 3.7 explains the optical FFT utilized based on MMIs and time delayers. The current study invented 16-optical FFT for 16 channels after developing 8-Optical FFT for eight channels. It can describe 8 and 16-Optical FFT with:

- ✓ **8-OFFT,** the first stage of optical delay has T_S-time delay, where Ts=25ps; in the second stage, each delayer has T_S/8-time delay.
- ✓ **16-OFFT**, first stage optical delay has T_S-time delay, second stage optical delays have T_S/4-time delay, third stage T_S/16-time delay.

Tables 3.4 and 3.5 illustrate the parameters of 8 and 16 OFFT, respectively.

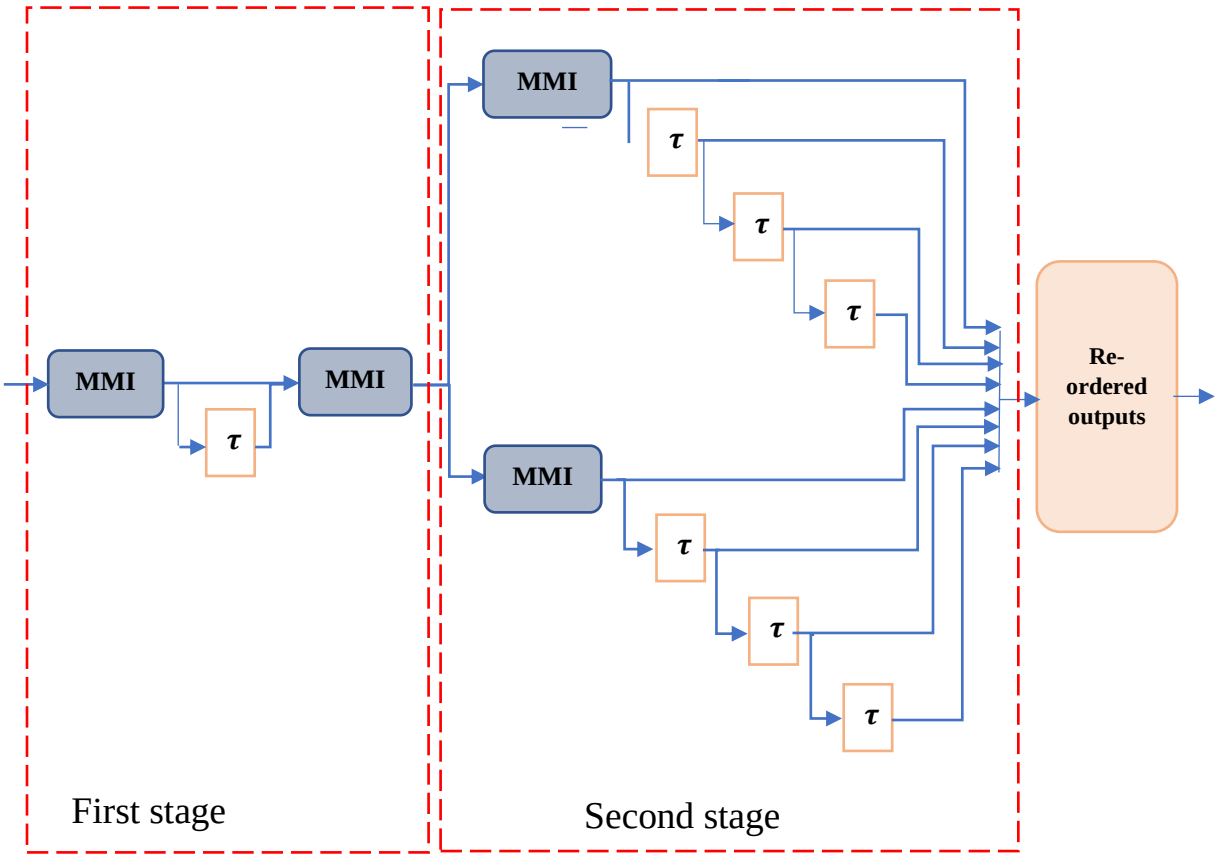
MMI
MMI
τ
MMI
τ
τ
τ
MMI
τ
τ
τ
Re-
ordered
outputs
First stage
Second stage

(a)

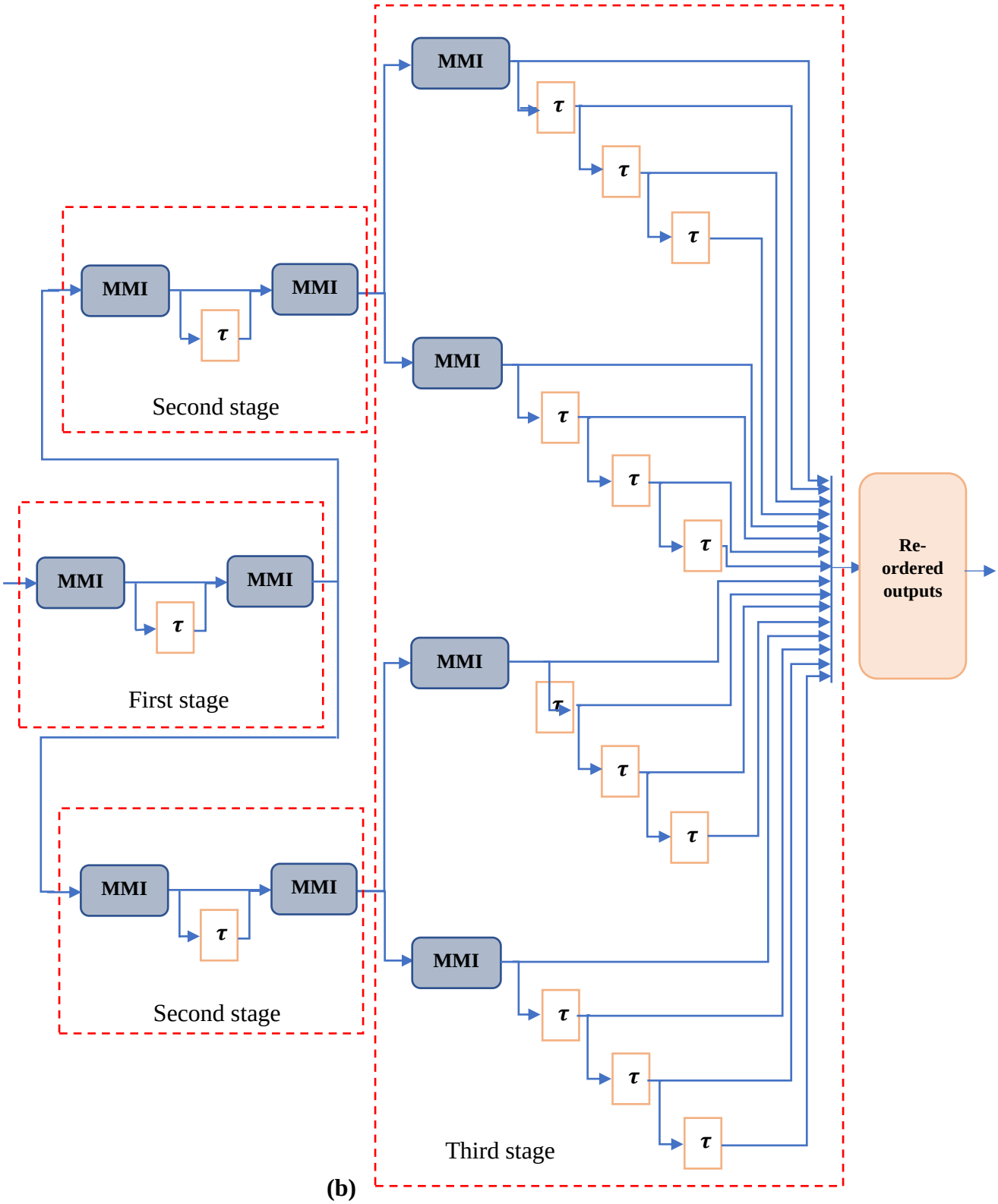

(b)

Figure 3.7 OFFT a) 8-OFFT b) 16-OFFT

Table 3.4 the parameters of 8- OFFT

Parameter	Value
OFFT size	8
No. of MMT	6
No. of delayers	7
Central frequency	500THz
Sample frequency	640GHz
Symbol rate Ts	1/20G symbol/s
First stage time delay	25ps
Second stage time delay	6.25ps

Table 3.5 the parameters of 16- OFFT

Parameter	Value
OFFT size	16
No. of MMT	10
No. of delayers	15
Central frequency	500THz
Sample frequency	640GHz
Symbol rate Ts	1/20G symbol/s
First stage time delay	25ps
Second stage time delay	6.25ps
Third stage time delay	3.125ps

ii. Optical gate

Optical gates cab be used to accomplish the sampling process. Their placement within the system—either before or after the OFFT—can be done without affecting overall system performance. Switching the optical data in a way to prevent ICI is helpful for optical gates. The switching mechanism enables the

appropriate frequency band to pass while blocking others by picking the time domain point at which the OFFT is synced to the OFDM symbols. As shown in Fig. 3.8, The optical gates were designed using

- ✓ Pseudo random binary sequence generator: Generated random bits with a bit rate equal to the system baud rate (20Gbps)
- ✓ On-Off code (OOK) driver: with modulation type RZ
- ✓ Time delay and
- ✓ AM modulator

Table 3.6 shows the optical gate parameters.

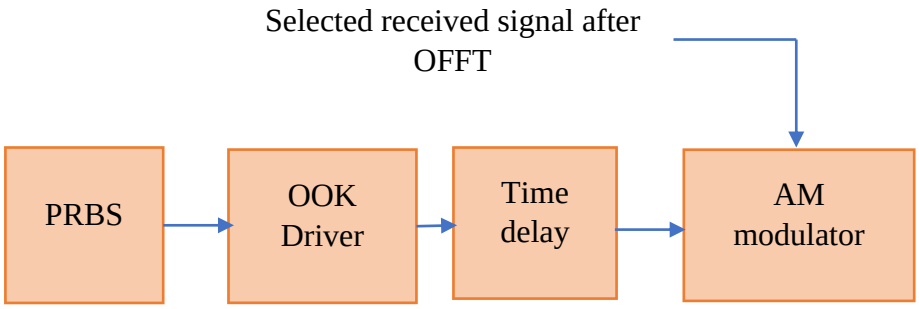

Figure 3.8 The sampling process scheme

Table 3.6 Optical gate parameter

The device	parameter	value
PRBS	Baud rate	1/20 GHz
OOK driver	Bite rate	20 Gbps
	Sample frequency	640 GHz
	Transition time	0.45/20 ns
Time delay	Delay time	0.45/20 ns

iii. Coherent receiver

After sampling, the demultiplexed optical signal was applied to a Dual polarization IQ coherent receiver operating with a specific LO optical signal. A homodyne coherent receiver was utilized, which required that the LO frequency equal the frequency of the corresponding unmodulated optical subcarrier. For this purpose, the AO-OFDM receiver should use a bank of LOs whose frequency is identical to those of unmodulated optical subcarriers used at the transmitter side. To estimate the phase offset is needed to use the optical phase lock loop (OPLL). However, the OPLL raised the cost and couldn't compensate for the channel impairment. But the receiver using ADC with a high-performance DSP algorithm implemented the coherent receiving and eliminated the need for OPLL. Thus, the baseband data was compensated by an electrical filter, ADC, and DSP to reduce most impairment caused through the transmission process. Fig. 3.9 shows the coherent receiver scheme. All-optical OFDM receiver parameters are illustrated in table 3.7.

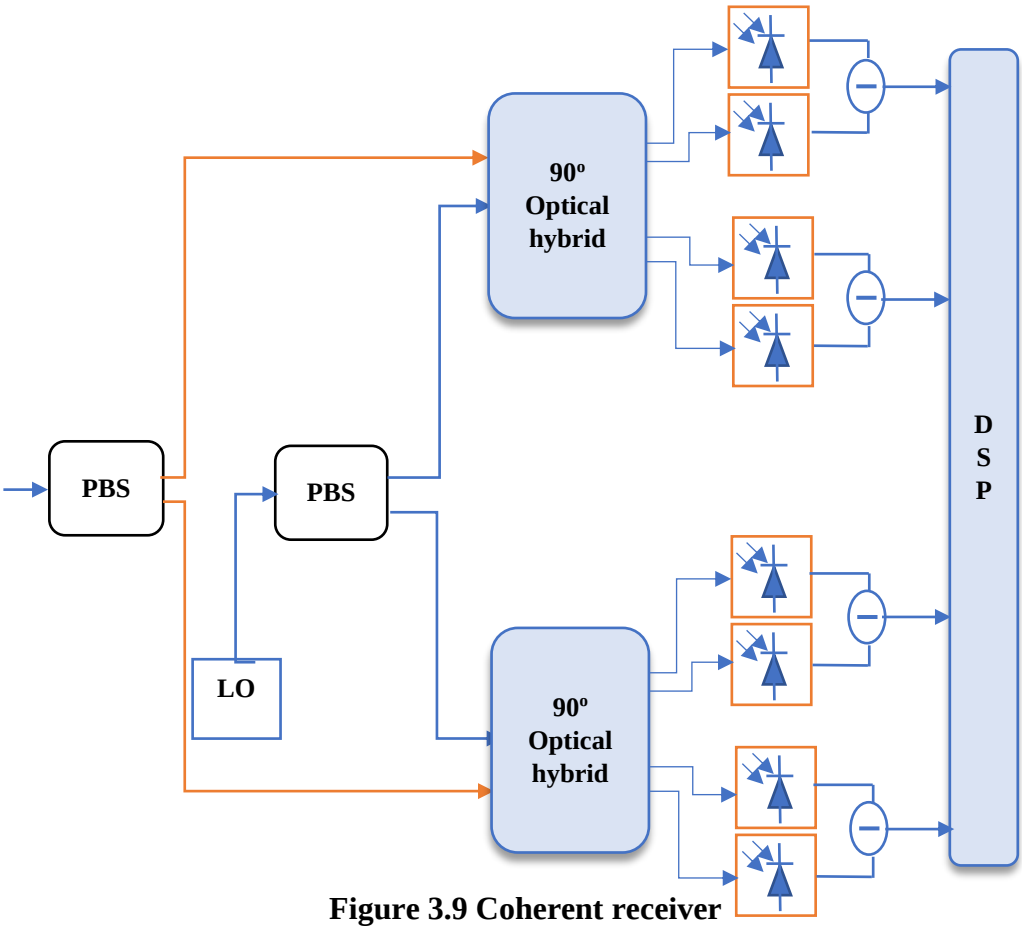

Figure 3.9 Coherent receiver

Table 3.7 The All-optical OFDM receiver parameters

The device		parameter	value
Receiver		dimeter aperture	10 cm
8-OFFT		Symbol rate Ts	25e-12
		No. of MMI	4
		No. of time delays	7
16-OFFT		Symbol rate Ts	25e-12
		No. of MMI	10
		No. of time delays	15
Optical Gate	**PRBS**	Baud rate	1/20 GHz
	OOK driver	Bite rate	20 Gbps
		Sample frequency	640 GHz

		Transition time	0.45/20 ns
	Time delay	Delay time	0.45/20 ns

iv. Digital signal processing DSP

A DSP analyses the constellation diagrams and computes the BER to complete the data evaluation. The Python was built on a single-carrier coherent transmission DSP library. The module handled floating-matrix representations of signal samples. Samples of [I Q] signal components for 2D and [Ix, Qx, Iy, Qy] signal components for 4D modulations were each stored in a row of the matrix. The module took the input sampling rate as input and produced a float value representing the postprocessing sampling rate. The DSP methods QPSK and 16-QAM phase estimation were put into practice. The recovered signal features a clear constellation diagram and a decent BER.

The overall proposed Li-Fi-based AO-OFDM parameters are listed in table 3.8.

Table 3.8 The overall Li-Fi system-based AO-OFDM parameters

Parameter	value
No. of channels (N)	8,16
Data rate for single channel	20 G symbol/s
Channel spacing	20 GHz
Modulation technique	AO-OFDM
Modulation scheme	BPSK, QPSK,16-QAM
No. of bit per symbol	1,2, 4
Optical source	CW laser
Emission frequency	500 THz
No. of laser source	One
Spectral efficiency	4,8 bps/Hz

PAPR	5~6 dB	
Channel link	Free space	
Channel Link range	1-10 (Km)	
Total transmitted Bit rate	8-OFFT& QPSK	$2 \times 2 \times 8 \times 20G$ = 640 Gbps
	8-OFFT&16-QAM	$2 \times 4 \times 8 \times 20G$ = 1.28 Tbsp.
	16-OFFT& BPSK	$2 \times 1 \times 16 \times 20G$ = 640Tbps
	16-OFFT& QPSK	$2 \times 2 \times 16 \times 20G$ = 1.28Tbps

3.3 System simulation

The designed Li-Fi-based AO-OFDM system was simulated in VPI photonics version 9.8 environment. A snapshot of the designed system simulation was shown in appendix A, Fig. 1 and 2 and illustrate this software environment for 8 and 16-AO-OFDM system respectively. Fig. 3 shows the proposed design of OFCG, Fig. 4 illustrate the DWDM construction, Fig 5 illustrate the DP-IQ modulator, Fig.6 shows the construction of free space channel with Scintillation affection, Fig.7 a and b explain all optical FFT at receiver side, Finally Fig.8 shows the coherent receiver with DP-IQ modulator.

Chapter Four

Obtain results and discussion

Chapter Four

Obtain results and discussion

4.1 Introduction

This chapter presents simulation results to access the Li-Fi system's transmission performance based on AO-OFDM. The data was collected from 8 and 16 channel modulated on OFCG sub-carriers each channel utilized DP-IQ modulated and perform the orthogonality between them through OIFFT after that transmitted over free space. The system is tested under different path lengths and channel turbulences/weather conditions based on previously mentioned channel modeling values. The transmission performance of the proposed system was tested to validate the configuration given in Chapter 3.

The simulation is carried out and analyzed in terms of BER, Constellation diagram, and received power with different FSO path links from 1-10 km and under different types of Atmosphere attenuation.

4.2 All-optical OFDM transmitter

The 8 and 16 subcarriers were multiplexed demultiplexed through optical inverse fast Fourier transform/fast Fourier transform (OIFFT/OFFT) for orthogonality. Optical IFFT was implemented at the transmitter side based on an optical frequency comb generator (OFCG), dense wavelength division multiplexing (DWDM), DP-IQ M-QAM and optical combiner.

4.2.1 OFCG

The proposed OFCG system generating optical comb lines for visible light communication and DWDM application, the CW laser diode was used as an optical source emitted at 500 THz. The optical spectrum of CW laser has a single optical carrier with center frequency f_0=500THz and many weak sidebands. Due to amplitude modulation of the laser light with RF signal source, these sidebands become stronger and produce multiple harmonics of the input signal on the two sides of CW center frequency of optical spectrum. Therefore, these harmonics are gradually decreased on both sides. Fig. 4.1(a), (b) show the output optical spectrum of the CW laser diode and the AM modulator.

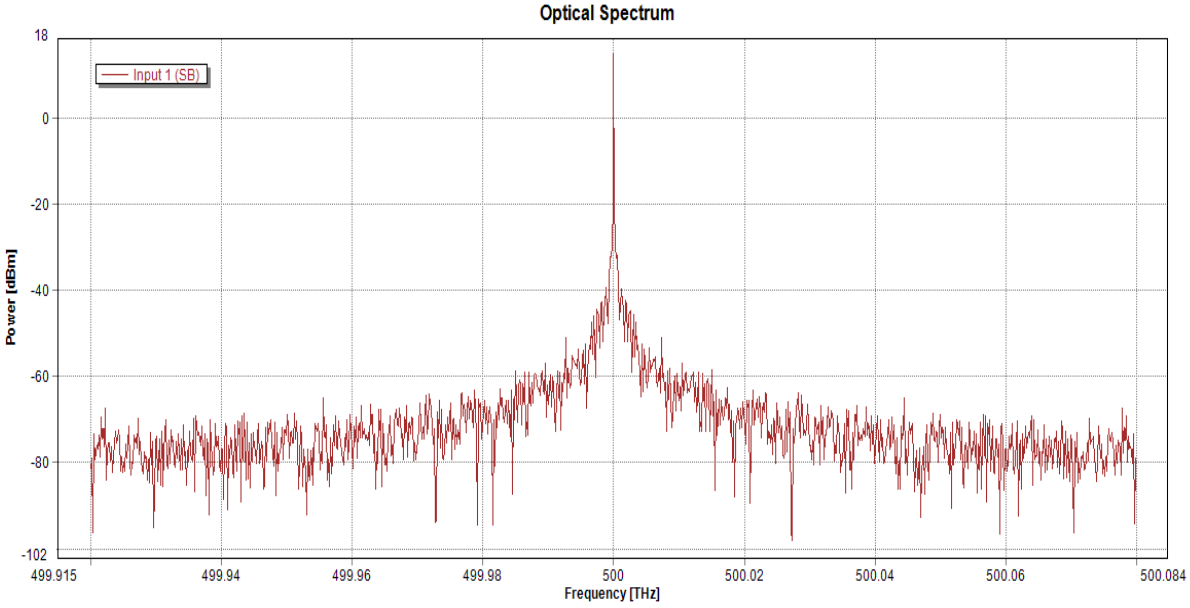

(a)

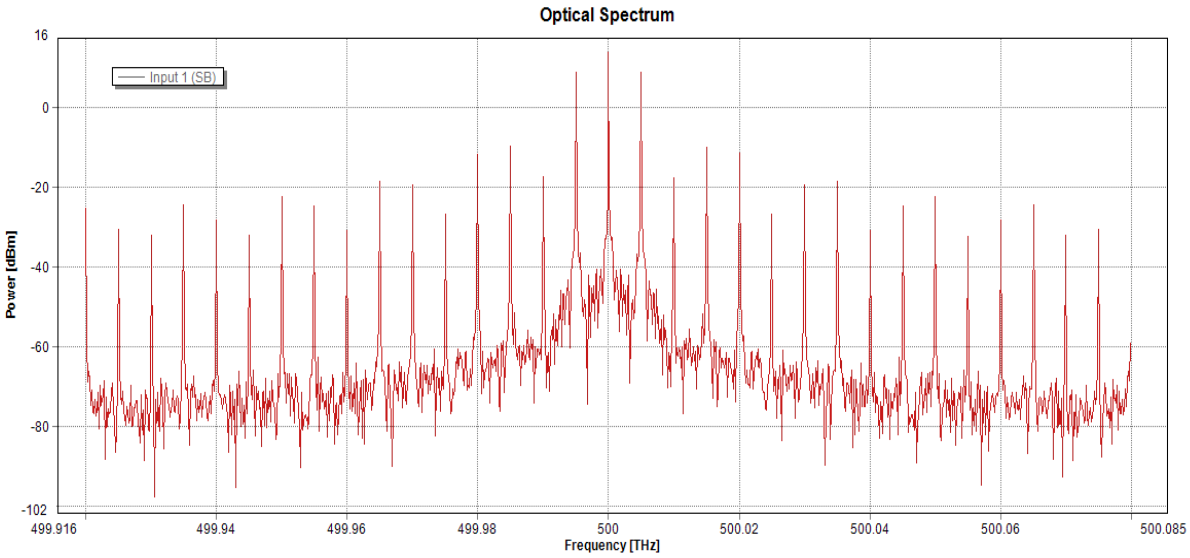

(b)

Figure 4.1 Optical spectrum of a) CW laser b) after AM modulator

The output of AM was separated into two branches by Fork, one of these directly passed through the MZM_2 and the other one shifted by phase shifter then passed through the MZM_1, frequency offset of the phase shift is equal to the AM bandwidth (160 GHz) this process takes advantageous in double the overall system bandwidth. The output harmonics after $MZM_{1,2}$ was stronger and flatter, then combined using an optical coupler to produce the final signal of OFCG lines over 470 GHz of bandwidth.

All the modulators were driven from the same FR signal. RF signal frequency was controlled on the duration of comb lined (Δf), so the spacing between generating optical lines was tuned by RF frequency. The spacing between optical comb lines was increased by increasing the frequency of RF signal generator.

MZM utilized different chirping/alpha factors α=3, 5, and 7 to experience the best behavior of OFCG system. The alpha-factor affected the flatness of these

harmonics, as demonstrated in Fig. 4.2(a), (b), (c). The best (extra flat comb lines) was associated with α=5.

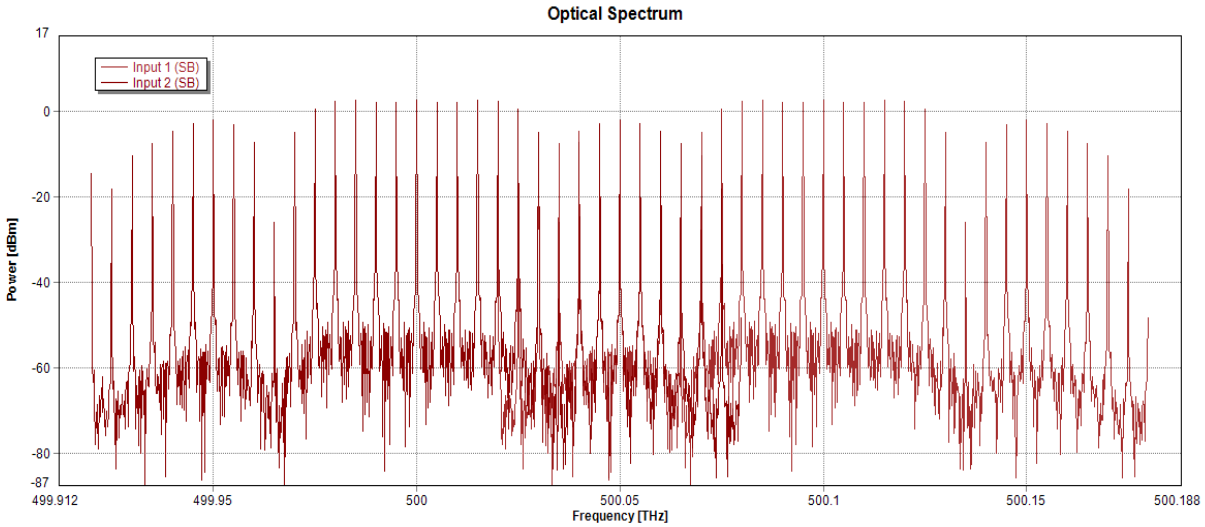

α=3

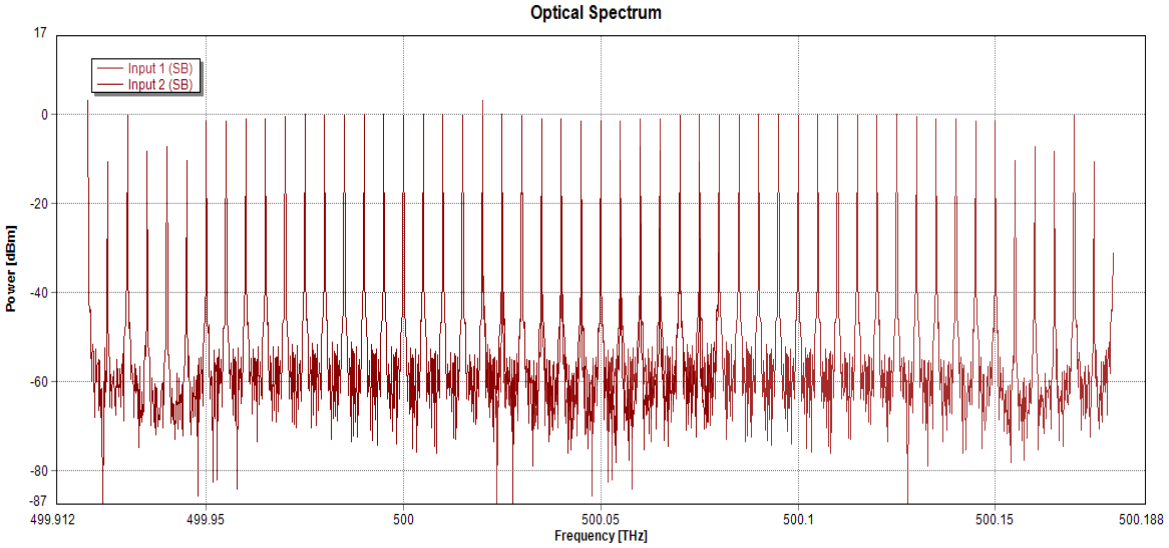

α=5

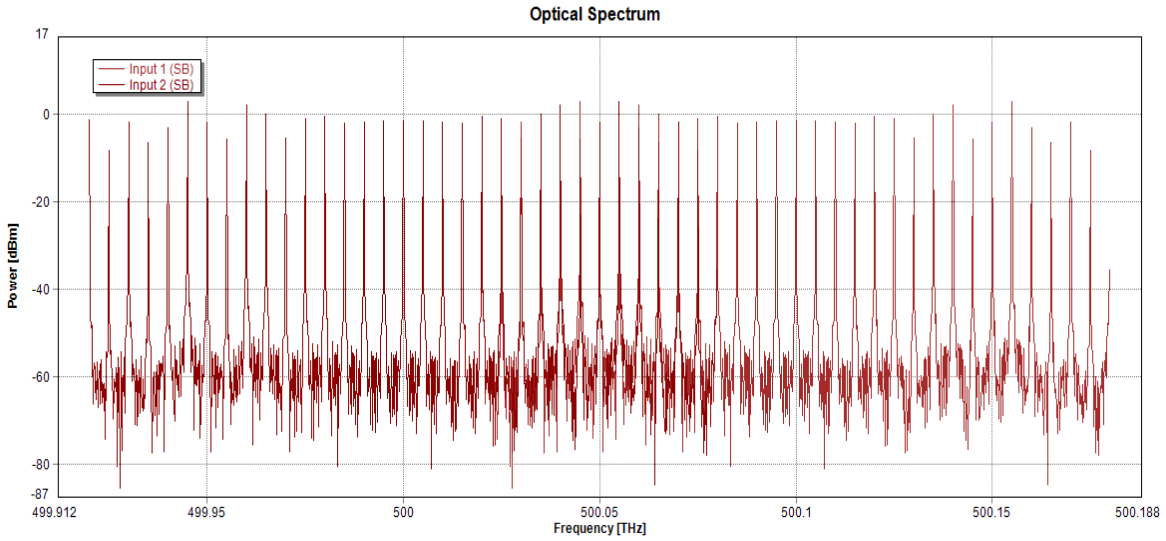

α=7.

Figure 4.2 OFCG lines under various alpha factor values

By increasing RF signal generator frequency, the spacing between comb lines (Δf) was increased and the number of comb lines was decreased. Fig. 4.3 shows the optical spectrum with α=5 and RF signals at 10, 20 and 40 GHz.

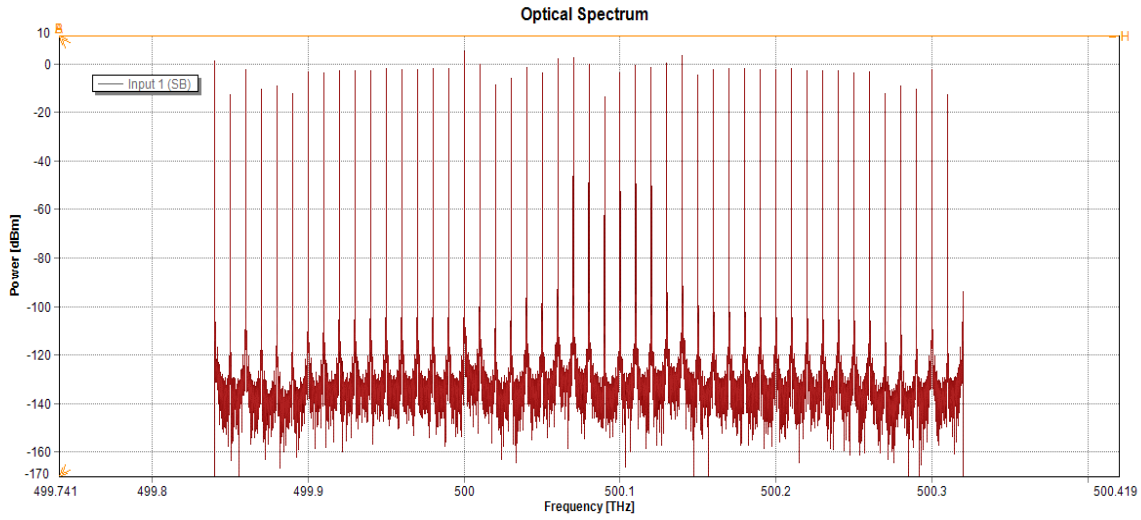

α=5, RF signal generator frequency= 10 Gbps

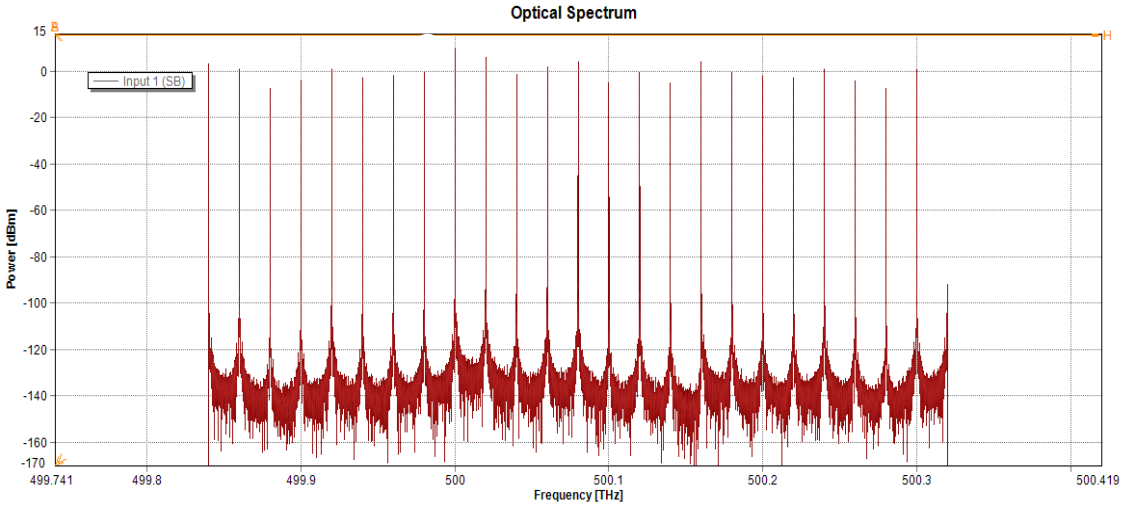

α=5, RF signal generator frequency= 20 Gbps

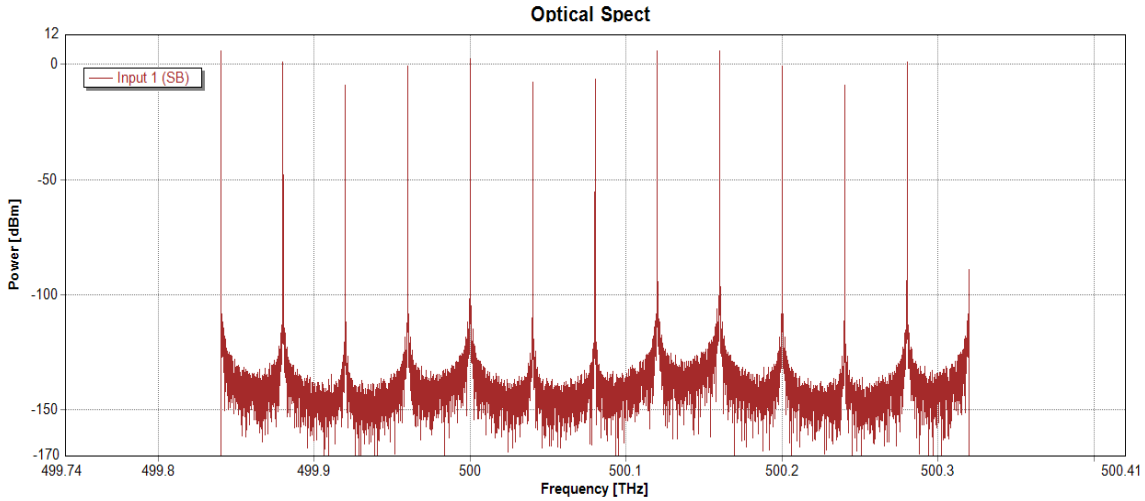

α=5, RF signal generator frequency= 40 Gbps

Figure 4.3 OFCG lines with different RF signal generator frequency

The proposed OFCG has outstanding flatness and output power compared to the many previous works, Furthermore the spacing between generated subcarriers are tunable, this is an important feature to perform the orthogonality between subcarriers optically. A single CW laser diode fed OFCG as optical source to generate set of frequencies between 24-52 flat comb lines for different frequency

spacing 5, 10, and 20 GHz over 470 GHz of bandwidth, the output power comb lines stronger than 2 dBm and fluctuation between 0.006-0.003 dB.

The measured results are explained in table 4.1. Furthermore, table 4.2 shows a Comparison of the proposed OFCG system with previous works.

Table 4.1 Simulation results of proposed OFCG

Frequency	**F=5GHZ**			**F= 10GHZ**			**F=20GHZ**		
Alpha factor	**α=3**	**α=5**	**α=7**	**α=3**	**α=5**	**α=7**	**α=3**	**α=5**	**α=7**
No. of comb line	52			48			24		
Maximum power(dBm)	3.27	0.81	3.40	-0.22	2.53	2.43	3.95	2.10	9.30
Minimum power (dBm)	-19.96	-6.71	-4.78	-16.85	-3.42	-12.52	-4.78	-2.34	-3.67
Fluctuation (dBm)	23.23	7.52	8.18	17	5.95	14.95	8.73	4.44	12.97
Fluctuation (mW)	210	5.64	6.57	50.11	3.93	31.26	6.46	2.77	19.8

As explained in results table 4.1, the number comb lines were constant and didn't vary with the alpha factor. Alpha factor effected on the comb lines flatness only. The best results belong to α=5 where OFCG produce 52 comb lines with fluctuation about 0.0056 W for RF signal source frequency=5 GHz, while 48 comb lines with fluctuation about 0.004 W for RF signal source frequency =10 GHz, and 24 comb lines with fluctuation 0.003 W for RF signal source frequency =20 GHz. However, the number of the comb lines was changed among different RF signal source frequencies, the number of comb lines were reduced with increasing RF signal frequency. Fig. 4.4 explains the relationship between the number of

comb lines and the RF signal source frequency of OFCG. Table 4.2 illustrate Comparison between the proposed OFCG performance and previous studies.

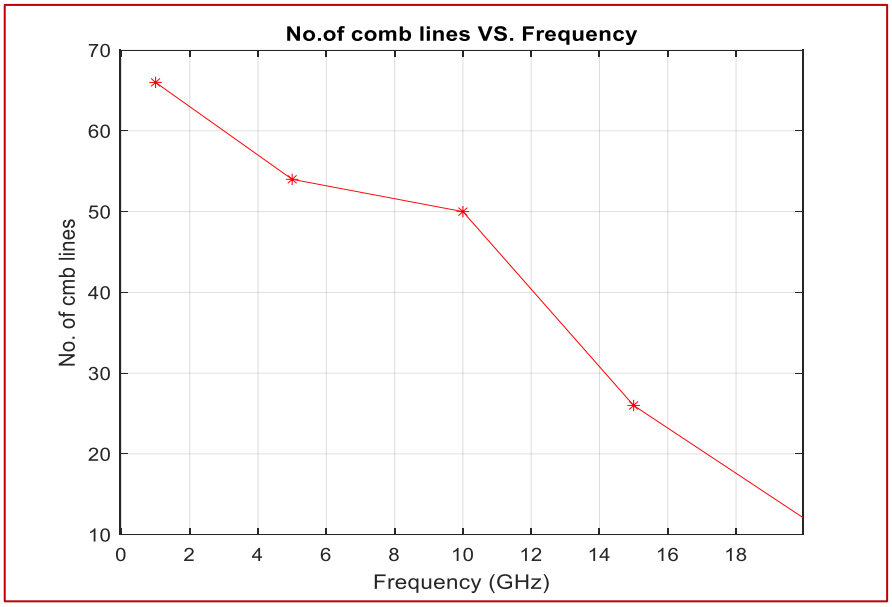

Figure 4.4 The RF Frequency vs OFCG lines

Table 4.2 Comparison of the proposed OFCG with previous works.

Ref.	year	Simulated system	laser			Comb Lines				
			Type	Output power	Line-width Hz	Fc (GHz)	α	No.	Max. power	Fluctuation [W]
[74]	Springer 2016	Opti-system	CW 1552.52nm	10mw	100K	5,10,20	5,7,9	15,21,27	-20dB	1.12
[75]	Science direct 2015	Opti-system	CW 193.1	10mW	100K	5,10,20,40	3,5,7,9	19,23,27,31	-10dB	-
[85]	IEEE 2018	Opti-system	CW	30mW	10M	-	-	61	-5dB	-
This work		VPI	CW	35mw	100K	5,10,20	3,5,7	52,48,24	2dB	0.003

4.2.2 DWDM and Modulation process

The comb lines with spacing Δf =20GHz were demultiplexed with DWDM into 8 and 16 subcarriers using 8 and 16 of bandpass gaussian filters respectively, with bandwidth 1GHz and central frequency is $f_0 + (n)\Delta f = 500THz + (n) \times 20GHz$; where n is channel number n=0, 1, 2…15. Each subcarrier, after demultiplexing represented the optical carrier for individual channel. Each channel modulated its data by dual polarization I/Q modulator with QPSK and 16-QAM with 20 G symbol/s (2 and 4 bits per symbol), so the total transmission bit rate is:

$2 \times 8 \times 20 \times 10^9 \times log_2 M = 640Gbps$ For 8-channel and QPSK

$2 \times 8 \times 20 \times 10^9 \times log_2 M = 1.28\,Tbps$ For 8-channel and 16-QAM

$2 \times 16 \times 20 \times 10^9 \times log_2 M = 640Gbps$ For 16-channel and BPSK

$2 \times 16 \times 20 \times 10^9 \times log_2 M = 1.28Tbps$ For 16-channel and QPSK

The value of 2 referred to the fact of dual polarization. Fig. 4.5 shows the signal spectrum of the first and last subcarriers after a modulation process. While Fig. 4.6 shows the constellation diagram of the first modulated signal.

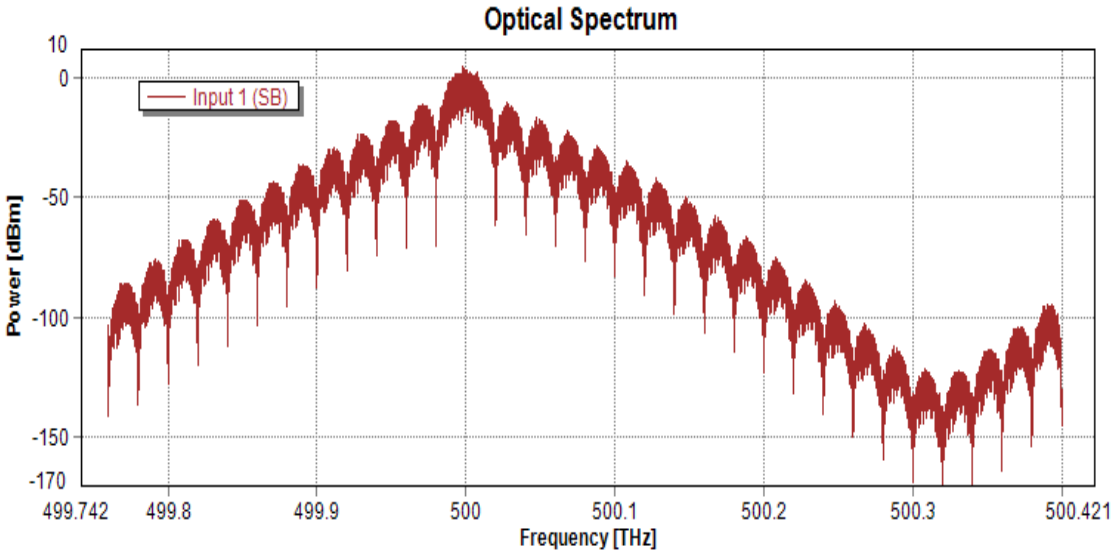

(a)

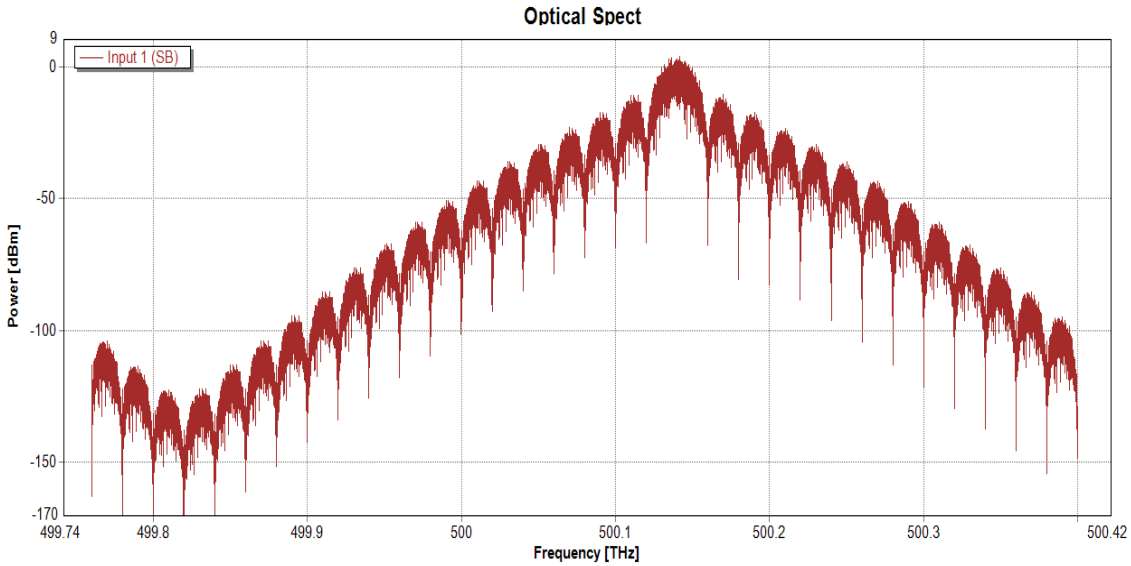

(b)

Figure 4.5 Optical spectrum of a) first channel b) last channel

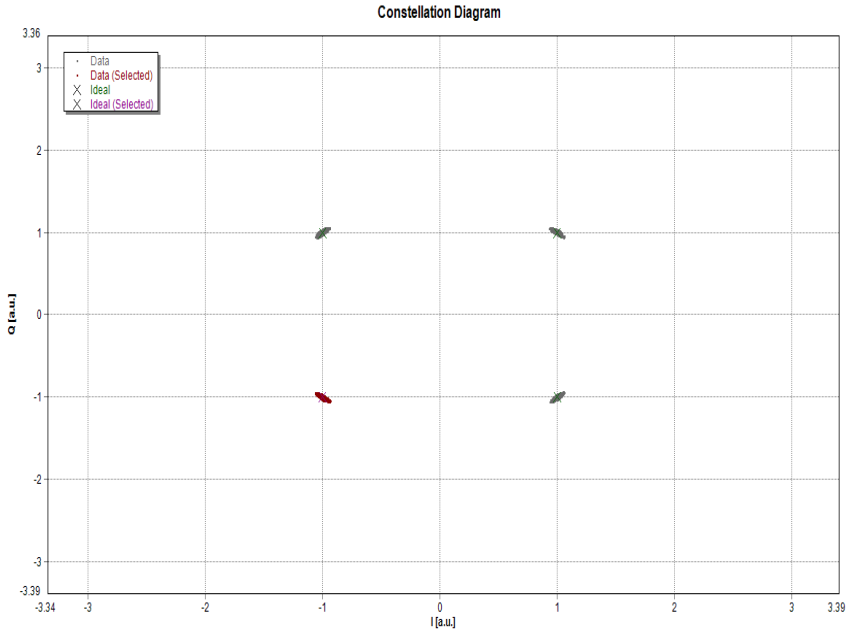

Figure 4.6 The constellation diagram of the first channel after QPSK coding

AO-OFDM symbols were generated by combining the output of the eight or sixteen channels using an optical combiner after the amplification process. They were propagated through a Line-of-sight FSO channel link, through utilized CW laser diode as optical sources of Li-Fi system with 35mW average power and 100KHz line width, the transmission distance was maximized through the free space channel links reaches to10 Km.

The proposed outdoor Li-Fi system-based AO-OFDM transmitted 640 Gbps and 1.28 Tbps for 8 and 16 channels respectively, the transmitted optical signal has acceptable value of PAPR about ~5dB over bandwidth 180 and 340 GHz for 8 and 16 channels, respectively. Furthermore, has 4 and 8 b/s/Hz of spectral efficiency for QPSK and 16-QAM respectively.

The transmitted signal waveform is illustrated in Fig. 4.7. In contrast, Fig. 4.8 shows the optical spectrum of the transmitted signal with 8,16 channels. Table 4.4

explains the transmitter parameters of Li-Fi system-based AO-OFDM architecture.

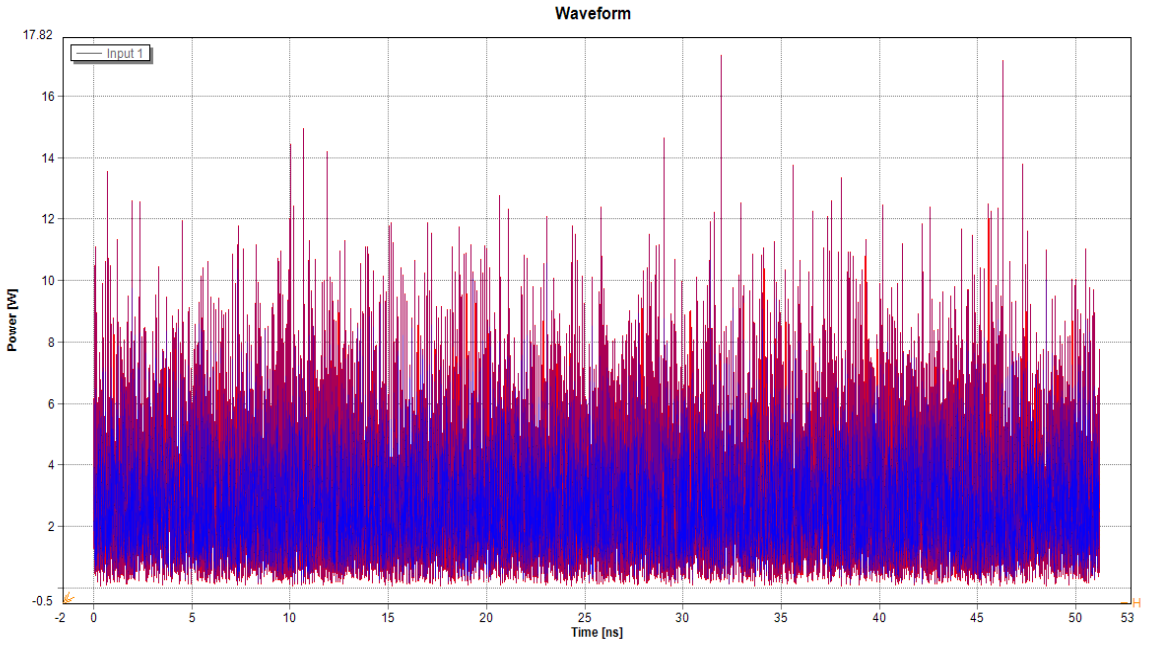

Figure 4.7 Transmitted signal waveform

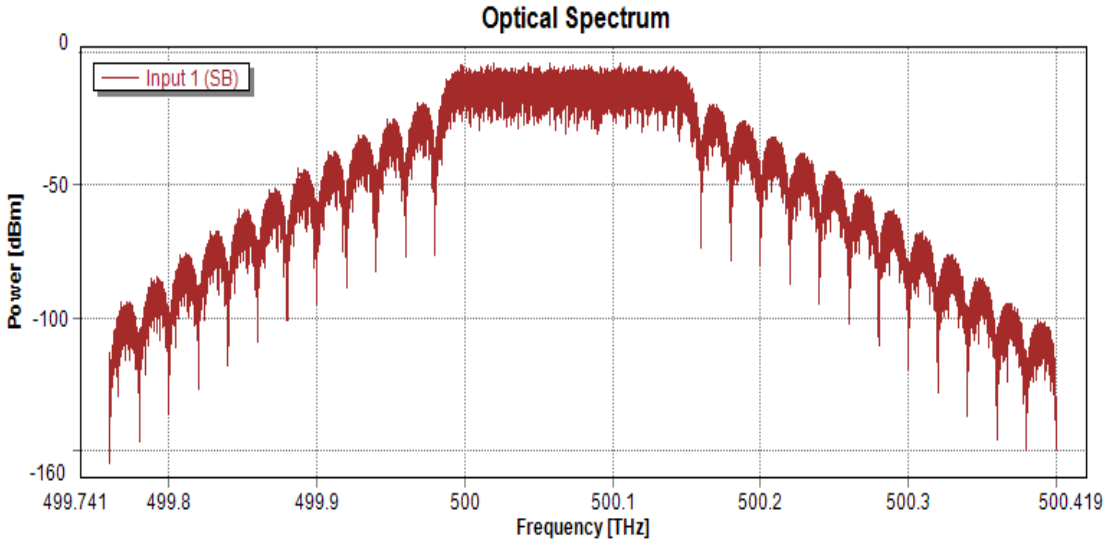

(a)

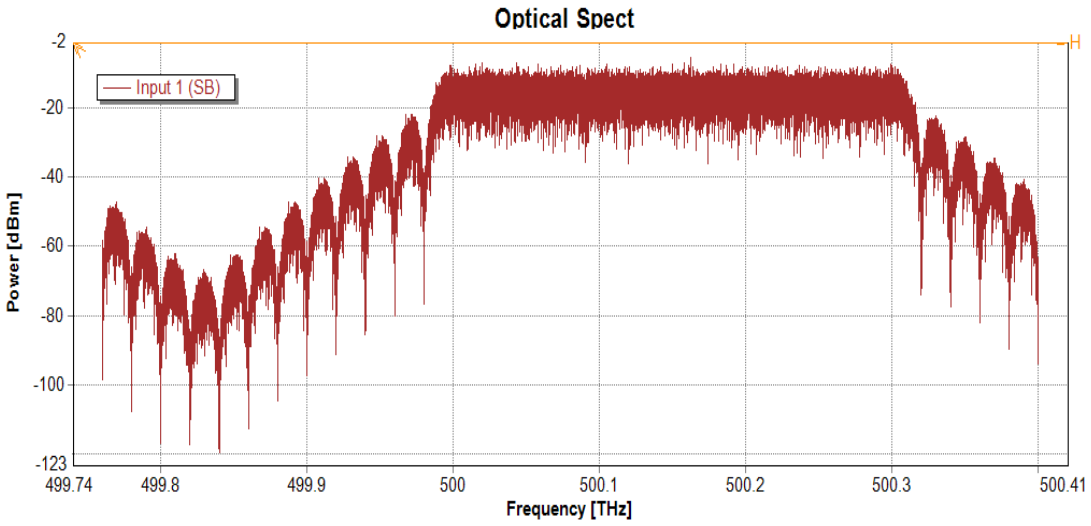

(b)

Figure 4.8 Optical spectrum of the transmitted signal for a) 8-channel AO-OFDM b) 16-channel AO-OFDM

4.3 All-optical OFDM receiver

After passing through the FSO channel with a 1-10 km LOS path length, the receiver received the propagated signal and utilized it into optical 8-OFFT and 16-OFFT (set of time delay and MMI). Fig. 4.9 shows the received signal waveform. Fig. 4.10 shows the received signal optical spectrum with 8 and 16 subcarriers, respectively. While Fig. 4.11 illustrated the optical signal spectrum after 8-OFFT and 16-OFFT.

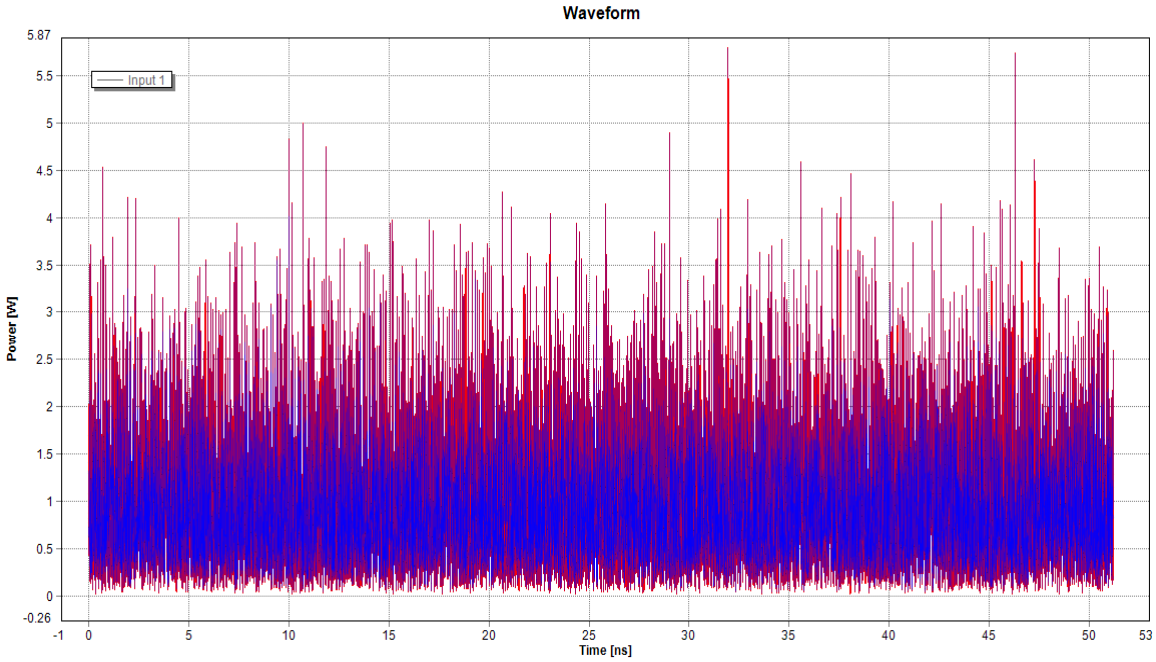

Figure 4.9 The received signal waveform

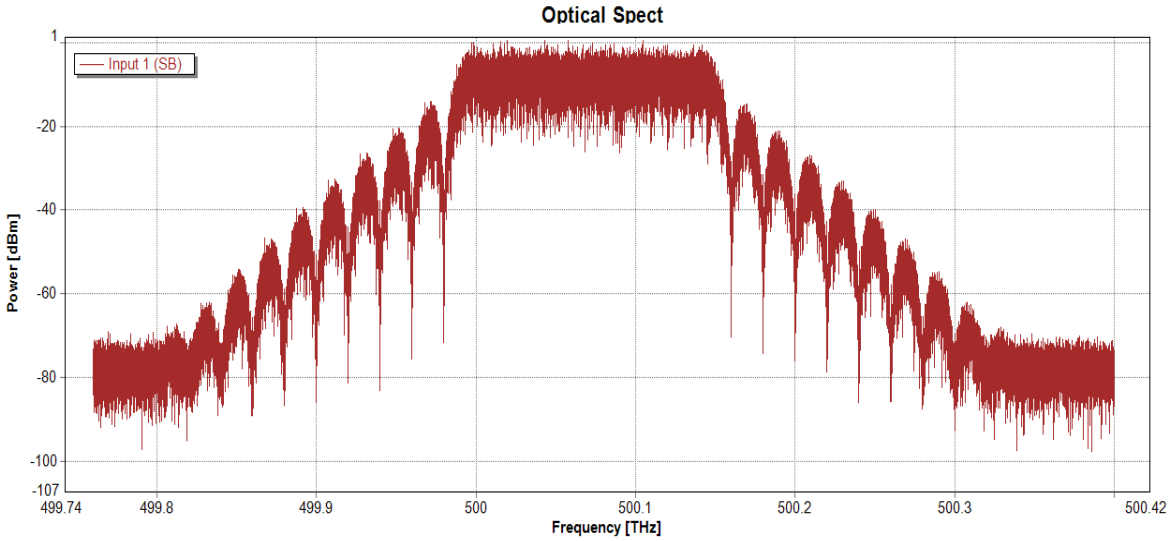

(a)

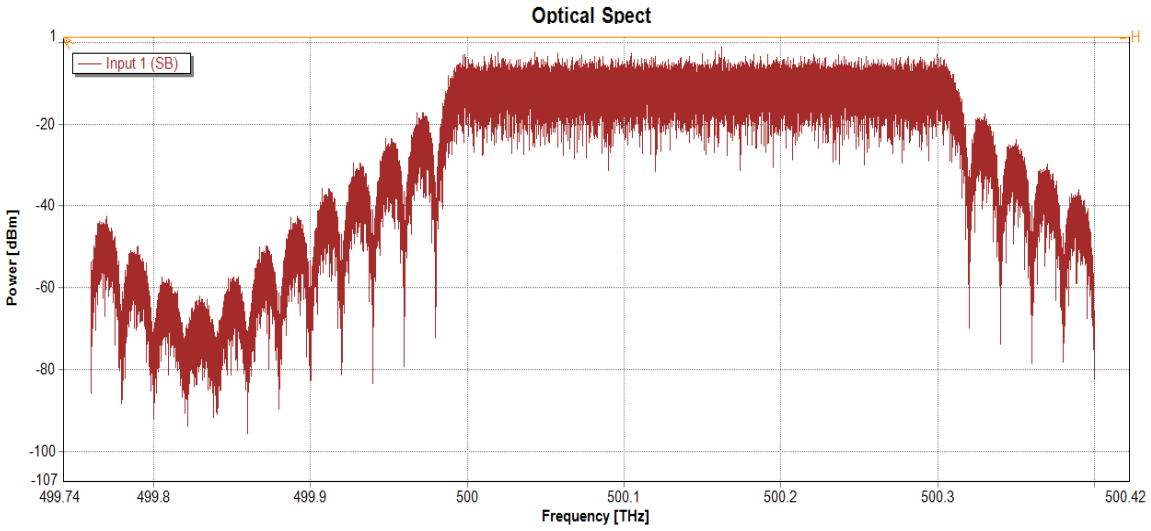

(b)

Figure 4.10 Optical spectrum of Received signal a) 8-OFFT b) 16-OFFT

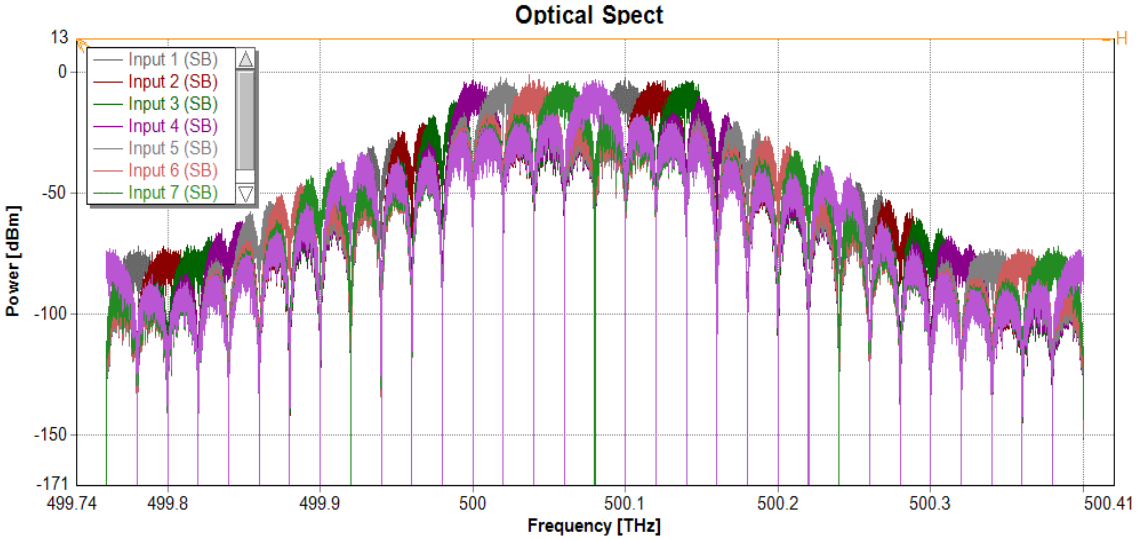

(a)

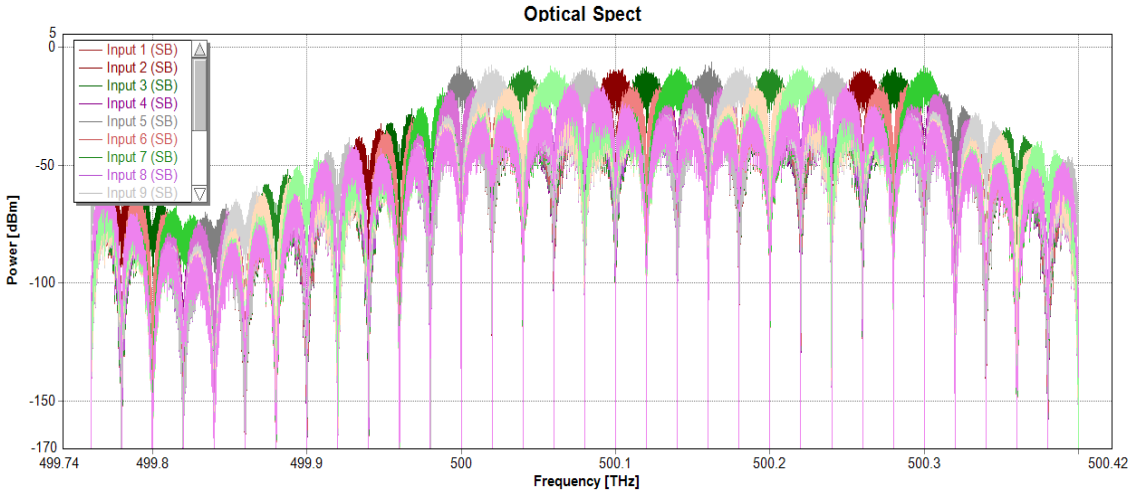

(b)

Figure 4.11 The signal optical spectrum after a) 8-OFFT b) 16-OFFT.

Afterwards, the selector was used to select the desired channel for the sampling process. The sampling process was performed using the optical gate and then applied to PBS and fed into dual-polarization coherent receiver, which contained eight photodetectors for detecting I/Q component. It produced an electrical signal, using DSP to recover the original signal. Fig. 4.12 illustrates the consultation diagram of BPSK, QPSK and 16-QAM received signal for proposed Li-Fi based AO-OFDM architecture.

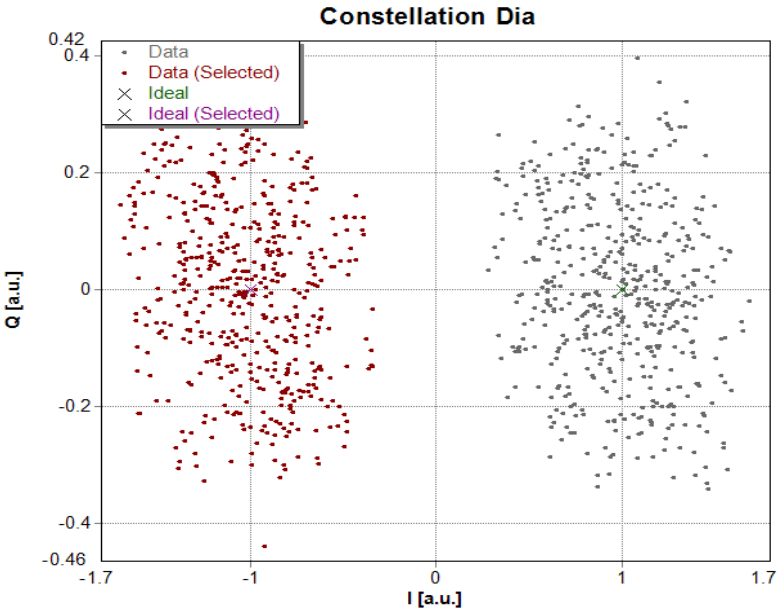
Constellation Dia
Data
Data (Selected)
Ideal
Ideal (Selected)
0.42
0.4
0.2
0
-0.2
-0.4
-0.46
Q [a.u.]
-1.7
-1
0
1
1.7
I [a.u.]

(a)

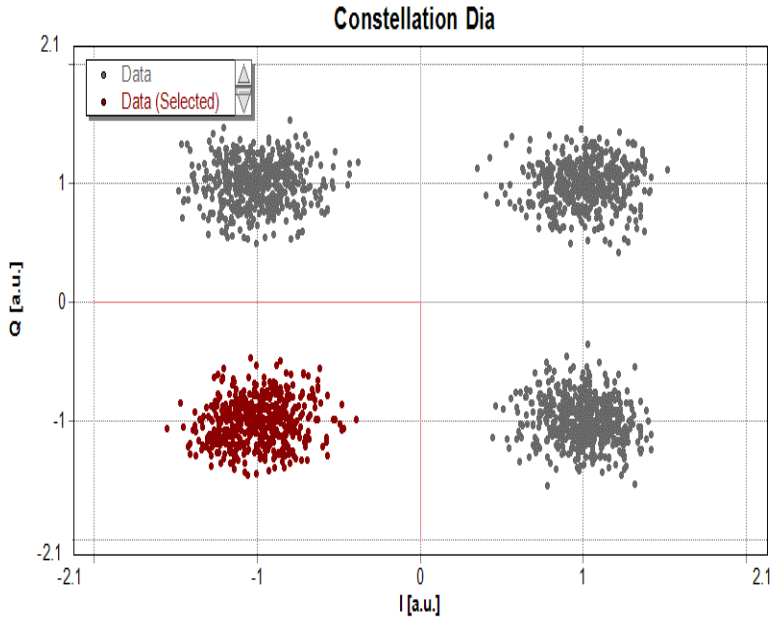
Constellation Dia
Data
Data (Selected)
2.1
1
0
-1
-2.1
Q [a.u.]
-2.1
-1
0
1
2.1
I [a.u.]

(b)

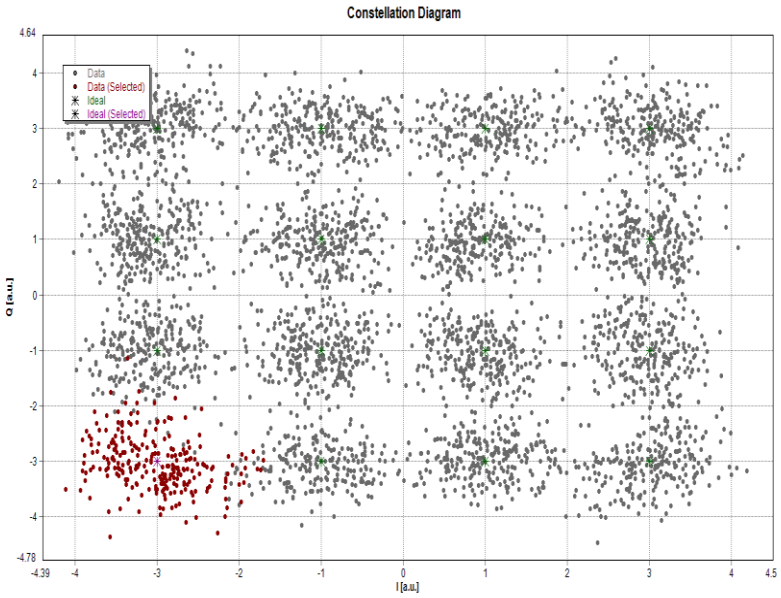

(c)

Figure 4.12 Received signal consultation Diagram of a) BPSK b) QPSK c)16-QAM

4.4 Tested the performance of the proposed system

4.4.1 Different OSNR values

The proposed system was tested under different OSNR (0-35dB) with observed effects on system BER and received signal power. Fig.4.13 shows the received signal with OSNR values 35 and 0 dBm, respectively. While table 4.3 illustrate the calculated received power and BER of the proposed system with different OFFT size and modulation scheme types under different values of OSNR.

The relationship between OSNR vs BER for both 8-OFFT and 16-OFFT for different modulation schemes is shown in Fig. 4.14.

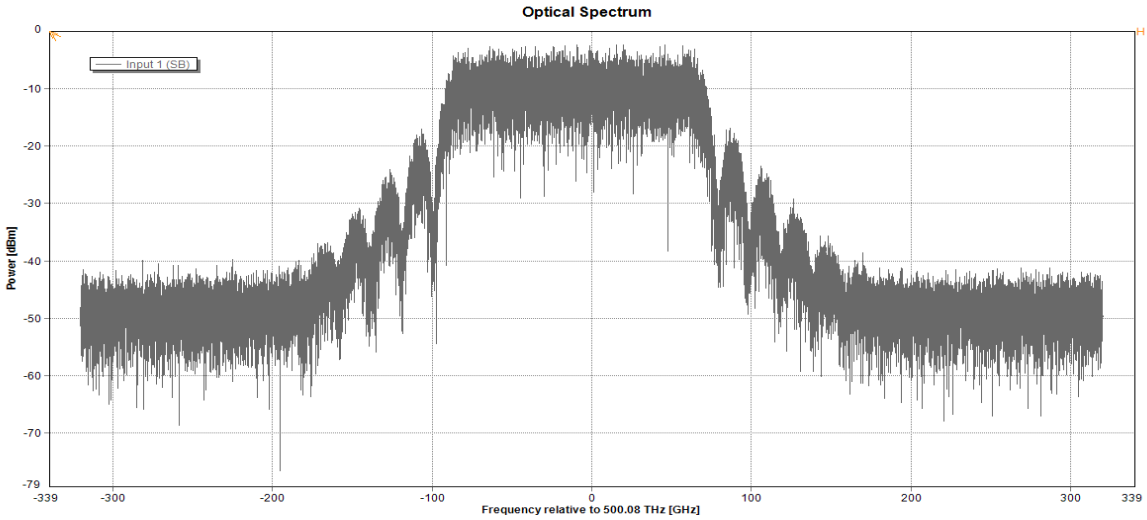

(a)

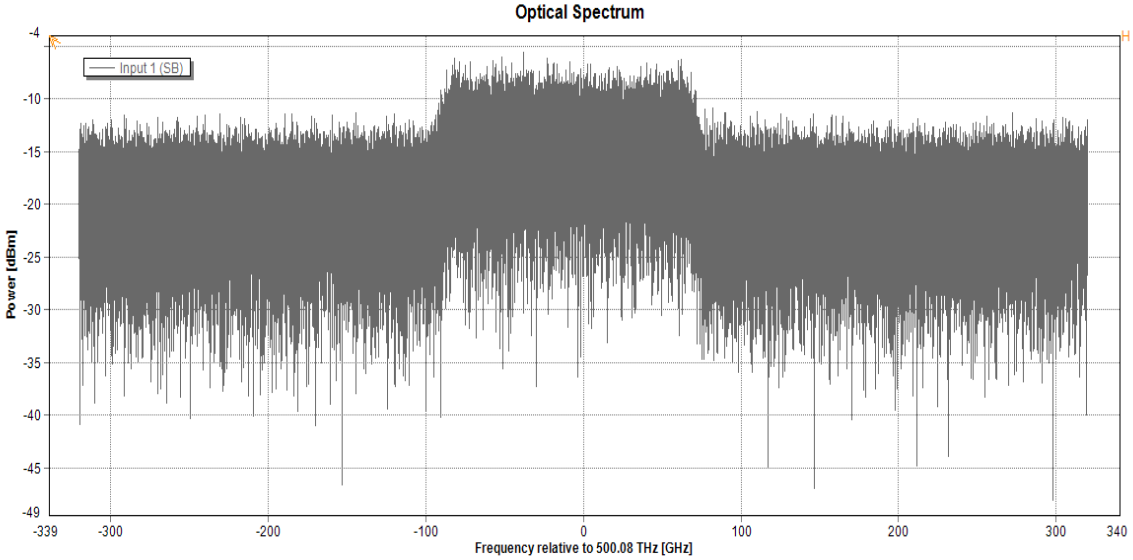

(b)

Figure 4.13 received optical signal with OSNR a) 35dB b) 0 dB

Table 4.3 OSNR vs BER for both 8-OFFT and 16-OFFT

OSNR	8-OFFT				16-OFFT			
	QPSK		16-QAM		BPSK		QPSK	
	BER	Received power	BER	Received power	BER	Received power	BER	Received power
0	0.67	~ -5 dBm	0.9	~ -7.8dBm	4e-3	~ -6.2dBm	1.2	~ -8dBm
5	0.01		0.55		1.5e-3		0.5	
10	1.3e-4		0.05		8.3e-4		0.41	
15	6.3e-7		9 e-3		7.7e-4		0.99	
20	1.08e-8		4.8 e-4		7.3e-5		7.3e-2	
25	1.39e-9		3.7 e-4		7.1e-5		5.3e-3	
30	5.89e-10		3.1 e-4		7.05e-5		5.7e-4	
35	4.15e-10		2.4 e-4		7 e-5		2.9e-4	

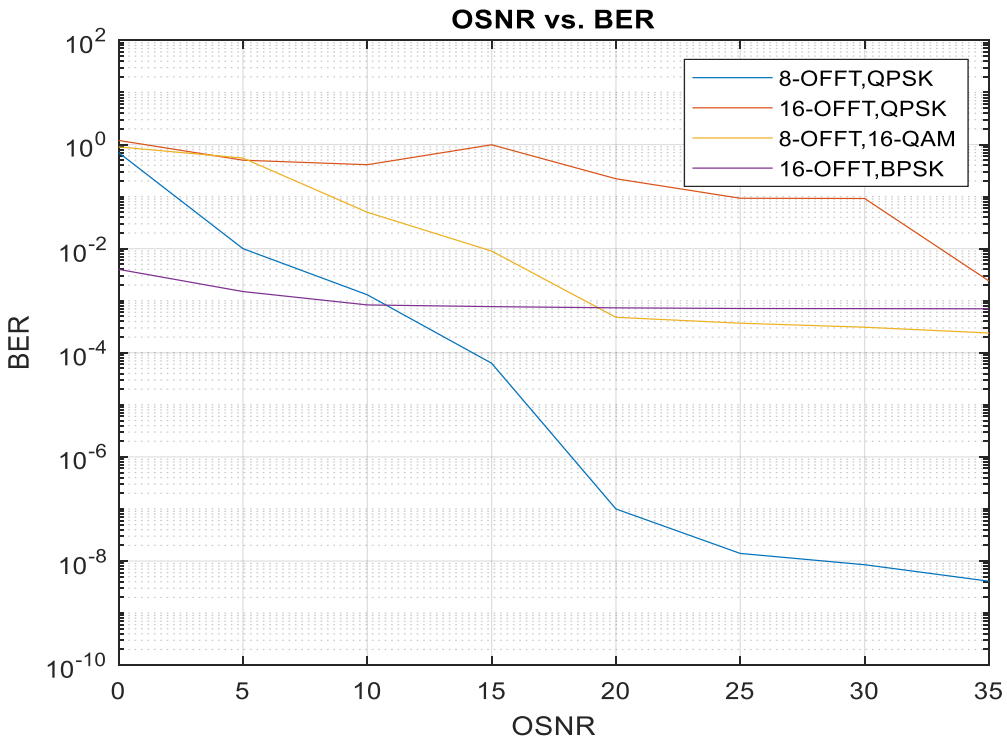

Figure 4.14 The relation between OSNR and BER

As shown in table 4.3, outdoor Li-Fi system shown a good performance in terms of strong received signal power and low BER for different OSNR compared with previous studies. The system offers a good received power of about -5dBm and -8dBm for 8-OFFT QPSK and 16-QAM respectively, for various values of OSNR (0-35 dB). In addition, the BER ranging between 1.08e-8 and 7.3e-2 at 20dB of OSNR for 8-OFFT and 16-OFFT respectivly.

Generally, the Li-Fi system-based AO-OFDM architecture performed better for QPSK and 8-OFFT than 16QAM and 16-OFFT in terms of BER. The proposed system was characterized by a good received signal for different OSNR as shown in table 4.3.

4.4.2 FSO channel link

The proposed simulated Li-Fi system-based AO-OFDM was tested under different FSO turbulence level and weather condition in terms of received power and BER, as explained in next sections.

I. Clear weather situation

The light signal produced by the proposed system was propagated over an FSO channel link and evaluated under various degrees of FSO scintillation and route length. Even in clear weather, the free-space propagated light signal suffers from scintillation (signal fading). The system was tested and analyzed under three situations of scintillation: strong, moderate, and low, with different path lengths (1-10Km) regarding BER and received power. The tables 4.4, 4.5, 4.6 and 4.7 shows the simulated system results for 8-OFFT and 16-OFFT with different modulation types (BPSK, QPSK, and 16-QAM). Fig. 4.15 shows the recorded received power at different path length for 8-OFFT&QPSK while Fig. 4.16

illustrate the optical spectrum of received signal after all OFFT at 10Km with 8-FFT and QPSK for low, Moderate, and strong turbulence.

Fig. 4.17, 4.18, and 4.19 shows the relations between the received signal power for different turbulence levels and path length for 8-OFFT&16-QAM, 16-OFFT&BPSK, and 16-OFFT&QPSK respectively.

Table 4.4 Received power for different atmosphere turbulence level (8-OFFT-QPSK)

Length (Km)	**Received power [dBm]**			
	8-OFFT& QPSK			
	Low turbulence	**Moderate turbulence**	**Strong turbulence**	**BER**
1	-5.58	-7.21	-15.02	5.3e-10 - 8.99e-10
2	-5.88	-7.90	-18.65	
3	-5.96	-8.26	-20.14	
4	-6.05	-9.21	-22.20	
5	-6.27	-9.94	-25.44	
6	-6.44	-10.04	-27.34	
7	-6.87	-10.22	-29.87	
8	-6.91	-10.89	-31.70	
9	-7.07	-11.40	-32.65	
10	-8.21	-11.88	-34.37	

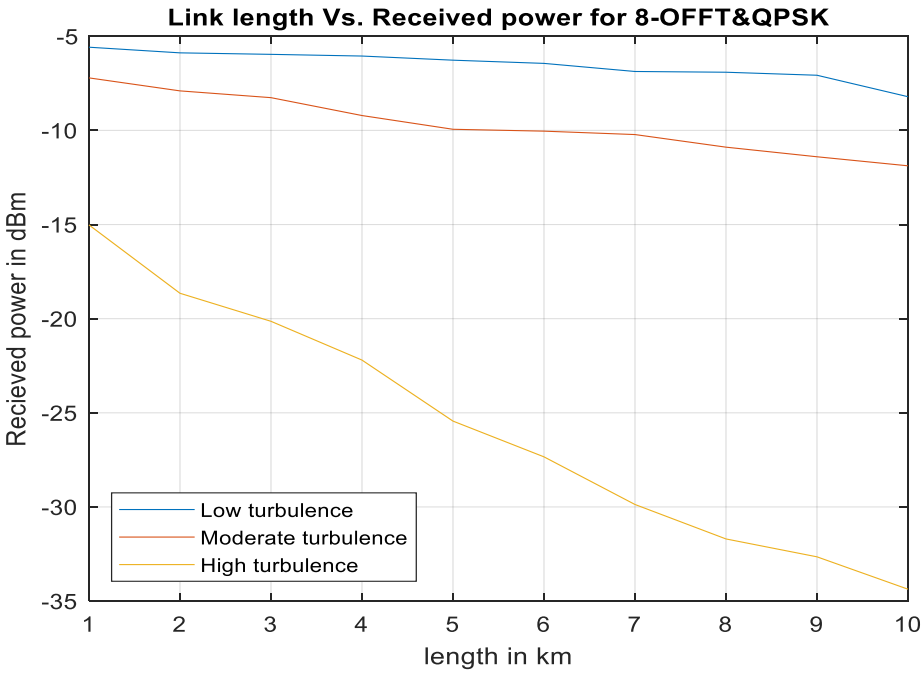

Fig. 4.15 Received power of (8-OFFT&QPSK) under different scintillation levels

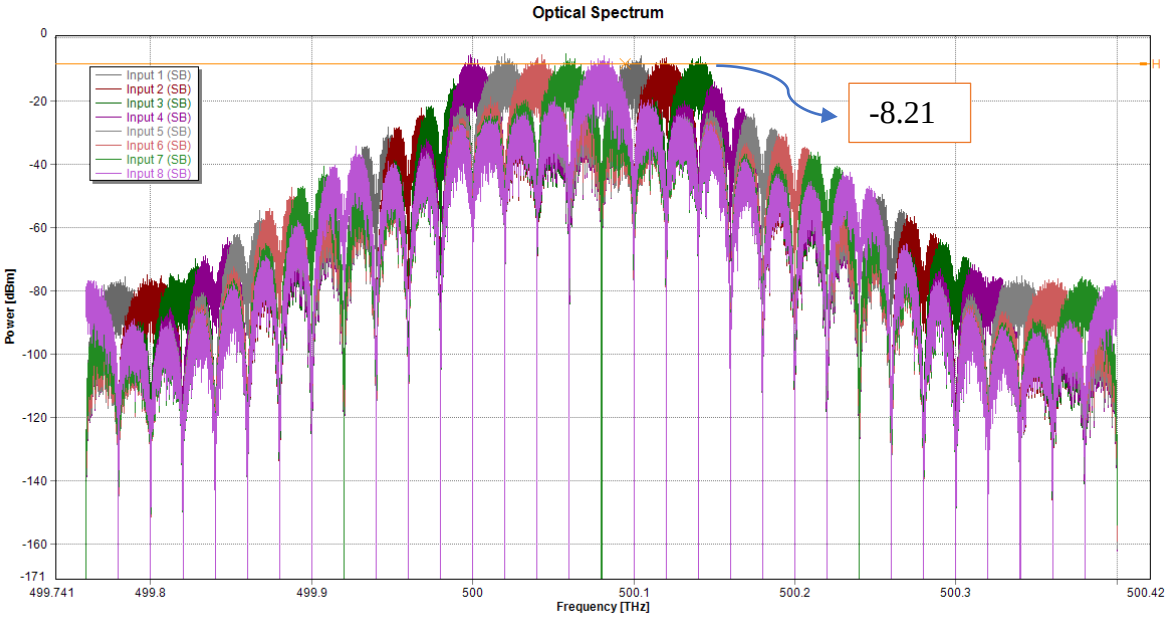

(a)

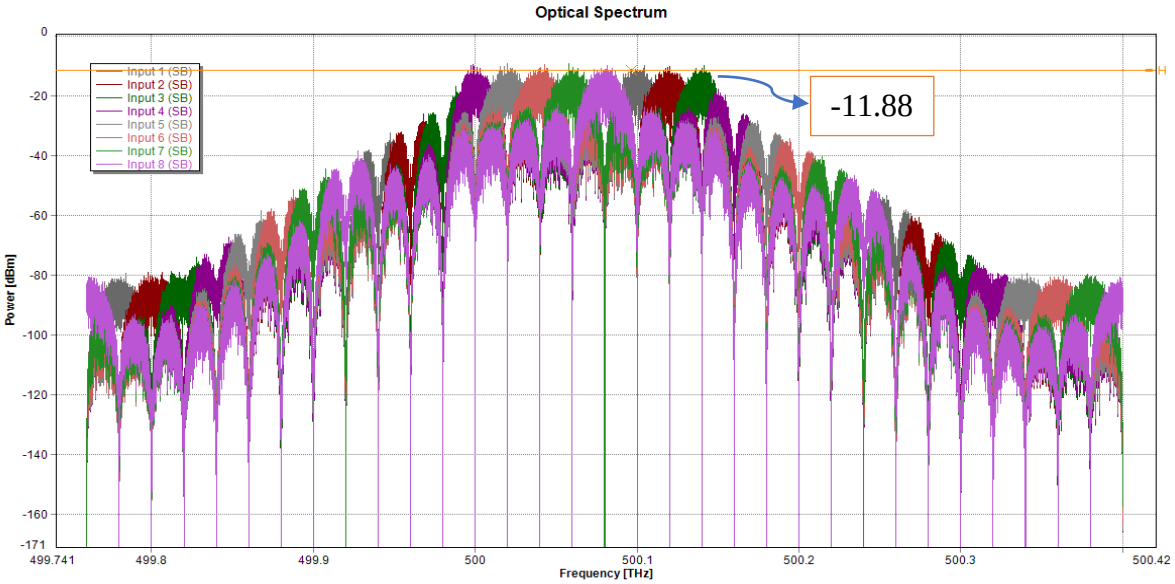

(b)

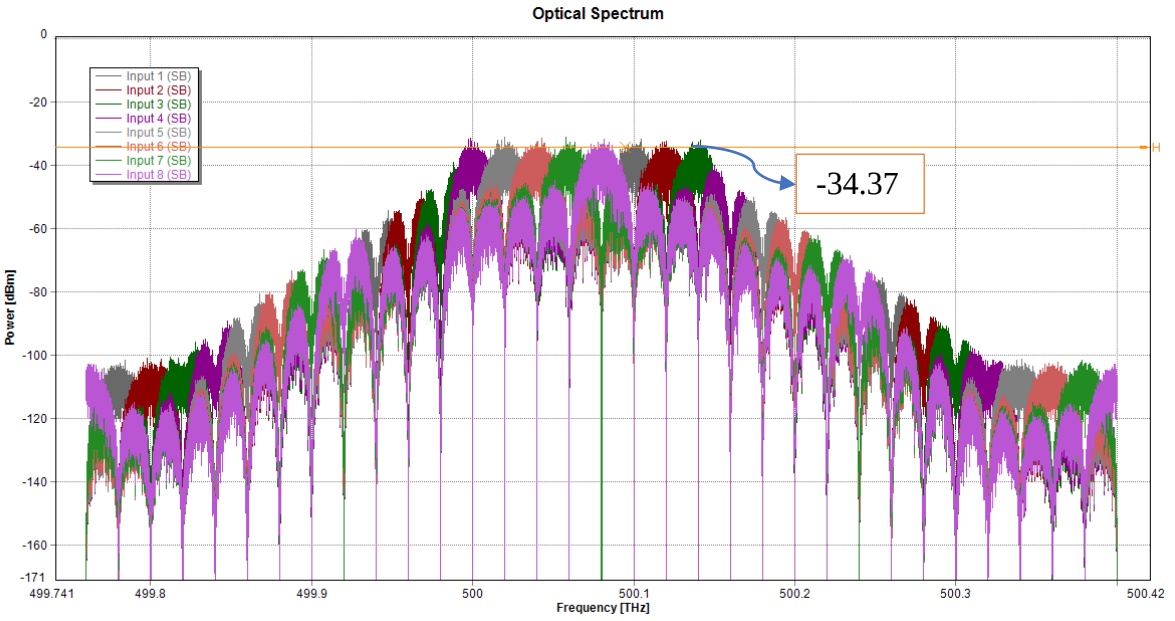

(c)

Figure 4.16 Optical spectrum of received signal after all optical FFT at 10Km with 8-FFT and QPSK for a) low turbulence b) Moderate turbulence c) Strong turbulence

Table 4.5 Received power and BER for different atmosphere turbulence level (8-OFFT-16-QAM)

Length (Km)	8-OFFT& 16-QAM			
	Received power [dBm]			BER
	Low turbulence	Moderate turbulence	Strong turbulence	
1	-6.70	-8.22	-26.77	4.1e-3 - 5.7e-3
2	-6.75	-8.50	-33.83	
3	-6.89	-8.96	-37.95	
4	-6.92	-9.21	-41.10	
5	-6.95	-9.54	-42.99	
6	-6.99	-9.75	-43.21	
7	-7.04	-10.20	-43.95	
8	-7.09	-10.56	-44.43	
9	-8.15	-11.02	-44.8	
10	-10.61	-12.6	-45.87	

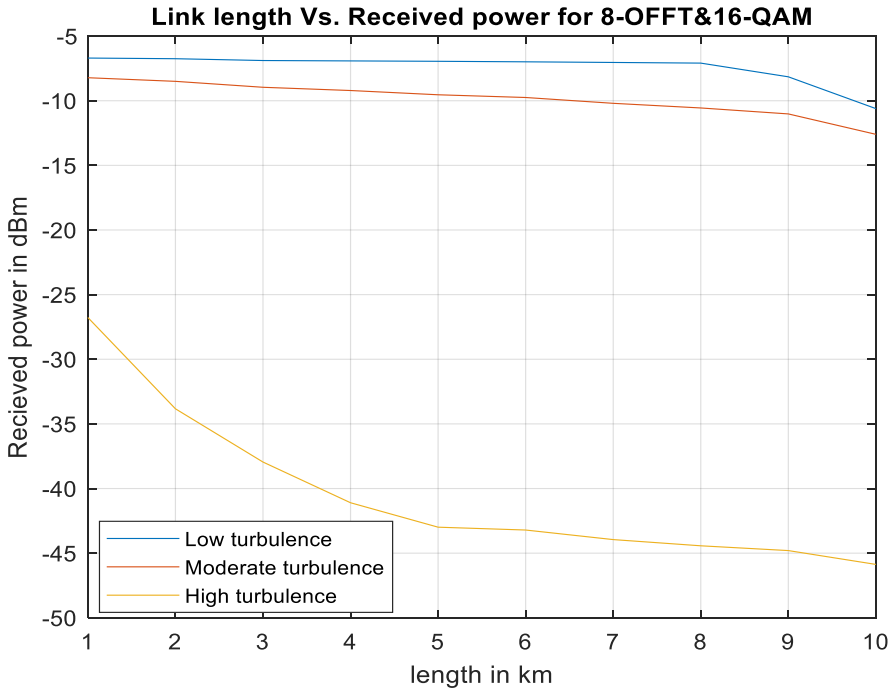

Fig. 4.17 Received power of (8-OFFT&16-QAM) under different scintillation levels

Table 4.6 Received power and BER for different atmosphere turbulence level (16-OFFT BPSK)

Length (Km)	16-OFFT& BPSK			
	Received power [dBm]			BER
	Low turbulence	Moderate turbulence	Strong turbulence	
1	-8.88	-9.29	-27.05	~ 5e-4
2	-8.94	-9.32	-27.65	
3	-8.99	-9.42	-28.09	
4	-9.12	-9.67	-29.62	
5	-9.43	-9.99	-30.4	
6	-9.55	-10.23	-31.54	
7	-9.89	-10.85	-32.03	
8	-10.02	-11.02	-33.72	
9	-10.22	-11.7	-35.66	
10	-10.34	-12.9	-36.54	

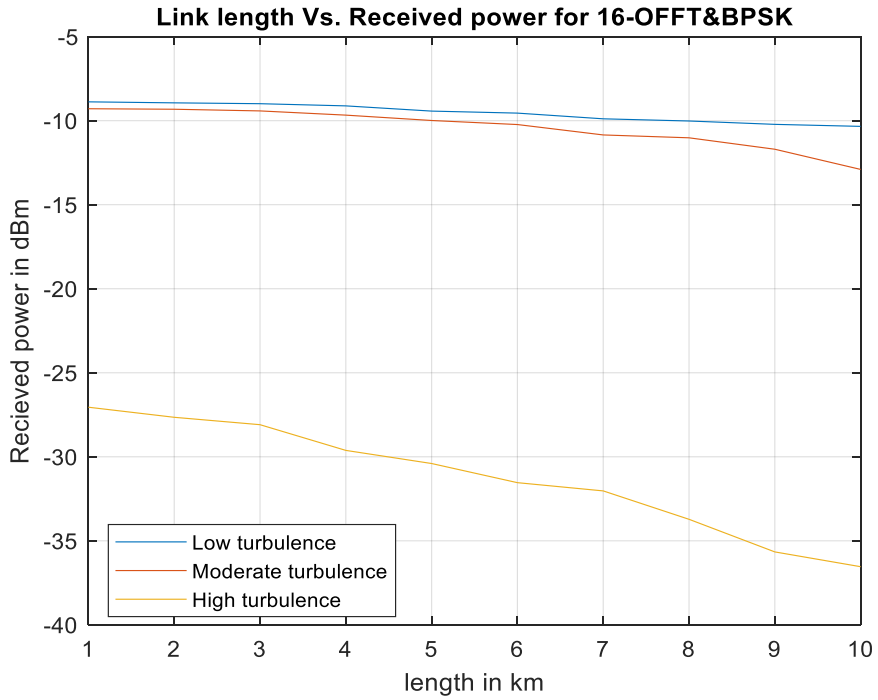

Fig. 4.18 Received power of (16-OFFT&BPSK) under different scintillation levels

Table 4.7 Received power and BER for different atmosphere turbulence level (16-OFFT QPSK)

Length (Km)	16-OFFT& QPSK			
	Received power [dBm]			BER
	Low turbulence	Moderate turbulence	Strong turbulence	
1	-8.27	-9.65	-19.09	5.5e-4 - 6.1e-4
2	-8.44	-9.81	-21.68	
3	-8.62	-10.21	-23.04	
4	-8.78	-10.37	-24.87	
5	-8.91	-10.71	-26.11	
6	-9.11	-11.04	-27.39	
7	-9.36	-11.39	-30.52	
8	-9.47	-11.87	-31.08	
9	-9.84	-11.98	-33.81	
10	-10.26	-12.31	-35.20	

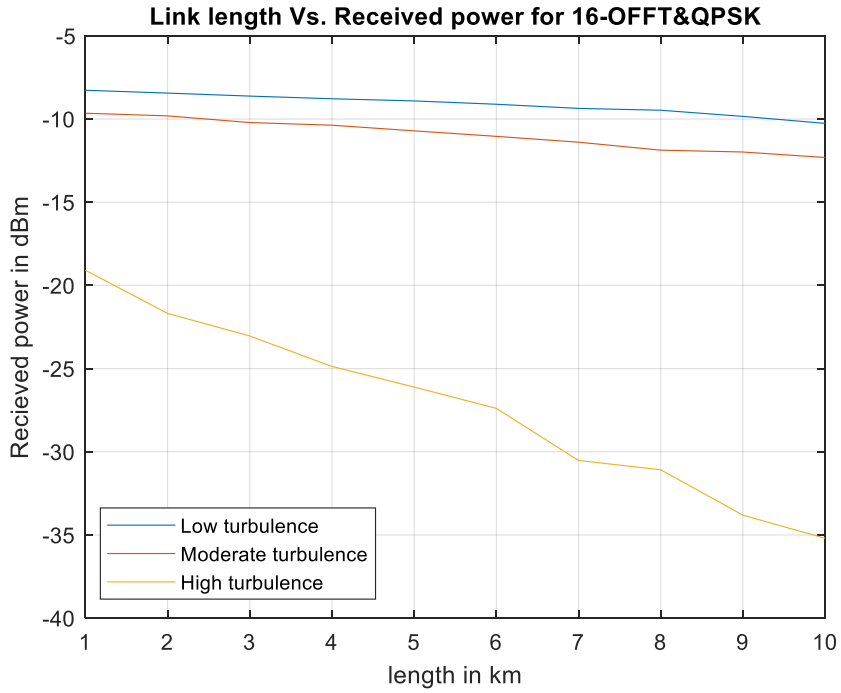

Fig. 4.19 Received power of (16-OFFT&QPSK) under different scintillation levels

As shown in tables 4.4, 4.5, 4.6 and 4.7, under three levels of scintillation the system decent an excellent performance with a clear constellation diagram, strong received power and good levels of BER. The path reaches 10 km of low turbulence free space and recorded about -5 and -12 dBm received power with ~5×10^{-10} and ~ 4×10^{-4} of BER for 8-OFFT and 16-OFFT, respectively. The system did not exhibit a large difference in its performance for moderate turbulence. While for strong turbulence, the system recorded -45 dBm and ~5×10^{-3} at 10 km of free space path length.

Generally, Outdoor Li-Fi system-based AO-OFDM shown a good performance in terms of high bit rate reaches 1.28 Tbps, low BER about 5×10^{-3} for worst case and strong received power, the received power ranging between 2 and -45 dBm with the different free space optic FSO - line of sight (LOS) path links (1-10Km) and different scintillation levels.

Fig. 4.20 shows a compression between the behavior of proposed systems in terms of received power of 8-OFFT and 16-OFFT for different modulation scheme under low, moderate, and strong turbulence, respectively. As shown with this figures the best behavior was belong to the 8-OFFT and QPSK modulation rather than other modulation methods for low, moderate and strong scintillation levels.

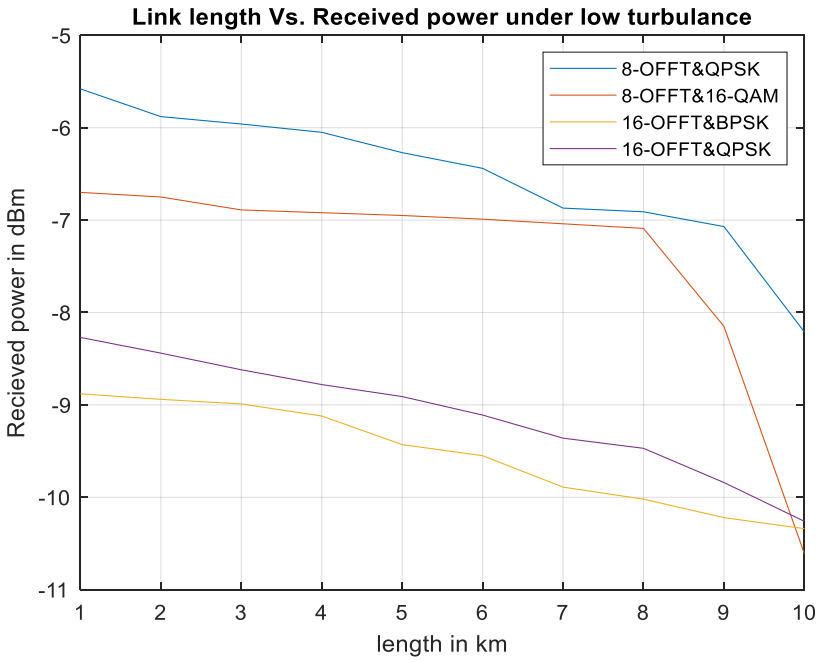
Link length Vs. Received power under low turbulance
8-OFFT&QPSK
8-OFFT&16-QAM
16-OFFT&BPSK
16-OFFT&QPSK
Recieved power in dBm
length in km
-5
-6
-7
-8
-9
-10
-11
1
2
3
4
5
6
7
8
9
10

(a)

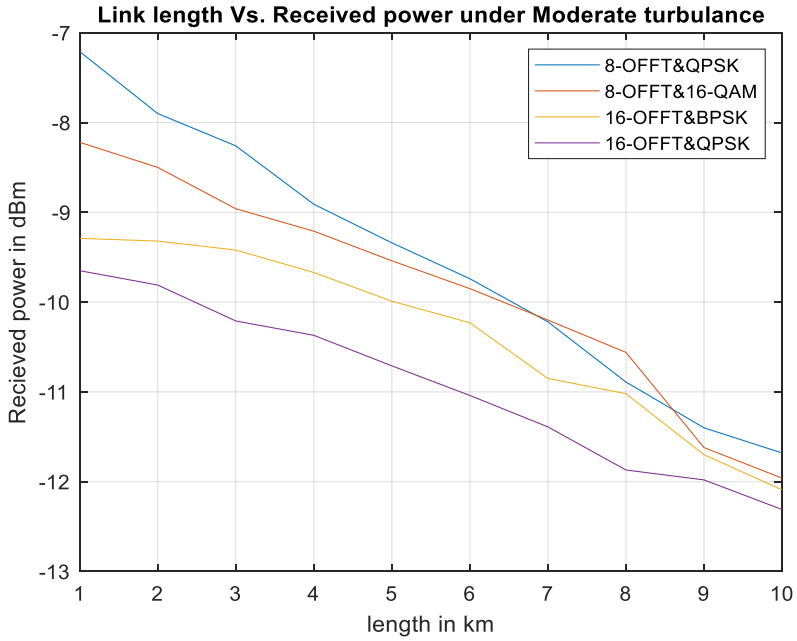
Link length Vs. Received power under Moderate turbulance
8-OFFT&QPSK
8-OFFT&16-QAM
16-OFFT&BPSK
16-OFFT&QPSK
Recieved power in dBm
length in km
-7
-8
-9
-10
-11
-12
-13
1
2
3
4
5
6
7
8
9
10

(b)

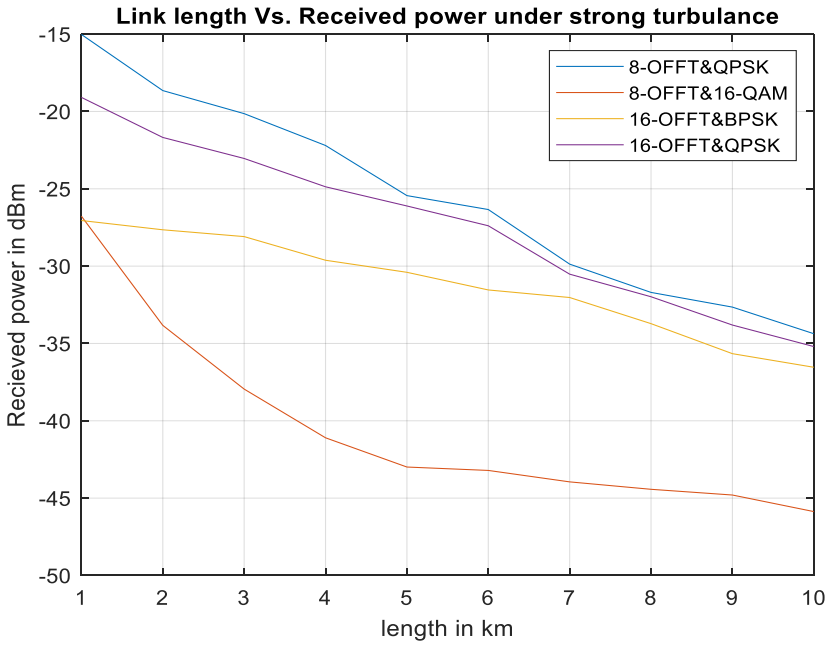

(c)

Fig. 4.20 The received signal power at different path length for 8 and 16-OFFT with different modulation scheme under a) Low turbulence b) Moderate turbulence c) Strong turbulence

II. Weather condition channel modelling

This study modelled the atmosphere channel using MATLAB through the utilization of the atmosphere attenuation formula as mentioned in chapter two. The signal behavior was tested with different visible band wavelengths (400, 500, 600, 700, and 800 nm) under this modelled channel, calculated the atmosphere attenuation for different path lengths 1-10 km based on visibility with two models Kim's and Kruse's as shown in Fig. 4.21 and Fig. 4.22. Fig. 4.23 illustrate the atmosphere attenuation for different wavelengths, as the wavelength increased, the atmosphere attenuation was reduced. 600nm was chosen as an emission wavelength of the laser source for the proposed Li-Fi system due to the fall with the visible band and low absorption property.

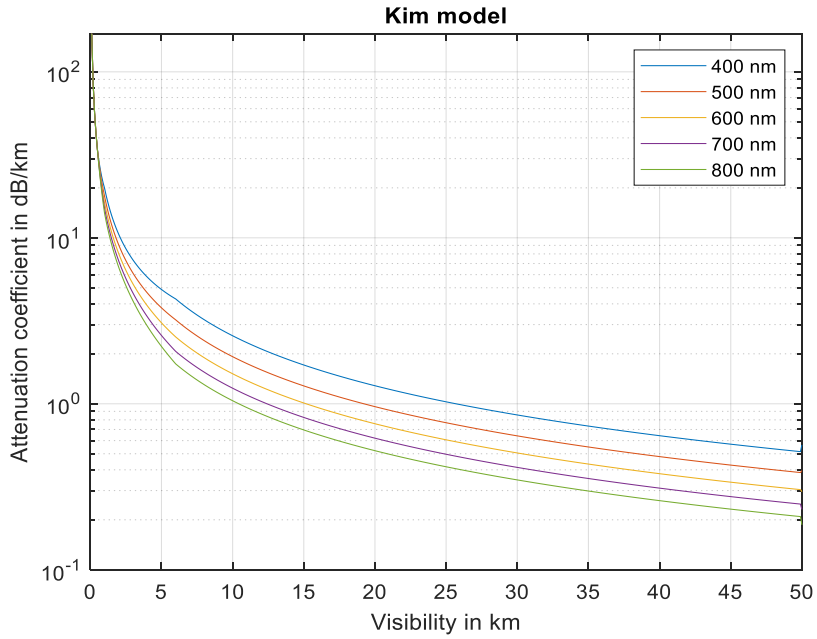

(a)

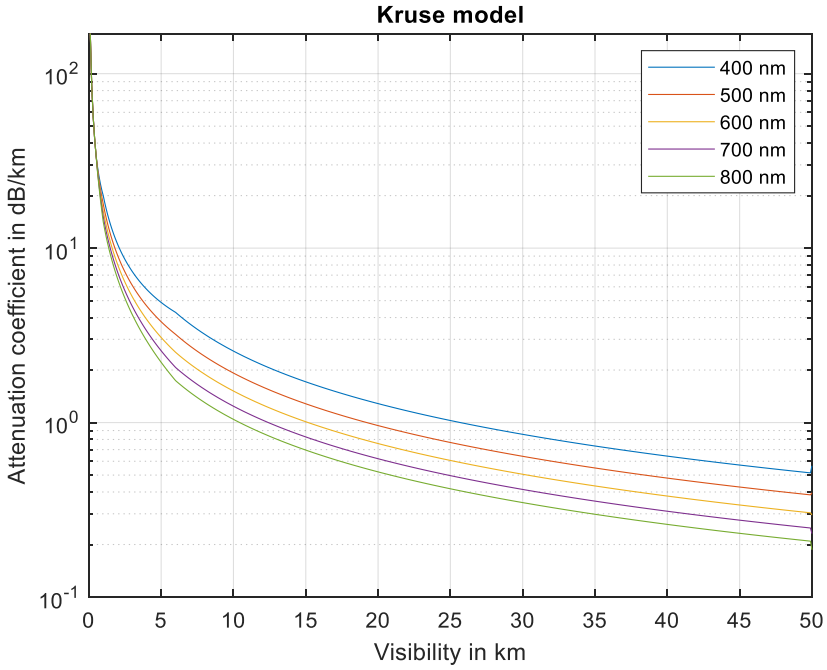

(b)

Figure 4.21 Attenuation coefficient for a) Kim model b) Kruse model

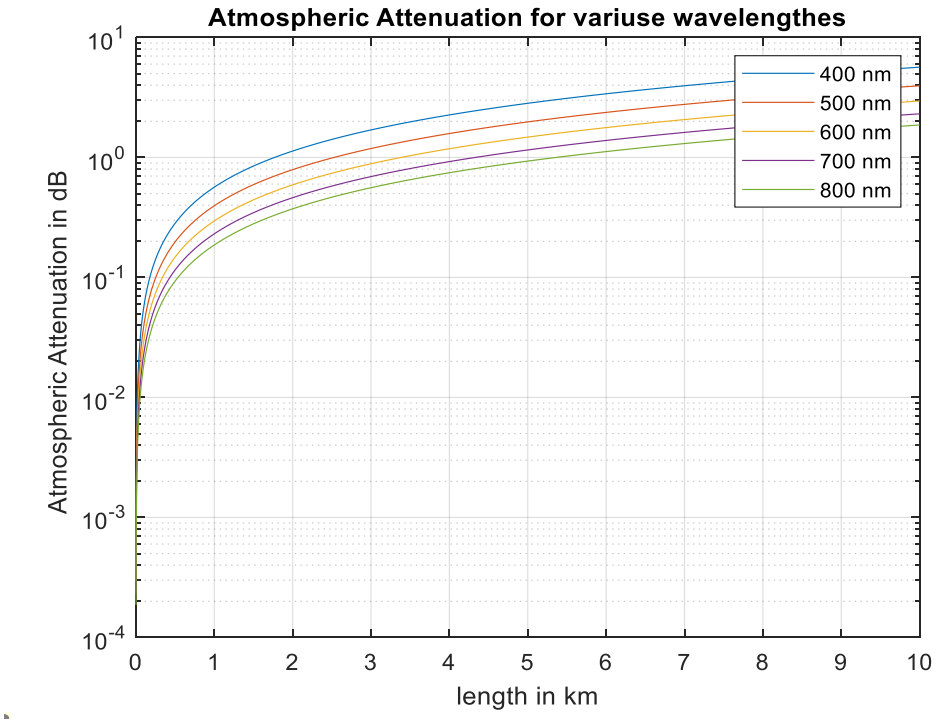

Figure 4.22 Atmosphere attenuation for different wavelength

Fog, Haze, and rain weather condition was utilized to test the proposed Li-Fi system.

a) Foggy or Hazy weather

600nm was chosen for the Li-Fi system optical source, utilized this wavelength under different Fog and Haze attenuation levels based on visibility in the modelled channel to calculate atmosphere attenuation values to this wavelength as shown in Fig. 4.23 and calculated the fog attenuation values as shown in table 4.8.

These attenuation values are utilized to the FSO channel link of the proposed simulated system in addition to the scintillation effect (Moderate level is chosen) to observe the behavior of the proposed system under these situations in terms of BER and received power as illustrated in Table 4.9, which is shows the calculated received signal power values and BER for 8-OFFT and 16-OFFT with different

modulation schemes under different level of fog weather condition. Fig. 4.24 shows this relation.

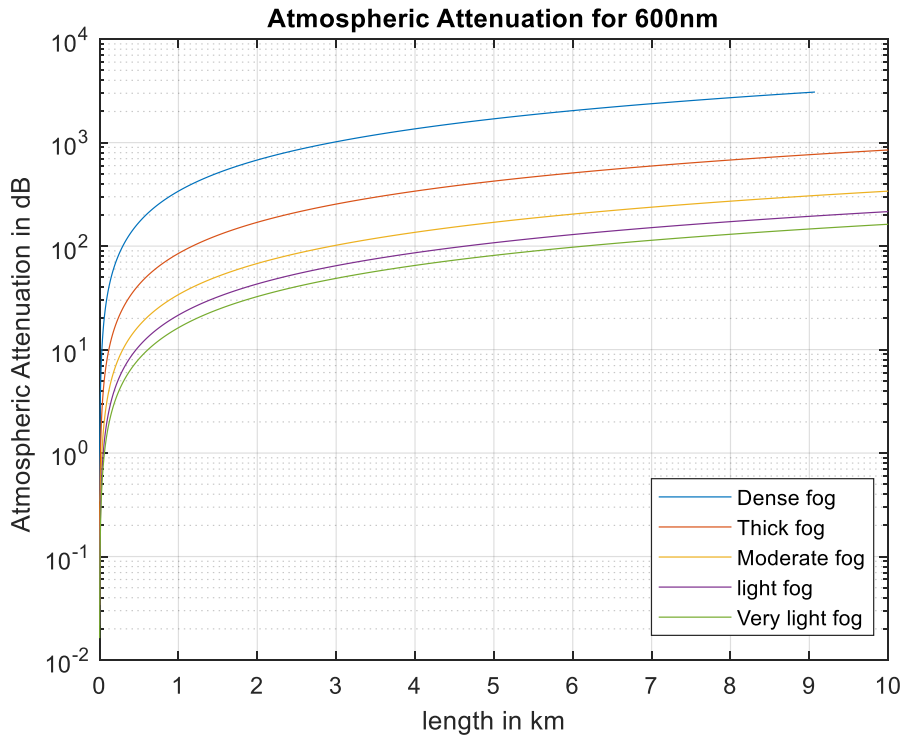

Figure 4.23 Atmosphere attenuation for 600nm

Table 4.8 Attenuation of 600nm for various levels of fog weather condition

Foggy weather condition	Visibility (m)	Attenuation (dB/Km)
Dense fog	50	331.7
Thich fog	200	83.72
Moderate fog	500	31.16
Light fog	770	20.32
Very light fog	1000	15.56

Table 4.9 Li-Fi system behavior for various foggy levels

Fog levels	8-OFFT				16-OFFT			
	QPSK		16-QAM		BPSK		QPSK	
	BER	Received power [dBm]	BER	Received power [dBm]	BER	Received power [dBm]	BER	Received power [dBm]
Dense	----	---	----	---	---	----	----	-----
Thick	4e-4 to 5 e-4	-80.9	5e-3 to 6e-3	-90.65	5e-4 to 7.2e-4	-86.33	5e-4 to 6 e-4	-88.9
Moderate		-30		-37.72		-34.02		-36.6
Light		-17.17		-25.96		-22.28		-24.8
Very light		-10.09		-21.97		-16.43		-18.26

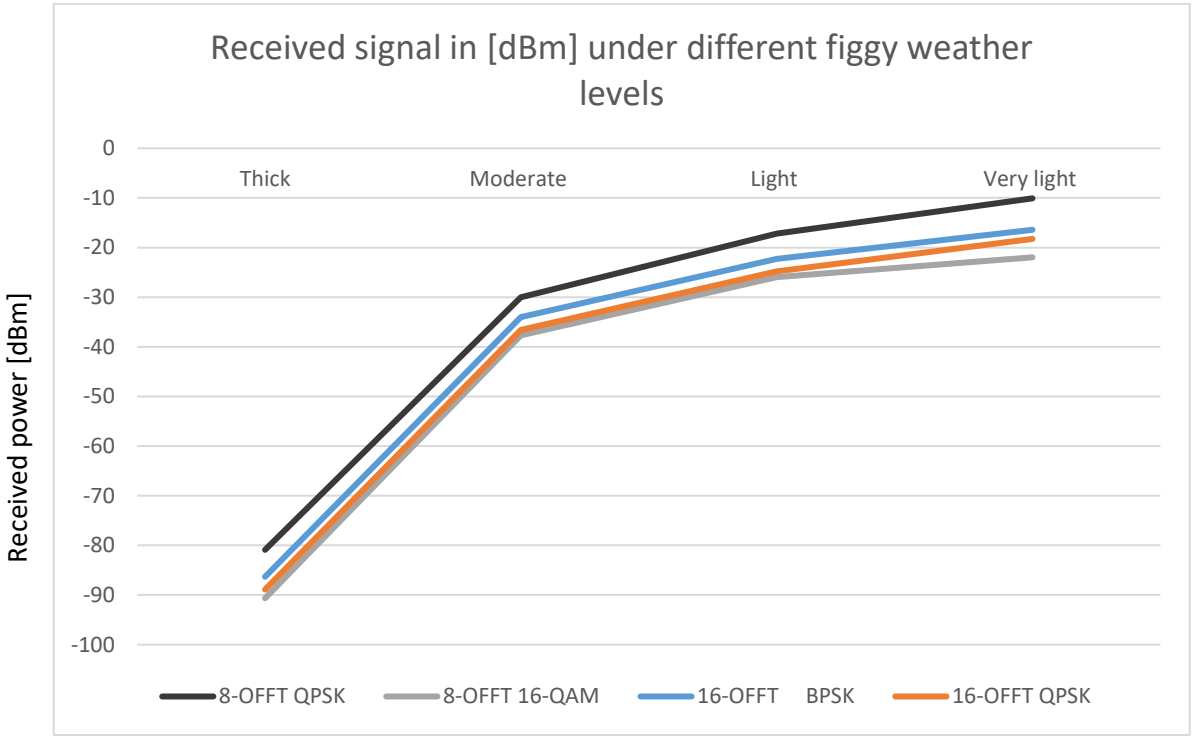

Fig. 4.24 The proposed system behavior for different modulation and OFFT size under different Fog attenuation levels.

As shown in table 4.9 and Fig.4.24 the proposed Li-Fi system decent an excellent performance for different OFFT size/ modulations schemes under different levels of foggy weather conditions in terms of strong received power with a clear constellation diagram, and good levels of BER performance.

Generally, the system did not exhibit a large difference in its performance for BER ranging between 6×10^{-3} and 4×10^{-4} for thick and very light fog levels respectively, while the received signal power ranging between -88 and -10 dBm for thick and very light fog condition, respectively.

Specifically, the best performance of the proposed system was belonging to 8-OFFT with QPSK modulation scheme in terms of received power compared with other types of OFFT size and modulation types.

b) Rainy weather

Rain attenuation is an independent wavelength; it depends on the rain precipitation intensity. Rain attenuation for different rain intensities is calculated based on its formula (eq. 2.78 in MATLAB) and Fig. 4.25 shows the calculated values of the relationship between precipitation intensity and rain attenuation, Rain attenuation in dB/Km for different intensity levels was calculated as shown in the table 4.10.

These attenuation values are utilized to the FSO channel link of the simulated proposed system in addition to the scintillation effect (moderate level was chosen) to observe the behavior of the proposed system under these situations in terms of received power and BER for 8-OFFT and 16 OFFT as shown in table 4.11 and Fig.4.26 shows the relation of received power for between different modulation schemes and OFFT size under various rain intensities values.

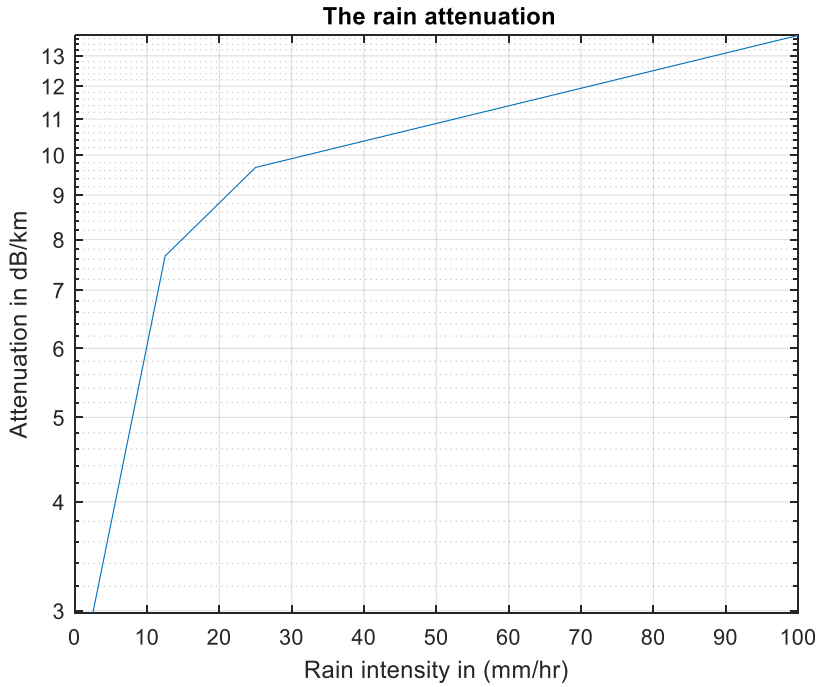

Figure 4.25 Rain attenuation for different rain intensity

Table 4.10 The Rain attenuation parameters

Rain weather condition	Precipitation intensity (mm/hr.)	Attenuation (dB/Km)
Storm	100	13.72
Strong rain	25	9.68
Average rain	12.5	7.66
Light rain	2.5	2.98
Drizzle	0.25	-3.72

Table 4.11 BER and Received power for different Rain path levels

Rain level	8-OFFT				16-OFFT			
	QPSK		16-QAM		BPSK		QPSK	
	BER	Received power [dBm]	BER	Received power [dBm]	BER	Received power [dBm]	BER	Received power [dBm]
Storm	5e-4 to 6.2e-4	-14.32	6e-4 to 7e-4	-16.44	7.2e-4 to 6.1e-4	-17.43	4e-4 to 5.5e-4	-17.04
Strong		-11.65		-13.8		-11.85		-12.56
Average		-9.05		-9.8		-9.91		-9.58
Light		-4.48		-6.17		-5.68		-8.12
Drizzle		-2.12		-2.84		-2.45		-2.52

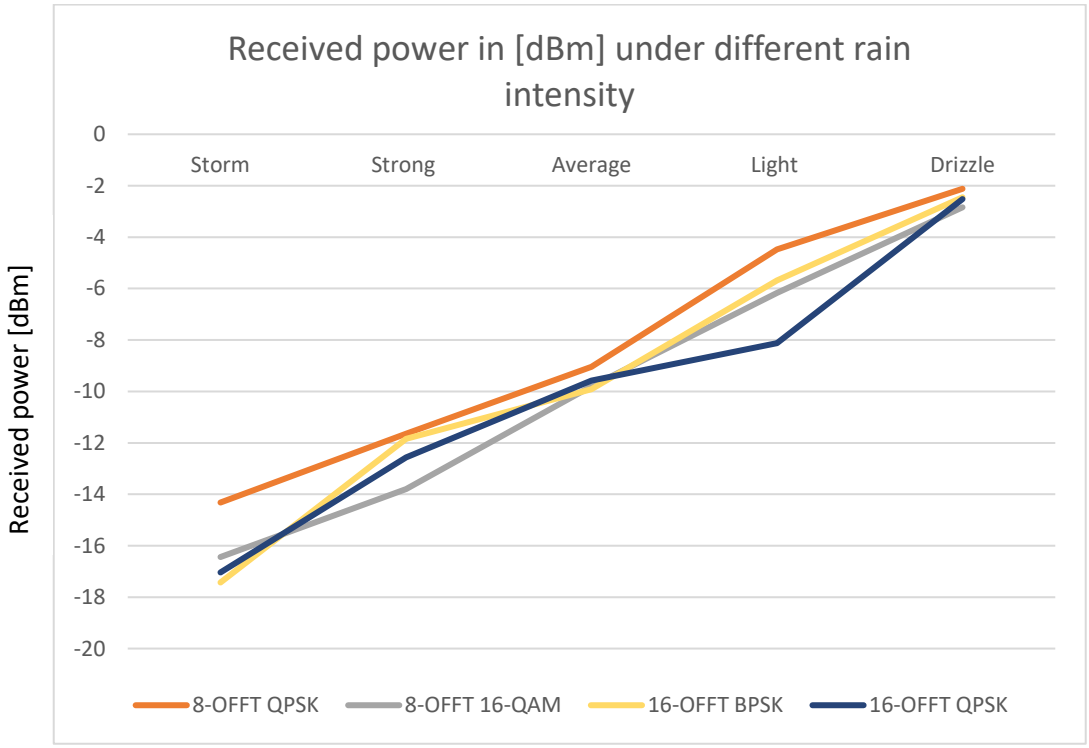

Figure 4.26 The proposed system behavior for different modulation and OFFT size under different rain intensity levels.

As illustrated in table 4.8 and Fig.4.26, the proposed Li-Fi system was tested under different level of rain precipitation intensity, the performance of the system not decent a large difference in the received power and BER under different level of rain intensity.

The proposed outdoor Li-Fi system successfully creates the orthogonality between eight and sixteen channels completely in the optical domain and performed AO-OFDM architecture at transmitter and receiver sides to design an ultra-high-speed Li-Fi system-based AO-OFDM with excellent performance compared with previous studies in terms of high bit rate reaches 1.28 Tbps, low BER, and strong received signal power.

The proposed system was immune against free space turbulence/weather conditions in terms of strong received power (ranging between 2 and -45 dBm) and low BER about 6×10^{-3} for the worst case with different OSNR (0-35 dB), FSO - LOS path links (1-10Km), different FSO turbulence levels (scintillation), and different weather condition situations (Foggy or hazy and rainy weather condition), table 4.12 show compression between previous studies and this work.

Table 4.12 highlights on the main difference between previous studies and present work

Parameters	**[13]**	**[21]**	**[29]**	**[30]**	**This work**
Work type	Simulated	Simulated	Simulated	Experiential	Simulated
Data rate for single channel (Gbps)	25	----	10	----	20
No. of channels	3	----	6	----	8&16
Optical carriers	LDs	LDs	LDs	LEDs	Single LD

Modulation scheme	QPSK	QPSK	----	IM/DD	BPSK, QPSK, 16-QAM
Multiplexing type	AO-OFDM optical interferometers	e-OFDM	AO-OFDM WSS	WDM	AO-OFDM
Channel spacing (GHz)		----	----	----	20
Channel link	Direct (Back-to-back)	FSO	Fiber	FSO Indoor	FSO (With different turbulence and weather condition)
Transmission distance	----	250 m	800 Km	1.6 m	1-10Km
Input power [mw]	----	-----	-----	----	35
Received signal power [dBm]	----	-----	-----	----	2-(-90)
BER or Q-Factor	10e-3 to 10e-16	Clear constellation diagram	20 Q-Factor	28×10^{-4}	1×10^{-10} to 6×10^{-3}
Total bitrate (bps)	75G	10 G	60 G	15.73G	640G &1.28T

Chapter Five

Conclusions and Future works

Chapter Five
Conclusions and future works

5.1 Conclusions

The proposed Li-Fi system uses an all-optical OFDM architecture to achieve the multi-carrier method. The study leads to the following key findings:

- ✓ CW laser diodes were utilized as optical sources of Li-Fi system to maximize the transmission distance through free space channel and overcome traditional LEDs' limitations.
- ✓ An effective optical frequency comb generator (OFCG) scheme was developed to minimize the optical sources on the transmission side while maximizing the transmission data rate. The system generated comb lines over VLC frequencies by utilizing the multi-carrier technique. It can be useful in VLC and DWDM applications. OFCG is characterized by its simplicity and tunability. Furthermore, the RF frequency signal's spacing between comb lines was easily tunable, making the proposed Li-Fi system more flexible for creating the orthogonality between multi-channels optically and implementing AO-OFDM architecture.
- ✓ Presented the effect of varying chirping factors of OFCG's modulators (MZMs) with three different values (α=3,5,7) on the performance of the proposed OFCG system.
- ✓ Successfully implemented Li-Fi system based on an All-optical OFDM architecture, this system suitable for outdoor applications to transmit the data collected from eight or sixteen channel through a free space channel link.

- ✓ AO-OFDM symbols were created by utilizing IFFT/FFT entirely in the optical domain between 8 and 16 channels. Each channel modulated its data on OFCG lines using dual-polarization I/Q modulator with QPSK and 16-QAM coding scheme.
- ✓ Optical IFFT was performed on the transmitter side based on OFCG and DWDM. However, optical FFT was successfully performed based on special structure of MMIs with time delays on the receiver side.
- ✓ 8-OFFT and 16-OFFT have been reported at the receiver.
- ✓ The Li-Fi system has shown a good performance compared with previous studies in terms of high bit rate, low BER, and strongly received power with different free space optic FSO - line of sight (LOS) path links and OSNR.
- ✓ The behavior of the proposed Li-Fi system-based AO-OFDM is tested under different levels of FSO turbulence and weather conditions.
- ✓ The system was more suitable for outdoor applications and immune to different atmospheric attenuation types due to utilizing AO-OFDM.

5.2 Suggestions for future works

1. Adopting an algorithm to compensates free-space channel turbulence in the design of the Li-Fi transmission system.
2. The MIMO system can solve issues related to free space channel impairments like physical obstructions and turbulence. It allows more data to be transmitted and received while differentiating data signals can be sent from different transceivers. It also minimizes the likelihood of errors.
3. Exploited A PAPR reduction techniques like selective mapping, interleaving, and partial transmit sequence for both IM/DD and coherent

detection systems can be utilized as future work to mitigate PAPR and improved the performance of optical OFDM systems.

4. Implementing Optical IFFT/FFT with more channels such as 32-OFFT and 64- OFFT.
5. A forward error correction technique can be utilized to improve the BER of the system.
6. Adopting a DSP process for the proposed Li-Fi system design to handle more data with higher modulation orders such as 16-QAM or 32-QAM

References

References

[1] A. Galisteo, "Visible light communication networks for iot and its applications," Universidad Carlos III de Madrid, Spain, 2020.

[2] A. T. Hussein and J. M. Elmirghani, "Mobile multi-gigabit visible light communication system in realistic indoor environment," *Journal of Lightwave Technology,* vol. 33, no. 15, pp. 3293-3307, 2015.

[3] R. Boluda-Ruiz, "On the performance of terrestrial free-space optical (FSO) links under the presence of generalized pointing errors," 2017.

[4] A. H. A. Kareem, "Design and Comprehensive Investigation of High Capacity Communication System Based on All Optical Orthogonal Frequency Division Multiplexing Processing."

[5] I. A. Murdas and A. N. Jabbar, "Light Fidelity Technology Technique and Parameters: A Review Paper," *Journal of University of Babylon for Engineering Sciences,* vol. 26, no. 9, pp. 35-41, 2018.

[6] H. Haas, "LiFi is a paradigm-shifting 5G technology," *Reviews in Physics,* vol. 3, pp. 26-31, 2018.

[7] W. Alheadary, "Free space optics for 5G backhaul networks and beyond," 2018.

[8] R. A. A. Othman, D. ap Sagaran, M. Mokayef, W. I. I. R. binti Wan, and M. Nasir, "Effective LiFi communication for IoT applications," in *2018 IEEE 4th International Symposium in Robotics and Manufacturing Automation (ROMA)*, 2018: IEEE, pp. 1-4.

[9] M. Abaza, "Cooperative MIMO techniques for outdoor optical wireless communication systems," Université de Bretagne occidentale-Brest, 2015.

[10] L. I. Albraheem, L. H. Alhudaithy, A. A. Aljaser, M. R. Aldhafian, and G. M. Bahliwah, "Toward designing a Li-Fi-based hierarchical IoT architecture," *IEEE access*, vol. 6, pp. 40811-40825, 2018.

[11] Z. Wang, D. Tsonev, S. Videv, and H. Haas, "On the design of a solar-panel receiver for optical wireless communications with simultaneous energy harvesting," *IEEE Journal on Selected areas in Communications*, vol. 33, no. 8, pp. 1612-1623, 2015.

[12] H. Haas, L. Yin, Y. Wang, and C. Chen, "What is lifi?," *Journal of lightwave technology*, vol. 34, no. 6, pp. 1533-1544, 2015.

[13] R. J. Ferreira, D. M. Dourado, M. M. Rodrigues, M. L. Rocha, S. M. Rossi, and D. M. Pataca, "All-optical fast fourier transform for processing an optical OFDM superchannel," in *2017 SBMO/IEEE MTT-S International Microwave and Optoelectronics Conference (IMOC)*, 2017: IEEE, pp. 1-5.

[14] V. Georlette, S. Bette, S. Brohez, R. Pérez-Jiménez, N. Point, and V. Moeyaert, "Outdoor visible light communication channel modeling under smoke conditions and analogy with fog conditions," *Optics*, vol. 1, no. 3, pp. 259-281, 2020.

[15] C.-L. Ying, H.-H. Lu, C.-Y. Li, C.-J. Cheng, P.-C. Peng, and W.-J. Ho, "20-Gbps optical LiFi transport system," *Optics letters*, vol. 40, no. 14, pp. 3276-3279, 2015.

[16] D. Tsonev, S. Videv, and H. Haas, "Towards a 100 Gb/s visible light wireless access network," *Optics express*, vol. 23, no. 2, pp. 1627-1637, 2015.

[17] M. Ayyash *et al.*, "Coexistence of WiFi and LiFi toward 5G: concepts, opportunities, and challenges," *IEEE Communications Magazine*, vol. 54, no. 2, pp. 64-71, 2016.

[18] H. Chun *et al.*, "LED based wavelength division multiplexed 10 Gb/s visible light communications," *Journal of lightwave technology*, vol. 34, no. 13, pp. 3047-3052, 2016.

[19] A. E.-N. A. Mohamed, A. N. Z. Rashed, M. S. Tabbour, and A. M. Ismail, "Performance enhancement of free space optical (FSO) systems using polarized DWDM-OFDM technique under atmospheric disturbances," in *2017 13th International Computer Engineering Conference (ICENCO)*, 2017: IEEE, pp. 8-13.

[20] R. Bian, I. Tavakkolnia, and H. Haas, "10.2 Gb/s visible light communication with off-the-shelf LEDs," in *2018 European Conference on Optical Communication (ECOC)*, 2018: IEEE, pp. 1-3.

[21] C. Verma and C. Selwal, "4QAM OFDM visible light communication using laser," in *2018 7th International Conference on Reliability, Infocom Technologies and Optimization (Trends and Future Directions)(ICRITO)*, 2018: IEEE, pp. 618-622.

[22] A. R. Ndjiongue and H. C. Ferreira, "An overview of outdoor visible light communications," *Transactions on Emerging Telecommunications Technologies*, vol. 29, no. 7, p. e3448, 2018.

[23] A. Israr, A. Israr, F. Khan, and F. Khan, "Optimal modulation technique for MIMO FSO link," *Wireless Personal Communications*, vol. 109, no. 2, pp. 695-714, 2019.

[24] R. George, S. Vaidyanathan, A. S. Rajput, and K. Deepa, "LiFi for vehicle to vehicle communication–a review," *Procedia Computer Science*, vol. 165, pp. 25-31, 2019.

[25] M. Adel, H. Seleem, M. Nasr, and H. El-Khobby, "Transmission of 128 Gb/s Optical QPSK Signal over FSO Channel under Different Weather Conditions

and Pointing Errors," in *Journal of Physics: Conference Series*, 2020, vol. 1447, no. 1: IOP Publishing, p. 012055.

[26] C. Lee *et al.*, "Advanced lifi technology: Laser light," in *Light-emitting devices, materials, and applications XXIV*, 2020, vol. 11302: SPIE, pp. 116-123.

[27] H. Haas *et al.*, "Introduction to indoor networking concepts and challenges in LiFi," *Journal of Optical Communications and Networking*, vol. 12, no. 2, pp. A190-A203, 2020.

[28] D. Wang, X. Tang, L. Xi, X. Zhang, W. Zhang, and H. Zhang, "A scheme to generate 16QAM-OFDM vector mm-wave signal based on a single MZM without optical filter and precoding," *Optics Communications*, vol. 475, p. 126227, 2020.

[29] J. Hoxha, S. Shimizu, and G. Cincotti, "On the performance of all-optical OFDM based PM-QPSK and PM-16QAM," *Telecommunication Systems*, vol. 75, no. 4, pp. 355-367, 2020.

[30] R. Bian, I. Tavakkolnia, and H. Haas, "15.73 Gb/s visible light communication with off-the-shelf LEDs," *Journal of Lightwave Technology*, vol. 37, no. 10, pp. 2418-2424, 2019.

[31] S. Arnon, J. Barry, G. Karagiannidis, R. Schober, and M. Uysal, *Advanced optical wireless communication systems*. Cambridge university press, 2012.

[32] H. Elgala, R. Mesleh, and H. Haas, "Indoor optical wireless communication: potential and state-of-the-art," *IEEE Communications Magazine*, vol. 49, no. 9, pp. 56-62, 2011.

[33] D. Kedar and S. Arnon, "Urban optical wireless communication networks: the main challenges and possible solutions," *IEEE Communications Magazine*, vol. 42, no. 5, pp. S2-S7, 2004.

[34] M. Z. Chowdhury, M. T. Hossan, A. Islam, and Y. M. Jang, "A comparative survey of optical wireless technologies: Architectures and applications," *ieee Access,* vol. 6, pp. 9819-9840, 2018.

[35] Z. Ghassemlooy, W. Popoola, and S. Rajbhandari, *Optical wireless communications: system and channel modelling with Matlab®*. CRC press, 2019.

[36] A. Parmar, A. Sharma, and C. Guleria, "Analysis of optical wireless communication systems," *Journal of Optical Communications*, vol. 42, no. 3, pp. 481-484, 2021.

[37] S. N. Pottoo, R. Goyal, and A. Gupta, "Performance investigation of optical communication system using FSO and OWC channel," in *2020 Indo–Taiwan 2nd International Conference on Computing, Analytics and Networks (Indo-Taiwan ICAN)*, 2020: IEEE, pp. 176-180.

[38] H. Haas, J. Elmirghani, and I. White, "Optical wireless communication," vol. 378, ed: The Royal Society Publishing, 2020, p. 20200051.

[39] F. V. Fiordigigli, "Transport protocols performance on visible light communication technology," Universitat Politècnica de Catalunya, 2018.

[40] M. Saadi, T. Ahmad, M. Kamran Saleem, and L. Wuttisittikulkij, "Visible light communication–an architectural perspective on the applications and data rate improvement strategies," *Transactions on Emerging Telecommunications Technologies,* vol. 30, no. 2, p. e3436, 2019.

[41] E. Gerhátné Udvary, "Visible light communication survey," *Infocommunications journal,* vol. 11, no. 2, pp. 22-31, 2019.

[42] F. Zafar, M. Bakaul, and R. Parthiban, "Laser-diode-based visible light communication: Toward gigabit class communication," *IEEE Communications Magazine,* vol. 55, no. 2, pp. 144-151, 2017.

[43] Y. Guo *et al.*, "A tutorial on laser-based lighting and visible light communications: device and technology," *Chinese Optics Letters*, vol. 17, no. 4, p. 040601, 2019.

[44] L. Yang, X. Gao, and M.-S. Alouini, "Performance analysis of free-space optical communication systems with multiuser diversity over atmospheric turbulence channels," *IEEE Photonics Journal*, vol. 6, no. 2, pp. 1-17, 2014.

[45] A. Malik and P. Singh, "Free space optics: current applications and future challenges," *International Journal of Optics*, vol. 2015, 2015.

[46] O. Bouchet, H. Sizun, C. Boisrobert, and F. De Fornel, *Free-space optics: propagation and communication*. John Wiley & Sons, 2010.

[47] H. Willebrand and B. S. Ghuman, *Free space optics: enabling optical connectivity in today's networks*. SAMS publishing, 2002.

[48] D. Tsonev, S. Videv, and H. Haas, "Light fidelity (Li-Fi): towards all-optical networking," in *Broadband Access Communication Technologies VIII*, 2014, vol. 9007: SPIE, p. 900702.

[49] J. Santos *et al.*, "Visible light communication using InGaN optical sources with AlInGaP nanomembrane down-converters," *Optics express*, vol. 24, no. 9, pp. 10020-10029, 2016.

[50] C. Basu, M. Meinhardt-Wollweber, and B. Roth, "Lighting with laser diodes," *Advanced Optical Technologies*, vol. 2, no. 4, pp. 313-321, 2013.

[51] M. A. N. Perera, "Design and implementation of a light-based IoT (LIoT) node using printed electronics," Master's thesis, University of Oulu, 2020.

[52] C. Lee, *III-nitride Laser Diode for Visible Light Communication*. University of California, Santa Barbara, 2017.

[53] X. Li, B. Hussain, L. Wang, J. Jiang, and C. P. Yue, "Design of a 2.2-mW 24-Mb/s CMOS VLC receiver SoC with ambient light rejection and post-

equalization for Li-Fi applications," *Journal of Lightwave Technology,* vol. 36, no. 12, pp. 2366-2375, 2018.

[54] V. M. Baeza, M. Sánchez-Fernández, A. G. Armada, and A. Royo, "Testbed for a LiFi system integrated in streetlights," in *2015 European Conference on Networks and Communications (EuCNC)*, 2015: IEEE, pp. 517-521.

[55] M. S. Mir, B. Majlesein, B. G. Guzman, J. Rufo, and D. Giustiniano, "LED-to-LED based VLC Systems: developments and open problems," in *Proceedings of the Workshop on Internet of Lights*, 2021, pp. 1-6.

[56] A. R. Ndjiongue, T. M. Ngatched, and H. C. Ferreira, "Access telecommunication systems using VLC technology: Cascaded LD-LED channel analysis," in *2018 IEEE Global Communications Conference (GLOBECOM)*, 2018: IEEE, pp. 1-6.

[57] Y. Wang, D. A. Basnayaka, X. Wu, and H. Haas, "Optimization of load balancing in hybrid LiFi/RF networks," *IEEE Transactions on Communications,* vol. 65, no. 4, pp. 1708-1720, 2017.

[58] J. K. Hmood and S. W. Harun, "PAPR reduction in all-optical OFDM based on time interleaving odd and even subcarriers," *Optics Communications,* vol. 437, pp. 237-245, 2019.

[59] D. Che, A. Li, X. Chen, Q. Hu, and W. Shieh, "Rejuvenating direct modulation and direct detection for modern optical communications," *Optics Communications,* vol. 409, pp. 86-93, 2018.

[60] A. Aloff and N. Mansor, "Coherent OFDM for optical communication systems," Master's Thesis, The Islamic University, Gaza, 2014. Web: http://hdl. handle …, 2014.

[61] J. K. Perin, A. Shastri, and J. M. Kahn, "Data center links beyond 100 Gbit/s per wavelength," *Optical Fiber Technology,* vol. 44, pp. 69-85, 2018.

[62] J. Armstrong, "OFDM for optical communications," *Journal of lightwave technology*, vol. 27, no. 3, pp. 189-204, 2009.

[63] W. Shieh and I. Djordjevic, *OFDM for optical communications*. Academic press, 2009.

[64] G. Azarnia, A. A. Sharifi, and H. Emami, "Compressive sensing based PAPR reduction in OFDM systems: Modified orthogonal matching pursuit approach," *ict express*, vol. 6, no. 4, pp. 368-371, 2020.

[65] R. Arthur, F. K. G. Hoshino, F. Fambrini, A. G. Silva, and J. H. Saito, "OFDM modulation simulation and analysis applied in new generation of optical networks," in *IECON 2018-44th Annual Conference of the IEEE Industrial Electronics Society*, 2018: IEEE, pp. 2998-3003.

[66] A. Alamir, H. Esmaiel, and H. S. Hussein, "Optical MIMO-TDS-OFDM with generalized LED index modulation," in *2018 International Conference on Computing, Electronics & Communications Engineering (iCCECE)*, 2018: IEEE, pp. 1-5.

[67] Y. Tang, *High-speed optical transmission system using coherent optical orthogonal frequency-division multiplexing*. University of Melbourne, St. Vincent's Institute of Medical Research …, 2010.

[68] L. A. Abdul-Rahaim, I. A. Murdas, and M. Razzaq, "Performance of coherent optical OFDM in WDM system based on QPSK and 16-QAM modulation through super channels," *International Journal of Engineering & Technology*, vol. 5, no. 3, pp. 141-158, 2015.

[69] S. D. Dissanayake and J. Armstrong, "Comparison of aco-ofdm, dco-ofdm and ado-ofdm in im/dd systems," *Journal of lightwave technology*, vol. 31, no. 7, pp. 1063-1072, 2013.

[70] H. Chen, X. Gu, M. Chen, and S. Xie, "All optical sampling orthogonal frequency division multiplexing systems," 2010.

[71] H. Supreem and M. Mahalakshmi, "Performance Analysis of Coherent Optical OFDM in FSO Communication System," in *2018 3rd IEEE International Conference on Recent Trends in Electronics, Information & Communication Technology (RTEICT)*, 2018: IEEE, pp. 2178-2182.

[72] V. V. Sudheer and A. Mandloi, "Enhanced coherent optical OFDM FSO link using diversity for different weather conditions," in *2016 IEEE International Conference on Recent Trends in Electronics, Information & Communication Technology (RTEICT)*, 2016: IEEE, pp. 1221-1225.

[73] J.-K. K. Rhee, S.-J. Lim, and M. Kserawi, "All optical OFDM transmission systems," in *2011 Asia Communications and Photonics Conference and Exhibition (ACP)*, 2011: IEEE, pp. 1-6.

[74] K. Qu, S. Zhao, D. Y. Liang, Z. Zhu, C. Dong, and X. Li, "High flatness optical frequency comb generator based on the chirping of modulators," *Optical Review*, vol. 23, no. 3, pp. 436-441, 2016.

[75] J. K. Hmood, S. D. Emami, K. A. Noordin, H. Ahmad, S. W. Harun, and H. M. Shalaby, "Optical frequency comb generation based on chirping of Mach–Zehnder Modulators," *Optics Communications*, vol. 344, pp. 139-146, 2015.

[76] F. Zhang, X. Ge, and S. Pan, "A two-stage optical frequency comb generator based on polarization modulators and a Mach–Zehnder interferometer," *Optics Communications*, vol. 354, pp. 94-102, 2015.

[77] R. Ferreira and M. Rocha, "Optical comb generation techniques," in *5th IWT 2013, International Workshop on Telecommunications*, 2013.

[78] R. Ullah *et al.*, "Pulsed laser-based optical frequency comb generator for high capacity wavelength division multiplexed passive optical network supporting 1.2 Tbps," *Optical Engineering*, vol. 55, no. 9, p. 096106, 2016.

[79] C. Shen, P. Li, X. Zhu, Y. Zhang, and Y. Han, "Ultra-flat broadband microwave frequency comb generation based on optical frequency comb with a multiple-quantum-well electro-absorption modulator in critical state," *Frontiers of Optoelectronics*, vol. 12, no. 4, pp. 382-391, 2019.

[80] V. Corral, R. Guzmán, C. Gordón, X. Leijtens, and G. Carpintero, "Optical frequency comb generator based on a monolithically integrated passive mode-locked ring laser with a Mach–Zehnder interferometer," *Optics letters*, vol. 41, no. 9, pp. 1937-1940, 2016.

[81] N. R. Doloca, K. Meiners-Hagen, M. Wedde, F. Pollinger, and A. Abou-Zeid, "Absolute distance measurement system using a femtosecond laser as a modulator," *Measurement Science and Technology*, vol. 21, no. 11, p. 115302, 2010.

[82] F. Zhang, J. Wu, Y. Li, and J. Lin, "Flat optical frequency comb generation and its application for optical waveform generation," *Optics Communications*, vol. 290, pp. 37-42, 2013.

[83] A. J. Metcalf, V. Torres-Company, D. E. Leaird, and A. M. Weiner, "High-power broadly tunable electrooptic frequency comb generator," *IEEE Journal of Selected Topics in Quantum Electronics*, vol. 19, no. 6, pp. 231-236, 2013.

[84] G. T. Harvey and L. F. Mollenauer, "Harmonically mode-locked fiber ring laser with an internal Fabry–Perot stabilizer for soliton transmission," *Optics letters*, vol. 18, no. 2, pp. 107-109, 1993.

[85] R. Ullah *et al.*, "Flattened optical multicarrier generation technique for optical line terminal side in next generation WDM-PON supporting high data rate transmission," *IEEE Access*, vol. 6, pp. 6183-6193, 2018.

[86] J. Pfeifle, *Terabit-rate transmission using optical frequency comb sources*. KIT Scientific Publishing, 2017.

[87] B. Song, C. Zhu, B. Corcoran, L. Zhuang, and A. J. Lowery, "Banded all-optical OFDM super-channels with low-bandwidth receivers," *Optics express*, vol. 24, no. 16, pp. 17968-17979, 2016.

[88] A. J. Lowery, "Design of arrayed-waveguide grating routers for use as optical OFDM demultiplexers," *Optics Express*, vol. 18, no. 13, pp. 14129-14143, 2010.

[89] Z. Wang, K. S. Kravtsov, Y.-K. Huang, and P. R. Prucnal, "Optical FFT/IFFT circuit realization using arrayed waveguide gratings and the applications in all-optical OFDM system," *Optics express*, vol. 19, no. 5, pp. 4501-4512, 2011.

[90] X. Yang, S. Yan, X. Li, and F. Li, "A unified spectrum formulation for OFDM, FBMC, and F-OFDM," *Electronics*, vol. 9, no. 8, p. 1285, 2020.

[91] J. Hoxha, G. Cincotti, S. Shimizu, and N. Wada, "FBG-and AWG-based AO-OFDM demultiplexing," in *2015 International Conference on Photonics in Switching (PS)*, 2015: IEEE, pp. 82-84.

[92] A. J. Lowery, L. Zhuang, B. Corcoran, C. Zhu, and Y. Xie, "Photonic circuit topologies for optical OFDM and Nyquist WDM," *Journal of Lightwave Technology*, vol. 35, no. 4, pp. 781-791, 2017.

[93] D. Hillerkuss *et al.*, "Simple all-optical FFT scheme enabling Tbit/s real-time signal processing," *Optics express*, vol. 18, no. 9, pp. 9324-9340, 2010.

[94] S. Hamid, "Performance Evaluation of Optically Preamplified M-ary PPM Systems for Free-Space Optical Communications," 2013.

[95] R. Hui, *Introduction to fiber-optic communications*. Academic Press, 2019.

[96] H. E. Nistazakis, T. A. Tsiftsis, and G. S. Tombras, "Performance analysis of free-space optical communication systems over atmospheric turbulence channels," *IET communications*, vol. 3, no. 8, pp. 1402-1409, 2009.

[97] B. Bag, A. Das, A. Chandra, and R. Róka, "Performance analysis of fso links in turbulent atmosphere," in *Design, Implementation, and Analysis of Next Generation Optical Networks: Emerging Research and Opportunities*: IGI Global, 2020, pp. 100-156.

[98] S. A. Zabidi, W. Al Khateeb, M. R. Islam, and A. Naji, "The effect of weather on free space optics communication (FSO) under tropical weather conditions and a proposed setup for measurement," in *International Conference on Computer and Communication Engineering (ICCCE'10)*, 2010: IEEE, pp. 1-5.

[99] N. Hameed, T. Mehmood, and H. U. Manzoor, "Effect of Weather Conditions on FSO link based in Islamabad," *arXiv preprint arXiv:1711.10869*, 2017.

[100] A. G. Alkholidi and K. S. Altowij, "Free space optical communications—theory and practices," *Contemporary Issues in Wireless Communications*, pp. 159-212, 2014.

[101] H. Kaushal, V. Jain, and S. Kar, "Free-space optical channel models," in *Free space optical communication*: Springer, 2017, pp. 41-89.

[102] K. Anbarasi, C. Hemanth, and R. Sangeetha, "A review on channel models in free space optical communication systems," *Optics & Laser Technology*, vol. 97, pp. 161-171, 2017.

[103] N. H. M. Noor, A. W. Naji, and W. Al-Khateeb, "Performance analysis of a free space optics link with multiple transmitters/receivers," *IIUM Engineering Journal,* vol. 13, no. 1, 2012.

[104] S. Dubey, S. Kumar, and R. Mishra, "Simulation and performance evaluation of free space optic transmission system," in *2014 International Conference on Computing for Sustainable Global Development (INDIACom)*, 2014: IEEE, pp. 850-855.

[105] A. Mostafa, "Measurement and modelling of a free-space optical link and in-field OFDM experiment," 2012.

[106] D. S. Kim, "Hybrid Free-Space and Radio Frequency Switching," 2008.

[107] A. A. Abdullah, "Study the effect of Iraqi weather parameter in FSO communication using different wavelength (650, 532) nm," *Iraqi Journal of Physics,* vol. 16, no. 36, pp. 104-112, 2018.

[108] A. Kumar, A. Dhiman, D. Kumar, and N. Kumar, "Free space optical communication system under different weather conditions," *IOSR Journal of Engineering (IOSRJEN),* vol. 3, no. 12, pp. 52-58, 2013.

[109] C. A. B. Dath and N. A. B. Faye, "Resilience of long range free space optical link under a tropical weather effects," *Scientific African,* vol. 7, p. e00243, 2020.

[110] M. A. Esmail, H. Fathallah, and M.-S. Alouini, "Channel modeling and performance evaluation of FSO communication systems in fog," in *2016 23rd International Conference on Telecommunications (ICT)*, 2016: IEEE, pp. 1-5.

[111] C. Bi *et al.*, "Estimating and measurement of atmospheric optical turbulence according to balloon-borne radiosonde for three sites in China," *JOSA A,* vol. 37, no. 11, pp. 1785-1794, 2020.

[112] I. Toselli, L. C. Andrews, R. L. Phillips, and V. Ferrero, "Free-space optical system performance for laser beam propagation through non-Kolmogorov turbulence," *Optical Engineering*, vol. 47, no. 2, p. 026003, 2008.

[113] A. Rafalimanana, C. Giordano, A. Ziad, and E. Aristidi, "Prediction of atmospheric turbulence by means of WRF model for optical communications," in *International Conference on Space Optics—ICSO 2020*, 2021, vol. 11852: SPIE, pp. 1856-1866.

[114] D.-N. Nguyen, S. Zvanovec, and Z. Ghassemlooy, "Mitigation of dispersion and turbulence in a hybrid optical fibre and free-space optics link using electronic equalisation," *Optik*, vol. 196, p. 163154, 2019.

[115] V. Sharma and G. Kaur, "Degradation Measures in Free Space Optical Communication(FSO) and its Mitigation Techniques- A Review," *International Journal of Computer Applications*, vol. 55, no. 1, pp. 23-27, 2012.

[116] H. Li and Y. Huang, "The architecture of blind equalizer for MIMO free space optical communication system," in *Optical Communication, Optical Fiber Sensors, and Optical Memories for Big Data Storage*, 2016, vol. 10158: SPIE, pp. 376-383.

[117] A. Abdullah and R. Fyath, "Towards optical frequency comb-based high-capacity superchannel transmission-part ii: Transmission performance," *International Journal of Networks and Communications*, vol. 10, no. 2, pp. 33-40, 2020.

Appendix

Appendix A

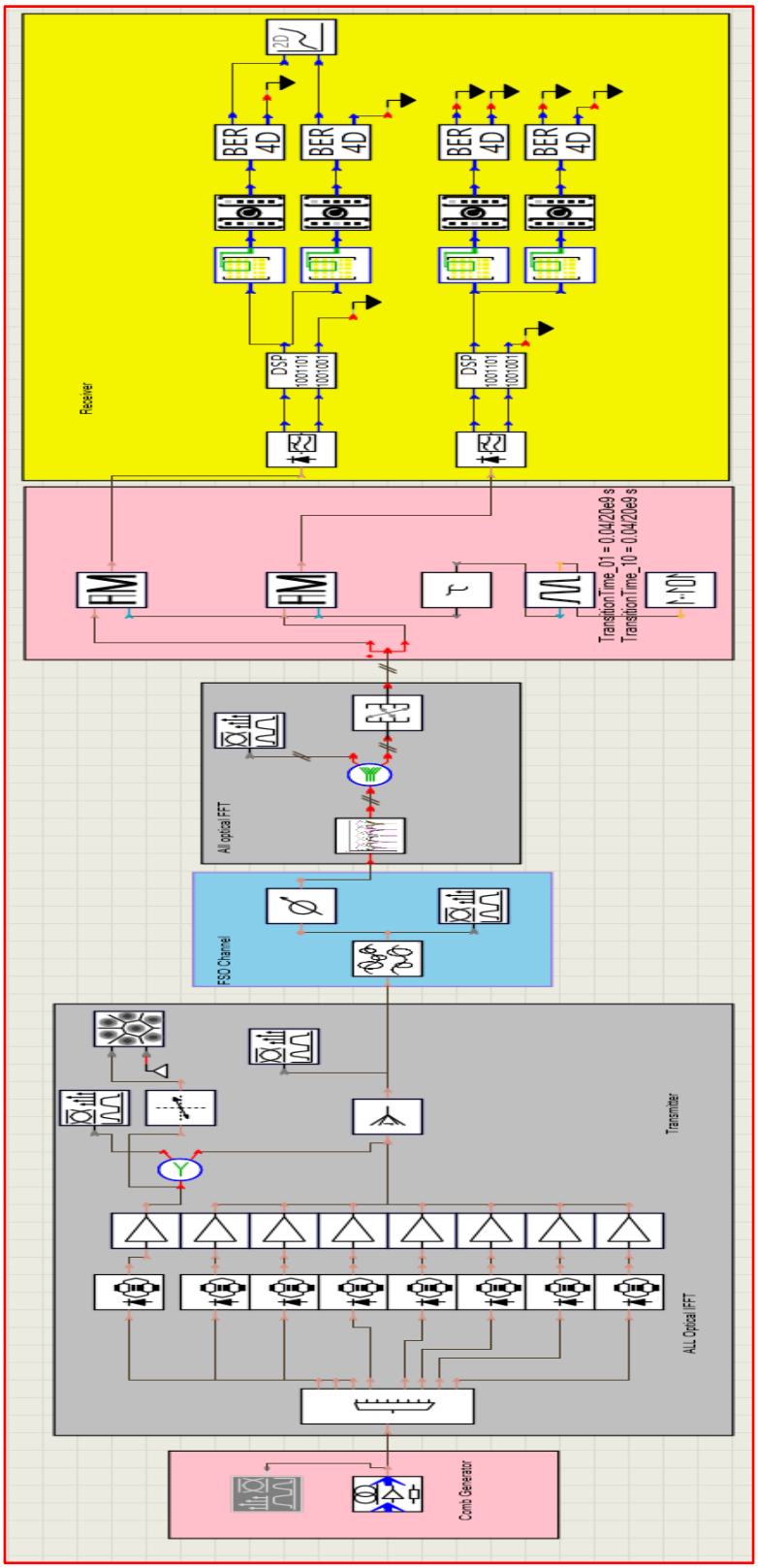

Figure 1 The VPI photonic design suite simulations of 8-channels Li-Fi system-based AO-OFDM architecture

Appendix A

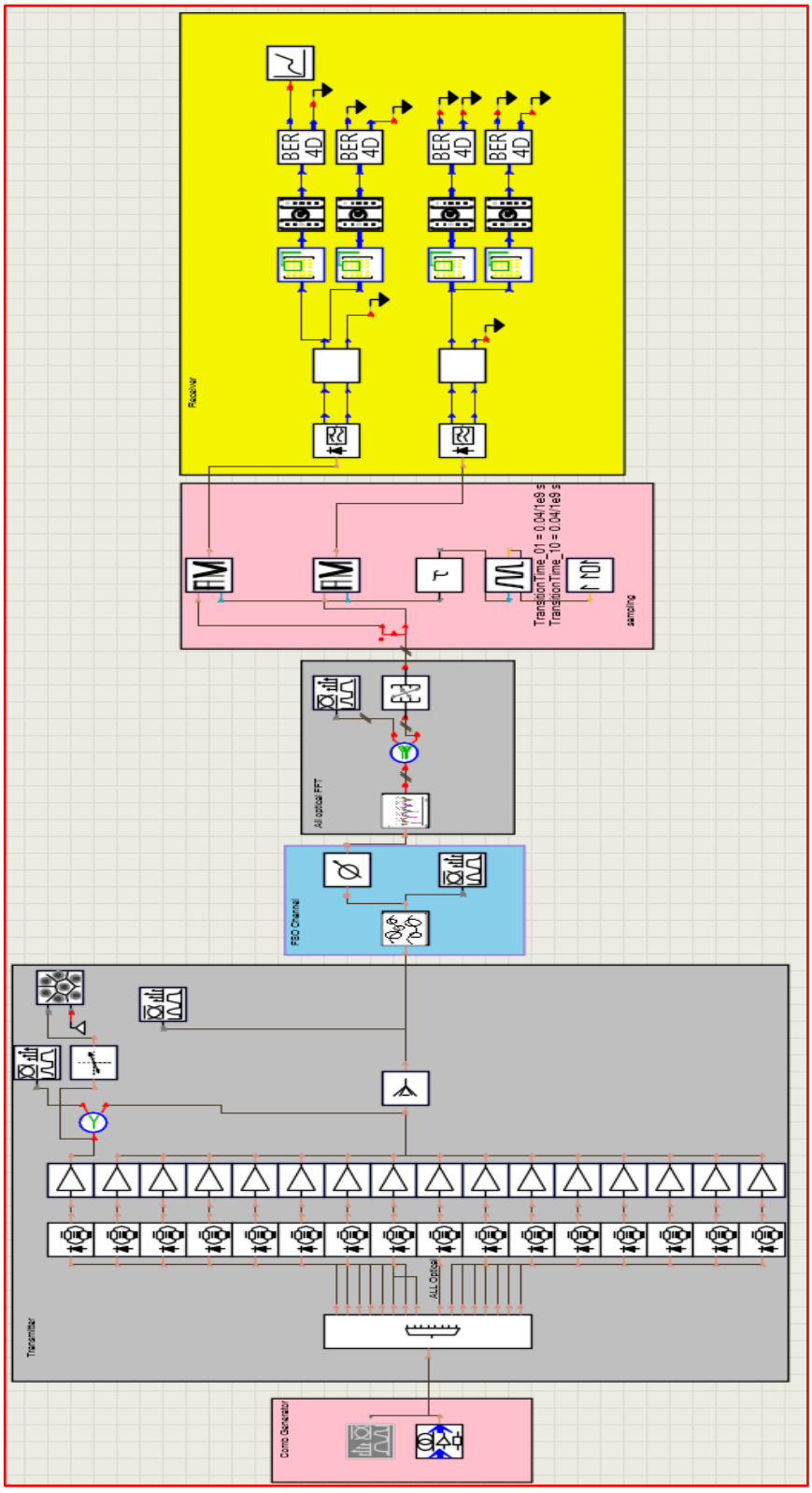

Figure 2 The VPI photonic design suite simulations of 16- channels Li-Fi system-based AO-OFDM architecture

Appendix A

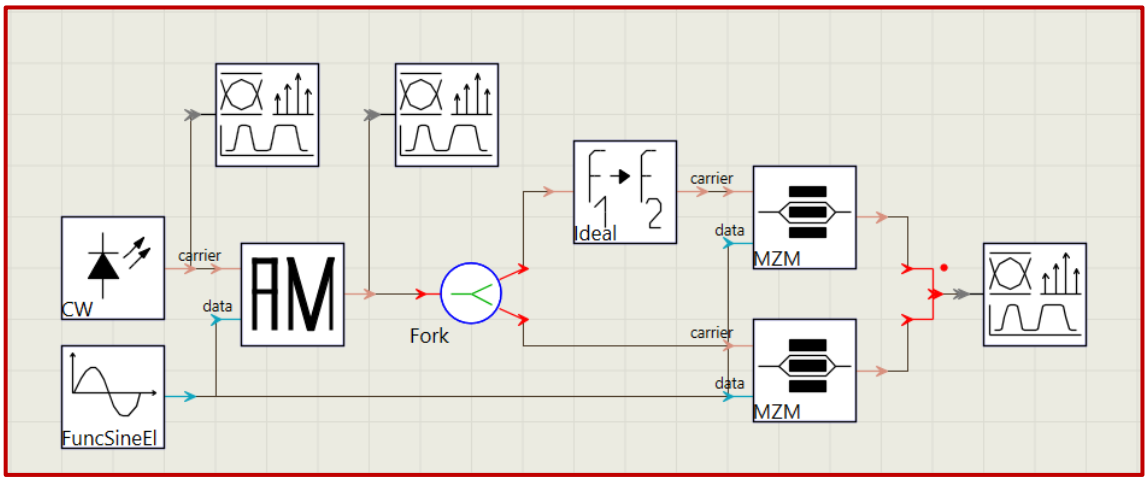

Figure 3 Simulation figure of proposed OFCG

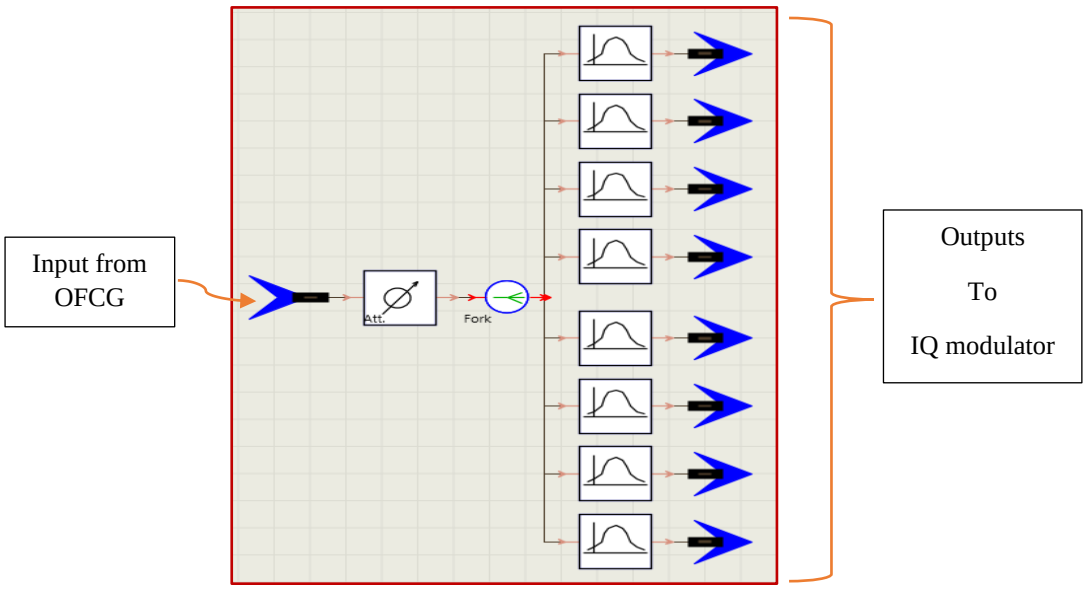

Figure 4 DWDM construction

Appendix A

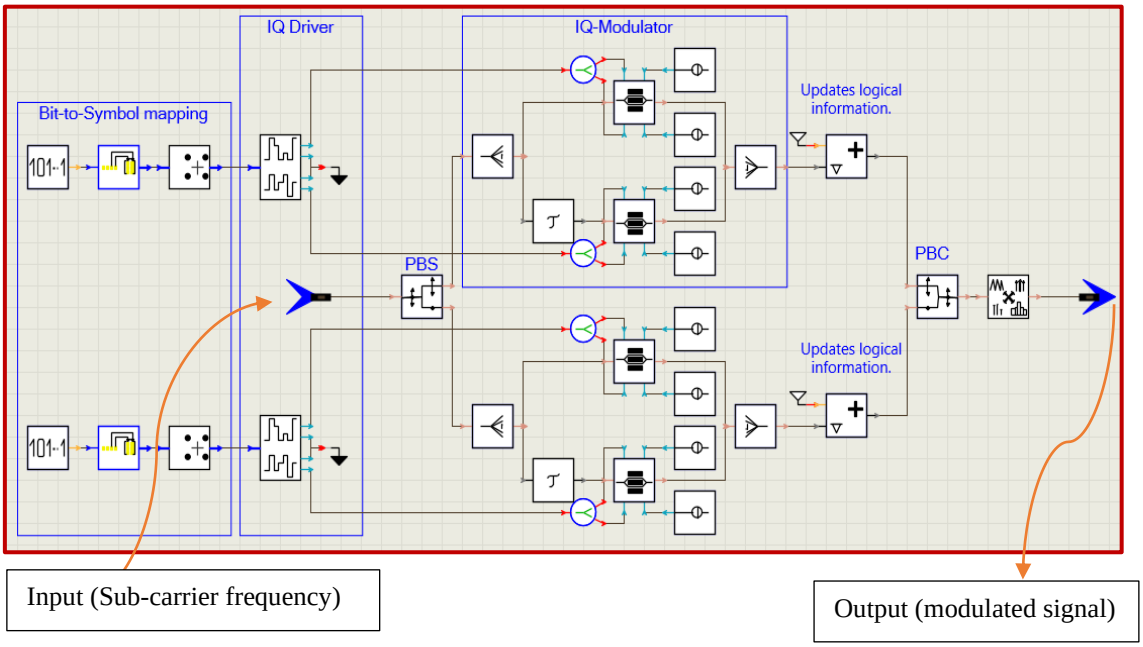

Figure 5 Dual polarization IQ modulator

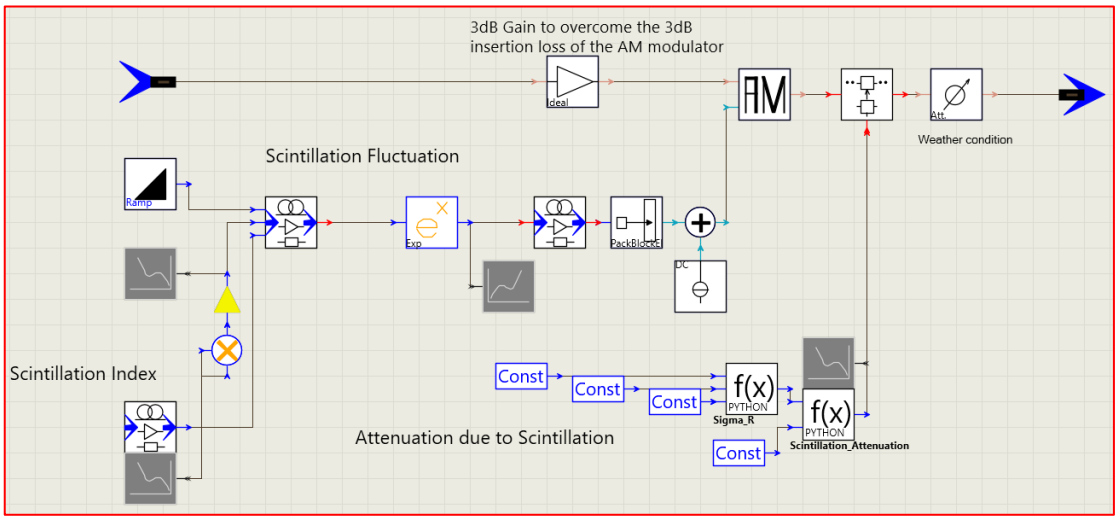

Figure 6 FSO channel modeling under scintillation effects

Appendix A

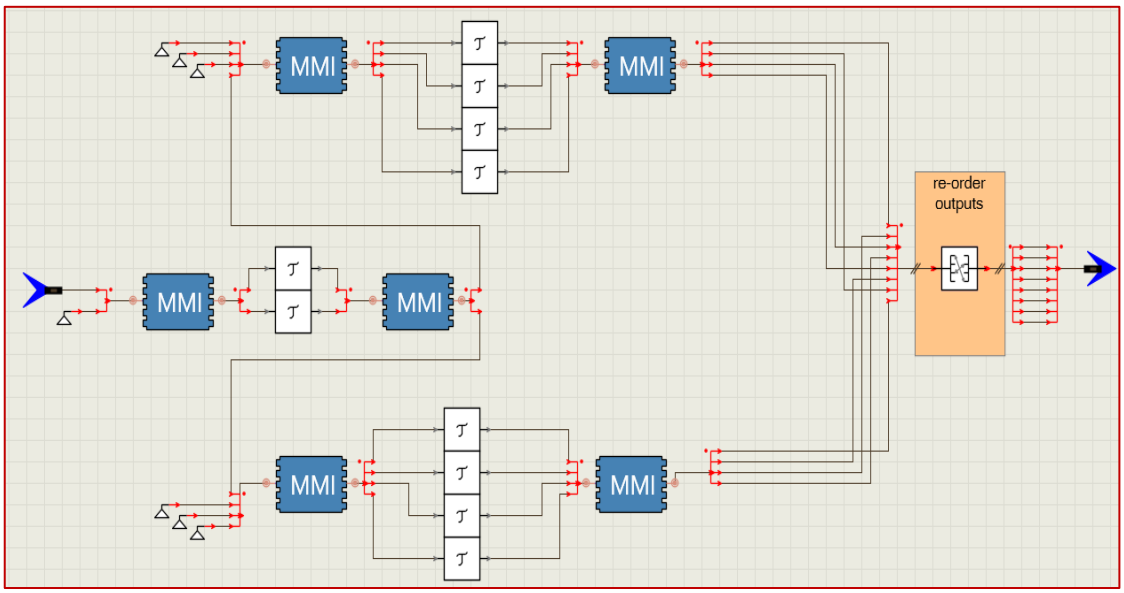

(a)

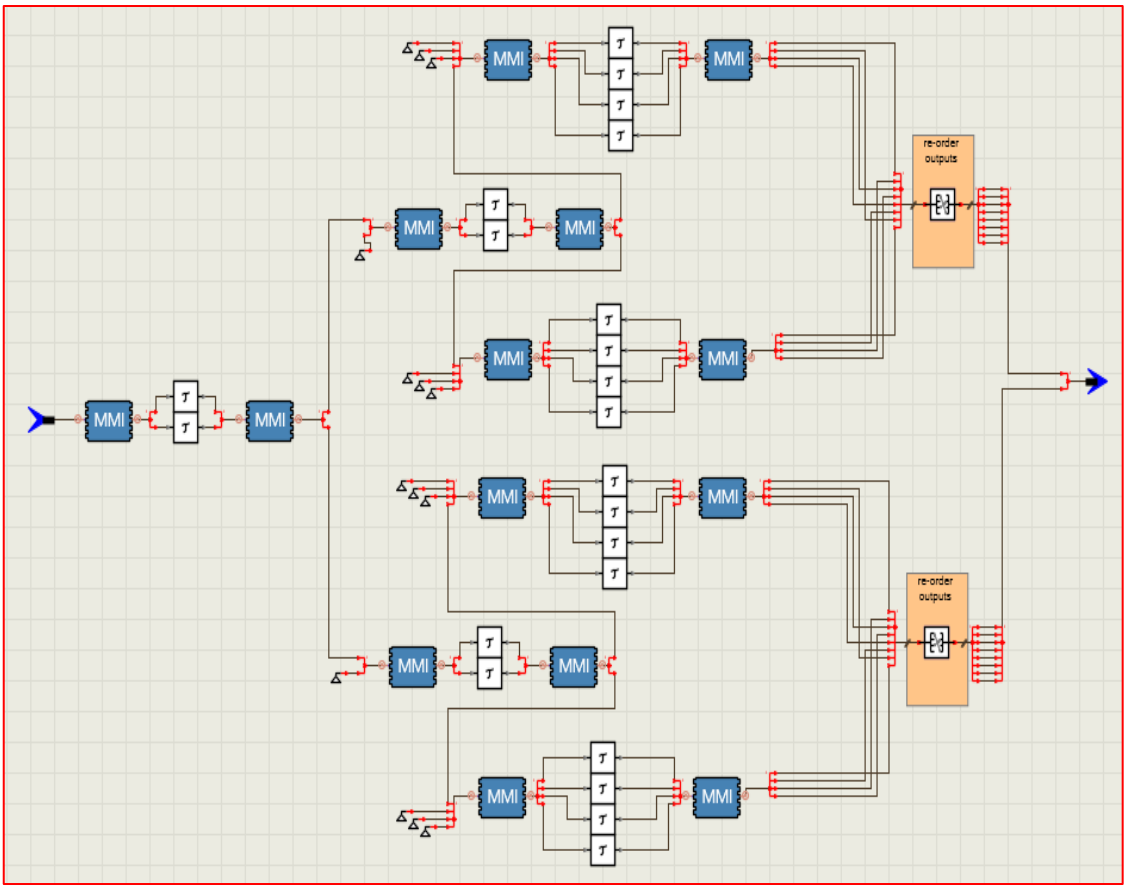

(b)

Figure 7 OFFT a) 8-OFFT b) 16-OFFT

Appendix A

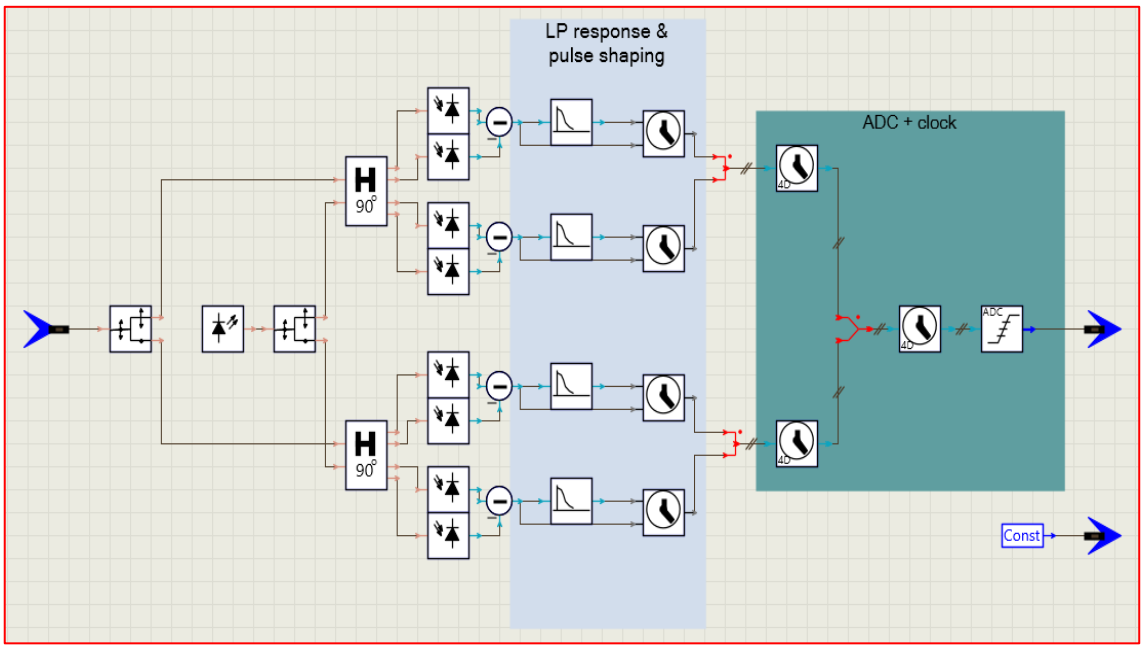

Figure 8 Coherent receiver with Dual polarization IQ modulator

الخلاصة

تُعتبر تقنية ال (Li-Fi) تقنية واعدة للجيل الخامس وما بعده للتغلب على أزمة الطيف الترددي اللاسلكي (RF) في شبكات الاتصالات اللاسلكية وإجراءعملية إرسال عالية السرعة ، فهي بديلاً ممتازًا للترددات الراديوية في الشبكات اللاسلكية خلال السنوات القليلة الماضية لما لها من فوائد عديدة.

تم اقتراح نظام Li-Fi في هذه الدراسة كشبكة لاسلكية ضوئية تتميز بأمان وقدرة وسرعة ارسال اعلى مقارنتا مع شبكة Wi-Fi. اقترحت هذه الدراسة محاكاة لنظام Li-Fi عالي الاداء مُناسبًا للتطبيقات الخارجية حيث يتم إرسال إشارة الضوء عبر مسار غير موجه وغير محدود يسمى قناة الفضاء الحر FSO. تم استخدام الصمام الثنائي الليزري LD كمصدر بصري للتخلص من قيود أنظمة Li-Fi التقليدية من حيث عرض النطاق الترددي لل LED ومعدل نقل البيانات ومسافة الإرسال.

نظام ال Li-Fi المقترح عالي الاداء ومحصن ضد توهين قناة الفضاء الحرة بسبب استخدام بنية OFDM الضوئية بالكامل من خلال تنفيذ تحويلات فورير IFFT / FFT بالكامل في المجال البصري دون الحاجة للمكونات الكهربائية التي تحد من سرعة النظام وأدائه. نجحت هذه الدراسة في إنشاء التعامد بصريًا بين ثمانية إلى ستة عشر قناة من خلال اقتراح مخطط جديد لمولد مشط التردد البصري (OFCG) خاص لتطبيقات النطاق المرئي لتوليد ناقلات متعددة من صمام لثنائي ليزري مستمر واحد مع خاصية الضبط التحكمي، وهي ميزة مهمة لإنشاء التعامد بين الموجات الحاملة الفرعية المتولدة. إن OFCG المقترح بسيط مع طاقة و كفاءة عالية وتسطيحًا ممتازًا للخطوط المتولدة ، وكان عدد خطوط الترددية المولدة 52 مع قدرة قوية حوالي2 ديسيبل وتذبذب أقل من 0.5 ديسيبل على عرض نطاق حوالي 470 جيجاهرتز. تم بنجاح إنشاء إشارة AO-OFDM بين ثمانية وست عشرة قناة عبر 180 أو 340 جيجاهرتز من عرض النطاق الترددي على التوالي ، من خلال تنفيذ تحويل فوريير السريع العكسي البصري بالكامل (OIFFT) في جهة الارسال بناءً على OFGC و DWDM والجامع البصري ، كل قناة تحتوي على 20 G رمز / ثانية وتستخدم مضمن DP-IQ مع QPSK و 16- QAM مما يجعل إلاشارة المرسلة تحتوي على حوالي 5 ديسيبل من (PAPR) وكفاءة طيفية بالغة 4 و 8 بت / ثانية / هرتز لكل من QPSK و QAM-16 على التوالي. اما في الجانب المستقبل لاستعادة إشارة كل قناة ، يتم تنفيذ تحويل فورير السريع البصري بالكامل (OFFT) بلاعتماد على هيكلية خاصة مُقترحه من (MMI) والتأخيرات الزمنية.

تمت محاكاة النظام بواسطة مجموعة تصميم VPI وتم تحليله من حيث BER ، ومخطط البُعد ، والطاقة المستقبلة ، وحقق النظام قوة استقبال جيدًة بمعدل بيانات مرتفع يصل إلى 1.28 تيرا بت في الثانية و BER منخفض يبلغ حوالي 1×10^{-10} .

تم استخدام عدة قيم لل (OSNR) (0-35 dB) ومسافات مختلفة للفضاء الحر (من 1 إلى 10 كم) تحت عدة اضطرابات وظروف جوية مختلفة لاختبار سلوك النظام المقترح.

تعتبر ظروف الطقس من الخصائص الحرجة التي تؤثر على موثوقية وجودة أنظمة Li-Fi الخارجية. قامت هذه الدراسة بفحص ومحاكاة التوهين الجوي على نطاق واسع باستخدام MATLAB مع ظروف مختلفة وتقييم تأثير هذه الظروف على تصميم نظام Li-Fi المقترح. أظهر النظام أداءً لائقًا مع معدل الخطأ في البتات (BER) عند حوالي 1×10^{-3} وإشارة مستلمة تبلغ -45 ديسيبل مللي واط عند مسافة 10 كيلومترات وتحت اضطرابات جوية عالية.

جمهورية العـراق
وزارة التعليم العالي والبحث العلمي
جامعـــة بابـل
كليـــــة الهندســـة
قسم هنـدسـة الـكـهربـاء

الأداء ألعالي لنظام Li-Fi ألخارجي المستند على OFDM البصري الكامل في الاتصالات الخارجية

أطـروحــه
مـقدمـة إلى كليــة ألــهندسـة في جامعـة بـابـل
وهي جزء من متطلبات ألحصول على درجة ألدكتوراه فلسفة في هندسة الألـكتـرونيـك والأتـصـالات

من قبـل
مـروة جـليـل مـحسـن الـموسـوي

بإشــراف
أ.د. أبـراهيـم عـبـد الله مـرداس

١٤٤٤هـ ٢٠٢٣ م